Terrain Corrections for Gravity Gradiometry

by

Ou Huang

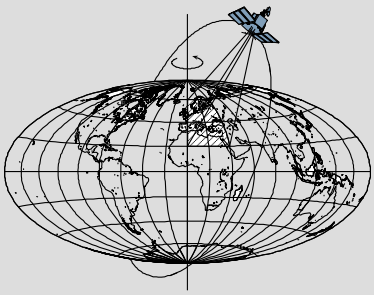

Report No. 500

Geodetic Science

The Ohio State University
Columbus, Ohio 43210

June 2012

PREFACE

This report was prepared for and submitted to the Graduate School of the Ohio State University as a dissertation in partial fulfillment of the requirements for the PhD degree.

Abstract

This study developed a geostatistical method to determine the required extent of terrain corrections for gravity gradients under the criterion of different applications. We present the different methods to compute the terrain corrections for gravity gradients for the case of ground and airborne gravity gradiometry. In order to verify our geostatistical method and study the required extent for different types of terrain, we also developed a method to simulate topography based on the covariance model. The required extents were determined from the variance of truncation error for one point, or furthermore from the variance of truncation error difference for a pair of points, and these variances were verified with that from the deterministic method. The extent of terrain correction was determined for ground gradiometry based on simulated, ultra-high resolution topography for very local application, and also was determined based on mountainous topography of large areas. For airborne gradiometry, we compute the terrain corrections and the required extent based on Air-FTG observations at Vinton Dome, LA and Parkfield, CA area; also they were verified with the results of Bell Geospace. Finally, from the mostly flat, medium rough and mountainous areas, an empirical relationship was developed which has the properties that the required extent has 4 times relationship corresponding to the amplitude of PSD has 100 times relationship between mountainous and mostly flat areas, and it can be interpolated for other types of topography from their geostatistics.

Table of Contents

Chapter 1

Introduction

1.1 Terrain Correction of Gravity and Gradiometry

The gravimetric technique has been used for over a century to study the surface and interior of the earth and the planet as well. Also for geophysics, gravity together with other techniques are used extensively in exploring the subsurface for energy and mineral resources, geological hazards, and other features of societal significance. Gravity exploration is concerned with measuring gravity anomaly components to learn the mass density contrast and subsurface anomaly body's depth, shape and size.

Gravity gradiometry is used by oil, gas and mining companies to measure the density of the subsurface, effectively the rate of change of rock properties. Then by applying the inverse theory, geophysicists can map and locate the target oil, gas and mineral deposits if a picture of subsurface anomalies can be obtained by removing the noise of unwanted features from the observed signal.

As the result of recent advances in instrumentation and field procedures, gravity gradiometers are becoming increasingly available (Difrancesco, 2007). Generally speaking, gravity gradiometers are more sensitive to mass anomaly than the gravimeter since gravity gradients are the second-order derivative of gravity potential. On the other hand, gravity gradiometers also show disadvantage because of its high sensitivity of topographic mass in land and airborne surveys which will be considered as noise if our application is the subsurface exploration. A terrain correction, computed from a model structure, accounts for the variation of topographic mass and so the procedure of computing terrain correction is most necessary and important in dealing with gravity and gravity gradiometry data. However, the high sensitivity signal from the gradiometer due to subsurface structures will not be correctly obtained if the terrain corrections were not computed properly using the high resolution terrain. For example, in rough topography, the magnitude of terrain corrections for gradient can reach about hundreds of E (1 E (Eötvös) $=10^{-9}$ s^{-2}) while the anomaly of ore-body usually will only generate a signal of about several tens of E (Nabighian et al., 2005). So the application of high accuracy gradiometer is limited by the ability to estimate inner-zone terrain corrections precisely and by the quality of the digital elevation model. Not only the relative proximity of the terrain to the gravity gradiometer, but also the relative magnitude of the density contrast

often result in a terrain correction that is larger than the anomaly signal of interest in subsurface exploration (Chen and Macnae, 1997; Dransfield and Zeng, 2009). Therefore, the increased sensitivity of the second-order derivative of the potential will limit their utility in subsurface exploration, especially in areas of rugged relief if we cannot obtain the terrain corrections of the second-order derivative of the potential more accurate than that of the first-order derivative of the potential. In the past several decades, many efforts have been put into developing different methods and algorithm of computing terrain corrections for gravity gravimeter. However the proper extent and resolution of terrain, also, the effect of varying surface density on the computation of terrain corrections for the gravity gradiometer are still not deeply researched and no consistent results were obtained, so it gives the motivation of this dissertation study.

1.2 Background

The gravity gradients have been quickly applied for mineral, oil and gas exploration since Baron Lorand von Eötvös invented the torsion balance instrument and the surveys were mainly carried out in Hungary throughout the last century (Bod et al., 1990), and were also used in the U.S. and Western Europe extensively. However due to the cumbersome field procedures and the long observation time needed for each station, especially in the rugged terrain, the instrument was largely displaced by high accuracy gravimeter in the 1940s.

Recent developments in airborne gravity gradiometry such as the FTG (Full Tensor Gradient) system by Bell Aerospace (now Lockheed Martin) and the Falcon system by BHP Billiton (recently acquired by Fugro) have sparked renewed interest in the use of gravity gradients for subsurface exploration (e.g., Nabighian et al., 2005). The airborne systems can survey large areas quickly on any type of terrain with advertised measurement accuracies of 5 Eötvös for the gradients (Asten, 2000), this is the main reason for its rapid development in the recent 20 years.

A major limitation of using gravity gradients in subsurface exploration, especially in areas of rugged relief, is stripping out the gradient effects of the terrain with commonly variable physical properties (e.g., Dransfield and Zeng, 2009; Chinnery, 1961). Many methods and algorithms have been developed to compute the terrain corrections of gravity and gravity gradients and the conventional terrain modeling schemes involve solutions that are closed formulas derived from mass prism that are cumbersome to implement efficiently. Substituting the mass prism using the equivalent point source, the closed mass prism formula can be approximated by point source formula and can be computed using Gauss-Legendre Quadrature methods which will significantly reduce the formula terms especially for the high order derivatives of potential (e.g., Grant and West, 1965; Ku, 1977). Terrain effect computations from the fast Fourier transform (FFT) of

the DEM have also been devised (e.g., Forsberg, 1985; Sideris, 1985). Furthermore, Jekeli and Zhu (2006) compared different algorithms for calculating the gravity-gradient terrain effect from gravity data and topographic data, providing useful information on the relative speed and accuracy of these algorithms.

The terrain correction model together with its analytical formula for airborne gravity anomaly and gravity gradients has been discussed extensively in the literature (Chinnery, 1961; Hammer, 1976; Tziavos et al., 1988; Parker, 1995). In Hammer's optimistic opinion, the gradient noise generated from the local terrain or the shallow variations in soil density is not serious for the expected gradient methods. However, there exists a reverse conclusion about the topographic corrections. Chinnery (1961) points out that the average terrain will generate the gradients at an aircraft altitude of the same order as that due to some common ore bodies. And the vertical gradient data are much more sensitive to near surface masses than the normal gravity data. Therefore the terrain corrections for the gradient will be more important than for the gravity. The simulation result of Chen and Macnae (1997) seems support the above second point of view. Their results show that the terrain effects of topography will seriously affect both the airborne gravity and gradient measurements. For the gravity, this can be corrected by using the standard Bouguer correction; while for gravity gradients, this effect remains a problem even if the terrain correction is carried out with a density error of only 100 kg/m^3. Thus, the conclusion is that it is hard to detect the anomaly from an airborne gradiometer since it is severely affected by regolith, bedrock topography even if the terrain corrections are made.

Different algorithms and methods on computation of terrain corrections were applied for the different application, most of them are only focused on the gravity, not the gradients, and there is no deep, systematic research carried out on the necessary extent and resolution of the terrain correction of the gravity, especially of the gradients for the application of subsurface exploration. Badekas (1967) assumed the topography is varying linearly in radial and azimuthal direction, the terrain correction is computed by directly integrating within the area of different radius and azimuth and applied these corrections to the torsion balance observations in Southwest Ohio in 1966. The total extent reached $5^o \times 5^o$ and the different resolutions of DEM data were used for different section of extent. Parker (1972) developed the gravity potential formula in frequency domain through the frequency transform of the topography height, while Tziavos et al., (1988) computed the effect of the terrain on airborne gravity and gradiometry using FFT method and studied effects of terrain representation (mass lines or prisms), height data resolution needed, and the number of expansion terms required to approximate the basically nonlinear terrain effect integrals. The total extent of the original grid was 56.6 km $\times$ 36.7 km with a DEM grid spacing of 0.1 km. From their results, they concluded that in order

to obtain terrain gravity effects at accuracy of 0.3~0.5 mGal (1 mGal=10^{-5} m/s^2) and terrain gravity gradient effects at accuracy of 1 E respectively, the grid spacing should be 0.5 km$\times$0.5 km for a flying altitude of 1 km above the highest topography. The extent of terrain correction they used roughly agrees with the required extent we determined considering the different flight altitude and characters of the terrain. If the flying altitude is below 600 m, then the height spacing needs to increase to 0.25 km$\times$0.25 km. The terrain correction integral was expanded to third-order terms in both cases. And they suggest that in order to obtain an RMS accuracy of gradient effects better than 1 E, a ratio of 1/3 between grid spacing and flight altitude above maximum elevations seems to be reasonable. Hwang et al. (2003) compared the computation of terrain corrections for gravity by using Gaussian quadrature, prism and FFT methods. By comparing different pairs of inner zones, it is concluded that if the required accuracy of terrain correction is 0.1 mGal, an inner radius of 20 km is sufficient; and by comparing different pairs of outer zones (fixed inner zone 20 km), it is concluded that to meet a 0.1 mGal accuracy in terrain correction, an outer radius of 200 km is sufficient, also an outer radius of 100 km is sufficient at elevations below 1000 m. It is also shown that among the three methods the Gaussian quadrature method recovers higher resolution of the terrain correction signal than the other two methods, however, still smaller than the highest grid data resolution, i.e., the corresponding Nyquist frequency. The needed computation time is most for Gaussian quadrature and least for FFT method and it is suggested that the Gaussian quadrature method is intended for point-by-point computation not for wide area grid point computation. From their computation results, the Gaussian quadrature method has the highest accuracy and the standard deviation of the terrain correction difference for gravity between Gaussian quadrature method and FFT method is 7.28 mGal, it is concluded that the achieved accuracy in terrain correction is worth the extra computing time.

Kass and Li (2008) extended Parker's (1972) formula in frequency domain to the gradient formula in frequency domain and applied this frequency method to the computation of terrain correction for gradient. They used this algorithm to examine the spatial extent and resolution of terrain model required for performing accurate terrain correction in airborne gravity gradiometry. Also a Gaussian hill was used to simulate the topography and compute the terrain correction of each gradient for different extent size of the topography. By analyzing the RMS difference of the terrain correction between each different extent pairs, they show that the empirical rule for the spatial extent can be approximated by 9 times the relief which assumes the needed maximum terrain correction extent is proportional with respect to the relief height. The extent of terrain correction from their results does not agree with the required extent of ours. According to results of our study, an extent of 400 km is needed with respect to the relief about 4000

m. Through computing the energy lost with respect to the resolution, their results show that 20 m resolution is sufficient for the terrain correction computation of the gradient.

Also, Dransfield and Zeng (2009) pointed out that the relative proximity of the terrain to the gravity gradiometer and the relative magnitude of the density contrast often result in a terrain correction that is larger than the geologic signal of interest in resource exploration. According to the terrain correction integral, the errors in density, the errors in DEM elevation, the errors in the evaluation point position and the errors in the DEM that is too coarsely sampled will result in the residual errors in the terrain correction.

Less effort has been concentrated on the topic of density variations effect on the terrain correction in the literature since the surface density variation is complicated and it is time consuming and laborious to measure the density variations for an area by sampling. Grant and Elsaharty (1962) proposed the concept of "Bouguer density" which is a weighted average of real density. It varies with respect to each observation point and they provide a procedure to compute it by minimizing the correlation between the local gravity anomalies and topography. Using their procedure the Bouguer density map can be generated and contoured. In their example, the correspondence between their results and the known geology appears to be good and indicates that Bouguer density variations due to changing surface conditions can be used routinely in the reduction of gravity data.

However, Tziavos et al., (1996) worked on the other side of this topic, provided that the surface density grid data are known. They investigated the effect of the variations of surface density values to the computation of terrain corrections on the gravity using the algorithm of mass prism topographic representation. They compute the terrain correction effect by applying the efficient FFT technique that they already derived (Tziavos et al., 1988), the only difference is to do the Fourier transform with respect to $\rho \cdot h$ terms instead of only h terms. The numerical examples on the computation of terrain corrections were carried out in Austria, where both the terrain (DEM) and density (DDM) files are available at the same grid with the same resolution of $11.25'' \times 18.75''$. It is also concluded that the differences in the mass prism model when using a uniform density value instead of an actual density grid are correlated with the topography and existing density variations. Their numerical tests showed that the differences are close to 0.4 mGal with a maximum absolute value close to 9.5 mGal and a variation which reached the level of 11 mGal. They did not compute the terrain correction effects for the gravity gradient using the surface grid density variations.

Up to here, different terrain correction methods and algorithms for the gravimeter or gradiometer were reviewed; it was argued that the terrain correction for gravity gradiometry is significantly more important than the gravity gravimetry for the application of subsurface exploration especially in rugged terrain area. Among all the terrain effect computations using different models and methods, one common problem is

to determine the extension and resolution of terrain source, while the above review shows that no consistent results were given. Also there is no conclusion about the density variation effect on the terrain correction for gravity gradiometry, and it may play an important role on the gravity gradients reductions. The required resolution and the density variation of the terrain are not included in this dissertation and should leave for the future research.

Chapter 2

Terrain Correction for Gravity Gradiometry

2.1 Gravitational Gradient and Terrain Correction

The gravitational potential at a point, $\mathbf{x}$, due to the masses distributed at points, $\mathbf{x}'$, over the volume, v, is given by Newton's law of gravitation:

$$V(\mathbf{x}) = G\iiint_{v} \frac{\rho(\mathbf{x}')}{|\mathbf{x}-\mathbf{x}'|} d\mathbf{x}', \tag{2.1}$$

where $|\mathbf{x}-\mathbf{x}'| = \sqrt{(x_1-x_1')^2+(x_2-x_2')^2+(x_3-x_3')^2}$, is the Euclidian distance between the integration point (x_1', x_2', x_3') and the computation point (x_1, x_2, x_3), defined in the local coordinate system with axes pointing in the east, north and up directions, the $x_3 = 0$ plane is set as the plane approximating the local geoid. $\rho(\mathbf{x}')$ is the mass density distribution and G is the gravitational constant.

The gravitational acceleration vector is given by

$$g = (g_1, g_2, g_3)^T = (\frac{\partial V}{\partial x_1}, \frac{\partial V}{\partial x_2}, \frac{\partial V}{\partial x_3})^T . \tag{2.2}$$

The gravitational gradient tensor due to these masses is defined by

$$\Gamma = \nabla\nabla^T V = \left[\Gamma_{jk}\right] = \begin{bmatrix} \frac{\partial^2 V}{\partial x_1 \partial x_1} & \frac{\partial^2 V}{\partial x_1 \partial x_2} & \frac{\partial^2 V}{\partial x_1 \partial x_3} \\ \frac{\partial^2 V}{\partial x_2 \partial x_1} & \frac{\partial^2 V}{\partial x_2 \partial x_2} & \frac{\partial^2 V}{\partial x_2 \partial x_3} \\ \frac{\partial^2 V}{\partial x_3 \partial x_1} & \frac{\partial^2 V}{\partial x_3 \partial x_2} & \frac{\partial^2 V}{\partial x_3 \partial x_3} \end{bmatrix} \tag{2.3}$$

The diagonal gradients are called in-line gradients and the off-diagonal gradients are called cross-gradients.

The gradient tensor has the following properties:

(1) The gradient tensor is symmetric.

(2) The in-line gradients satisfy the Poisson's equation, $\Delta V = -4\pi G\rho(\mathbf{x})$. (2.4)

where $\Delta V = \frac{\partial^2 V}{\partial x_1^{\,2}} + \frac{\partial^2 V}{\partial x_2^{\,2}} + \frac{\partial^2 V}{\partial x_3^{\,2}}$ (2.5)

Outside the volume, v, in empty space, the density is zero, so $\Delta V = 0$, which is called Laplace's equation. Thus, the gradient tensor only has 5 independent elements, three off-diagonal elements and two diagonal elements.

The total terrain effect is the gravitational potential and its derivatives at a point due to all the topographic masses above the geoid (Figure 2.1). The residual terrain effect is due to the topographic masses relative to a level surface through the point, or relative to some other approximation to the terrain. That is, if we construct a topography by this level surface (or some other approximation to the terrain), the additional masses that have been included and those not yet included constitute the residual masses that generate the residual terrain effect. For the observation point, P, on the Earth's surface, the Bouguer plate is an infinite, flat plate between the geoid and the level surface passing through the point, both approximated as horizontal planes. The terrain correction is a procedure which is defined by taking into account (that is, removing) the gravitational attraction of the residual topography, that is, the deviation of the actual topographic masses from the Bouguer plate of the point, P (Fig. 2-1) (Heiskanen and Moritz, 1967).

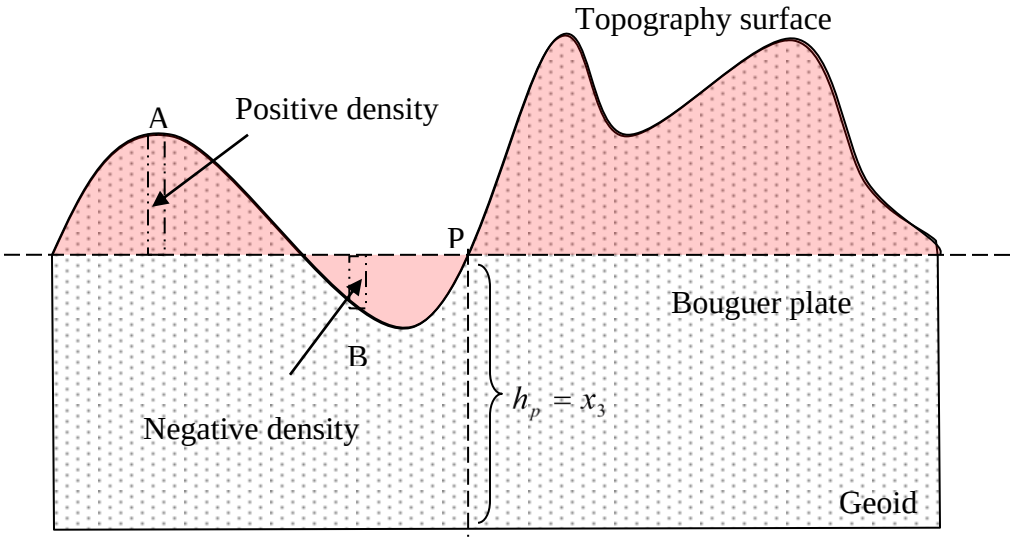

Figure 2.1 Terrain effect of topography (dotted area) and terrain correction of residual terrain (red area) w.r.t Bouguer plate

In our upward positive coordinate system, removing the mass above the Bouguer plane (mass attracts P upward, i.e., removing a positive value) will cause the terrain

correction to be negative; while adding mass below the Bouguer plane (mass attracts P downward, i.e., adding a negative value) will also cause the terrain correction to be negative. So the terrain correction is always negative for the vertical gravitational acceleration in our upward positive coordinate system if we define gravitation as the positive gradient of potential.

The same procedure can be used to compute terrain effect on the gravitational gradients at point, P. So, we have the total terrain effect on the gravitational gradients at point, P, from equation (2.1), (2.3) as

$$\Gamma_{jk} = \frac{\partial^2 V}{\partial x_j \partial x_k} = G \iiint_v \frac{\partial^2}{\partial x_j \partial x_k} \left(\frac{\rho(\mathbf{x}')}{|\mathbf{x} - \mathbf{x}'|} \right) d\mathbf{x}' \tag{2.6}$$

which can be written as

$$\begin{aligned} \Gamma_{jk} &= G \iiint_v \frac{\partial^2}{\partial x_j \partial x_k} \left(\frac{\rho(\mathbf{x}')}{|\mathbf{x} - \mathbf{x}'|} \right) d\mathbf{x}' \\ &= G \iint_A \int_0^{h_p} \frac{\partial^2}{\partial x_j \partial x_k} \left(\frac{\rho(\mathbf{x}')}{|\mathbf{x} - \mathbf{x}'|} \right) d\mathbf{x}' + G \iint_A \int_{h_p}^{h} \frac{\partial^2}{\partial x_j \partial x_k} \left(\frac{\rho(\mathbf{x}')}{|\mathbf{x} - \mathbf{x}'|} \right) d\mathbf{x}' \end{aligned} \tag{2.7}$$

where A is the horizontal area of topographic masses around the point, P. The area A can be separated into the sum of A_above and A_below, where A_above is the area of topography masses above the point, P; and A_below is the area of topographic mass voids below the point, P.

The terrain correction is the negative of the residual terrain effect, that is, residual to the Bouguer plate:

$$\begin{aligned} \delta\Gamma_{jk}^{TC} &= -G \iint_{A\_above} \int_{h_p}^{h} \frac{\partial^2}{\partial x_j \partial x_k} \left(\frac{\rho(\mathbf{x}')}{|\mathbf{x} - \mathbf{x}'|} \right) d\mathbf{x}' + G \iint_{A\_below} \int_{h}^{h_p} \frac{\partial^2}{\partial x_j \partial x_k} \left(\frac{\rho(\mathbf{x}')}{|\mathbf{x} - \mathbf{x}'|} \right) d\mathbf{x}' \\ &= -G \iint_{A\_above} \int_{h_p}^{h} \frac{\partial^2}{\partial x_j \partial x_k} \left(\frac{\rho(\mathbf{x}')}{|\mathbf{x} - \mathbf{x}'|} \right) d\mathbf{x}' - G \iint_{A\_below} \int_{h_p}^{h} \frac{\partial^2}{\partial x_j \partial x_k} \left(\frac{\rho(\mathbf{x}')}{|\mathbf{x} - \mathbf{x}'|} \right) d\mathbf{x}' \\ &= -G \iint_A \int_{h_p}^{h} \frac{\partial^2}{\partial x_j \partial x_k} \left(\frac{\rho(\mathbf{x}')}{|\mathbf{x} - \mathbf{x}'|} \right) d\mathbf{x}' \end{aligned} \tag{2.8}$$

So substitute (2.8) into (2.7), we have

$$\Gamma_{jk} + \delta\Gamma_{jk}^{TC} = G\iint_A \int_0^{h_p} \frac{\partial^2}{\partial x_j \partial x_k}\left(\frac{\rho(\mathbf{x}')}{|\mathbf{x}-\mathbf{x}'|}\right)d\mathbf{x}' \,. \tag{2.9}$$

It shows that the sum of the total terrain effect of topography and the terrain correction is the terrain effect of the Bouguer plate.

By moving the zero horizontal plane to the computation point, P, in (2.7), the terrain correction can also be written as

$$\begin{aligned}\delta\Gamma_{jk}^{TC} &= -G\iint_{A\_above} \int_0^{h-h_p} \frac{\partial^2}{\partial x_j \partial x_k}\left(\frac{\rho(\mathbf{x}')}{|\mathbf{x}-\mathbf{x}'|}\right)d\mathbf{x}' + G\iint_{A\_below} \int_{h-h_p}^{0} \frac{\partial^2}{\partial x_j \partial x_k}\left(\frac{\rho(\mathbf{x}')}{|\mathbf{x}-\mathbf{x}'|}\right)d\mathbf{x}' \\ &= -G\iint_{A\_above} \int_0^{h-h_p} \frac{\partial^2}{\partial x_j \partial x_k}\left(\frac{\rho(\mathbf{x}')}{|\mathbf{x}-\mathbf{x}'|}\right)d\mathbf{x}' - G\iint_{A\_below} \int_0^{h-h_p} \frac{\partial^2}{\partial x_j \partial x_k}\left(\frac{\rho(\mathbf{x}')}{|\mathbf{x}-\mathbf{x}'|}\right)d\mathbf{x}' \\ &= -G\iint_A \int_0^{h-h_p} \frac{\partial^2}{\partial x_j \partial x_k}\left(\frac{\rho(\mathbf{x}')}{|\mathbf{x}-\mathbf{x}'|}\right)d\mathbf{x}'\end{aligned} \tag{2.10}$$

The corresponding residual terrain effect is the negative of terrain correction (2.10), which can also be written as

$$\delta\Gamma_{jk} = G\iint_A \int_0^{h-h_p} \frac{\partial^2}{\partial x_j \partial x_k}\left(\frac{\rho(\mathbf{x}')}{|\mathbf{x}-\mathbf{x}'|}\right)d\mathbf{x}' \tag{2.11}$$

2.2 The Extent of DEM for Terrain Correction

The terrain effects are frequently decomposed into the effects of Bouguer plate and the terrain corrections in order to simplify the computations (Sjöberg, 2009).The model and the method of terrain correction computation for gravitation were well discussed in the literature, e.g. Forsberg (1984), Li and Sideris (1994), Nahavandchi and Sjöberg (1998) and Tsoulis (2001). With the application of airborne gravity gradiometry, the terrain corrections for the gradients were also discussed, e.g. Chinnery (1961), Chen and Macnae (1997), Dransfield and Walker (2005), Kass and Li (2008). In general, the computation method depends on the discrete representation of the topography. If the topography surface is modeled by specific, discrete height data, the topography can be modeled using concentric compartments and the terrain correction can be computed using the direct integral method (Mueller, 1964). More commonly, the topography is modeled by regular, equally spaced data, which then may be represented by many right rectangular prisms (Nagy, 1966), or polyhedrons (Paul, 1974). Thus the terrain correction can be

computed by summing up the gravitational effects due to all the right rectangular prisms, or polyhedrons, where the effects are closed analytic formulas. Alternatively, for large DEM (Digital Elevation Model) data grids, the Fast Fourier Transform method can be applied to speed up the computation. However, this method assumes that the data are periodic (period equal to the extent of the data) and that they are given with equal spacing. Also it has the limitation that the computation points need to be at a plane of constant height. Most representative in this respect are the algorithms of Parker (1972) and Forsberg (1985).

Many papers in the literature discuss these methods and the efficiency of computing the terrain correction based on different models and DEM data; however, few papers touch on the question: What is the extent of terrain needed for the desired accuracy of the correction? There is no consistent conclusion that can be found in the literature and each extent of terrain defined by investigators was based on their particular applications. For example, for the terrain correction on gravitation, Hammer (1939) took 21.944 km, whereas, Bullard (1936) went out to $1\frac{1}{2}^{o}$ or a distance of 166.735 km using tables by Cassinis et al. (1937). The complete Bouguer reduction includes the simple Bouguer slab correction (Bullard A), a curvature correction (Bullard B) and the terrain correction (Bullard C). The effect of an infinite Bouguer slab with the curvature correction equals the effect of a spherical cap with a surface radius of 166.735 km. It is hard to know otherwise from the literature why people choose 166.735 km as the surface radius of the spherical cap. Lafehr (1991) derived an exact solution for the gravity curvature correction as

$$BB = 2\pi G\rho\left\{h(-\eta+\frac{\eta^2}{3})-\frac{R}{3}\left[\begin{array}{l}(\delta^2-2+\delta\cos\alpha+3\cos^2\alpha)\sqrt{(\cos\alpha-\delta)^2+\sin^2\alpha}\\-6\cos^2\alpha\sin(\alpha/2)+4\sin^3(\alpha/2)\\-3\sin^2\alpha\cos\alpha\log_e\dfrac{2(\sin(\alpha/2)-\sin^2(\alpha/2))}{\cos\alpha-\delta+\sqrt{(\cos\alpha-\delta)^2+\sin^2\alpha}}\end{array}\right]\right\}$$

where $\delta = R_0 / R$ and $\eta = h/R$; $R = R_0 + h$, h is the elevation of the station , but measured from the station to R_0 (sea level); $\alpha = \frac{S}{R_0}$, S is the spherical surface distance.

He also pointed out that the 166.735 km radius (which is the outer radius of the Hayford-Bowie Zone O) is based on minimizing the difference between the effect of the cap and that of an infinite horizontal slab for a significant range of elevations between sea level

and about 4000 meters. Based on the terrain correction normally extended to a distance of 166.735 km, Nowell (1999) refined the process of terrain correction for the effects of height, nearby terrain or buildings, including correction ns for the sea or the lake bed instead of to the water surface and for the masses of water, as well as stations above and below ground level. More recently, Danes (1982) noted that 52.6 km is much further than most investigations would carry their terrain corrections. Chen and Macnae (1997) computed terrain corrections for airborne gravity gradiometer data using a 10 m resolution DEM with the extent of 10 km by 5 km for detecting an orebody of 100 m by 100 m by 100 m, located at 50 m beneath the surface.

Li and Sideris (1994) show that the limitation of the integration cap size to 100 km by 100 km results in a geoid undulation bias with an RMS of 10 cm compared with the extent of integration cap size of 600 km by 600 km. Comparing to literature papers which discuss the terrain correction extent for the gravimetry, there are fewer papers that discuss the terrain correction extent for gravity gradiometry. Kass and Li (2008) determined the minimum required spatial extent for a terrain correction of each gradient component to achieve 1 (Eötvös) RMS error. For example, for the T_{zz} component, the stated required radius of included terrain as a function of terrain relief should be $8.49 \times$ h, where h is the height of terrain relief which is a synthesized Gaussian-type terrain with slop of 45 degree. With the fast development of gravity gradiometry and the improving accuracy of the gradiometer instruments in recent years, the required extent of terrain corrections should be revisited in order to make efficient and correct utilization of gravity gradiometry.

Sprenke (1989) also devised a method for optimizing the distance to which terrain corrections are made based on a geostatistical analysis of the topography around a given area. Sprenke simulated the topography based on the geostatistics derived from a profile representative of the actual terrain. First, with the assumption of stationary and isotropic variability of elevations, the elevation Z_H of a radial zone centered on a station can be expressed as $Z_H = \left(\frac{c(r)}{\sigma^2}\right) Z_0 + \left(1 - \frac{c(r)}{\sigma^2}\right) Z_R$, where Z_0 is the station elevation, Z_R is the mean regional elevation; $c(r)$ is the covariance function, r is the mean radius of the zone and σ^2 is the variance of the elevations in the region. The detailed derivations can be found in Journel and Huijbregts (1978). Next, with the assumption of uniform distribution of elevation, the elevations in any subarea of the radial zone are evenly distributed between the lowest and highest elevation. Sprenke did his computation in the space domain using direct numerical integration with a maximum radius of the area equal

to the standard extent of 167 km. The necessary extent of the terrain correction for the gravity was derived from the criterion that the error should be smaller than the gravity accuracy of 0.1, 0.5, 1.0 and 1.5 mGal.

In this chapter, our object is to solve for the extent of terrain correction for gravity gradiometry. First, we develop our method to compute the terrain correction for gravity gradients in the spectral domain and compare this with other methods which are commonly used for, such as numerical integration and right rectangular prism methods. Next, we apply the truncation theory to our method for the purpose of computing the error in the terrain correction of gravity gradients due to neglecting the terrain beyond a certain extent. Through a statistical analysis of the truncation error, we can find the functional relationship between the variance of the error and the extent of the terrain correction. For the general application, we can set up a criterion that the variance of truncation error should be smaller than that of the instrument error, and this makes sure that the terrain correction under such an extent is enough and necessary considering the accuracy of our instrument for gravity gradiometry.

We also simulate the topography based on the stationary and isotropic properties of the topography, but our high frequency part of topography is simulated based on the empirical PSD (Power Spectral Density) of the given data, which contains relatively lower frequency, and making use of power-law extension in the frequency domain. Sprenke (1989) computed the terrain correction only for the gravity using the analytical formula in the space domain. The variance of the truncation error of the terrain correction is computed based on the simulated topography whose statistics come from a profile representative of the region. However, we compute the variance of truncation error (or variance of truncation error difference) for terrain correction of gravitational gradients through the FFT method in the frequency domain. The details about the topography simulation and extent determination are given in Chapters 3 and 4. Our method of extent determination is more general and can be applied to different observations, such as ground, airborne, and space gravity gradiometry. For the latter, the effect of total topographic mass above the geoid or residual topographic mass relative to a spherical Bouguer layer is computed at Earth's surface or at satellite altitude using the spherical coordinates (Martinec, 1998). By truncating the spherical integral limits as well as the spherical harmonic expression of topography data, the truncation error and its variance can also be computed and used to determine the extent of total topography or residual topography. This part is outside the scope of the present dissertation due to the time limitation and will be left for future research. Our computations are strictly for the planar approximation and Cartesian coordinates, which may be applied to ground and airborne data. For ground data, we compute the terrain correction using the residual terrain; for airborne data, we compute the total terrain effect since the observation point is usually

above all the terrain; and also this is consistent with the procedures implemented by Bell Geospace for their airborne gradiometer survey.

2.2.1 Terrain correction computation methods

For general gravimetric applications (gravity or gravity gradient measurements), we define the terrain correction as the appropriate gravitational effect due to the removal of masses above the plane of computation point, and the addition of masses below the plane in order to create a Bouguer plate. The removal of the mass corresponds to an effect with negative sign of the density; while adding mass below corresponds to a positive sign for the density. Thus the terrain correction can be interpreted as a gravitational effect due to negative density above the plane and positive density below the plane (see Figure 2.1).

For very local observations, we define the residual terrain relative to a point, P, on the Earth's surface as the difference between the actual elevation and the Bouguer plate through the point. More generally, for regional applications, we may also consider a higher-order reference topography instead of the Bouguer plate. For example, the reference topography can be high-degree harmonic expansion of the terrain, such as a global 5' × 5' Digital Topographic Model (DTM2006.0) with spherical harmonic expansion (to harmonic degree 2160) of Earth's topography and it is made available by the EGM2008 development team (Pavlis et al. 2007). DTM2006.0 relies heavily on elevation information made available from the Shuttle Radar Topography Mission (SRTM) and some other data sources, such as laser altimeter data over Greenland and Antarctica, and data of DTM2002 which includes bathymetry from altimetry data and ship depth soundings of Smith and Sandwell (1997). The residual topography model between SRTM and DTM2006.0 can be used to augment EGM2008 vertical deflection predictions and also for source-modeling of high-frequency gravity field signals. For example, Hirt et al. (2010) combined EGM2008 and SRTM/DTM2006.0 residual terrain model data to improve the quasigeoid computations in mountainous areas. For our regional terrain correction computations, we can set our reference using the mean elevation of the terrain, or using a higher-order reference surface such as DTM2006.0. The residual terrain in this case bounds the masses that are removed and added between the higher order reference surface and the actual topographic surface (Figure 2.2).

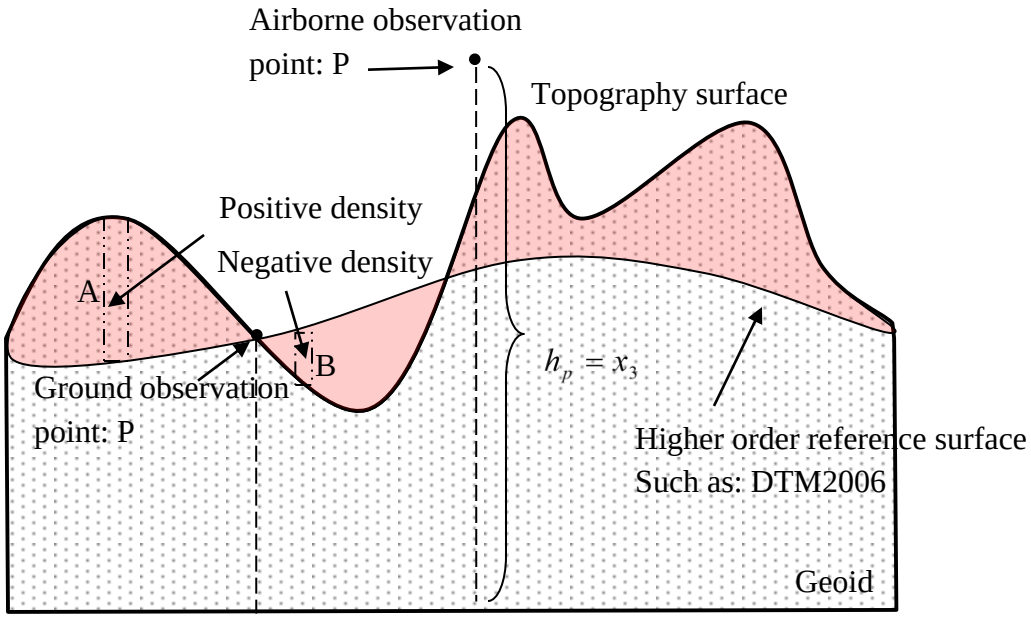

Figure 2.2 Terrain effect of topography (dotted area) and terrain correction of residual terrain (red area) w.r.t higher order reference surface

i. Right rectangular prisms for terrain corrections of ground data

One common method to compute the terrain correction and terrain effect is to represent the mass between the topography surface and the geoid (in planar approximation) using right rectangular prisms. The assumption of planar approximation is appropriate since for our local gradiometry application, the gravity gradient signal is presumed to be a very local phenomenon. We set up our coordinate system using the East-North-Up coordinate system and the x-o-y plane is the reference plane passing through observation point, P. For a topographic height above the reference plane, it is modeled by a negative density prism; for a topographic height below the reference plane, it is a positive density prism (Figure 2.3). The terrain correction can be computed by summing up the effect results of all $N \times M$ prisms around the point, P, if the topographic surface height is measured at $N \times M$ discrete points (equal spacing: length a along the x_1 direction; width b along the x_2 direction), where N is the number of heights along x_1; and M is the number of heights along x_2.

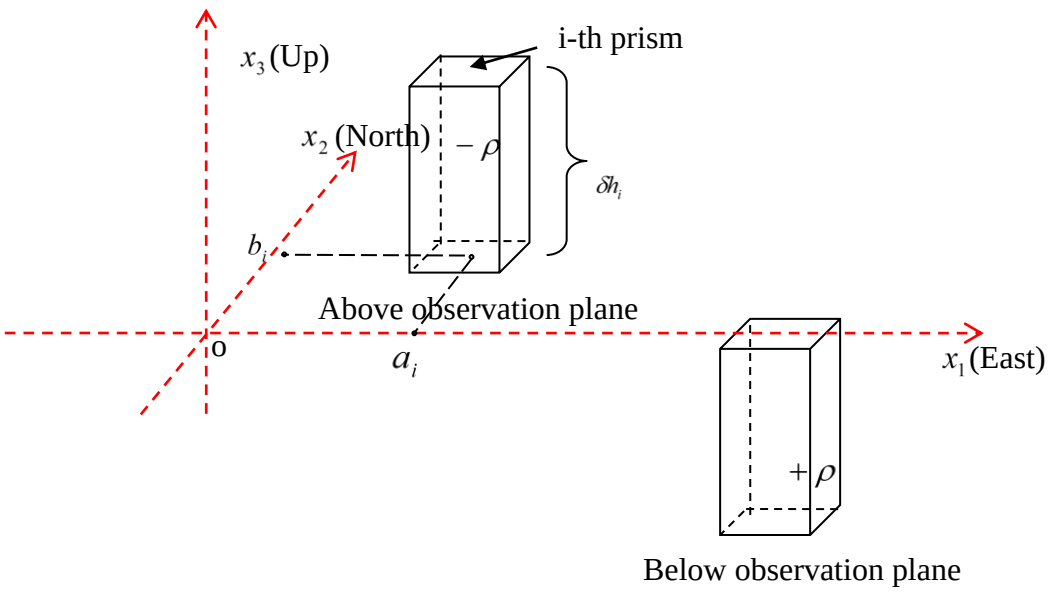

Figure 2.3 Coordinate System for residual terrain

The assumption of constant density was applied to the residual terrain. Then the terrain correction of gradients for the i-th prism element (length: a , width: b , height: $\delta h_i = h_i - h_p$, the center point coordinates (a_i, b_i)) either above (δh_i positive) or below (δh_i negative) the reference plane, can be derived from (2.6) , respectively (j=1,2,3; k=1,2,3)

$$\delta\Gamma_{jk}^{i}(x_1,x_2,0) = -G\rho \int_{a_i-a/2}^{a_i+a/2}\int_{b_i-b/2}^{b_i+b/2}\int_{0}^{\delta h_i} \frac{\partial^2}{\partial x_j \partial x_k}\frac{1}{r} dx_1' dx_2' dx_3', \tag{2.11}$$

It can be shown that the integral of (2.11) for in-line and cross gradients (Zhu, 2007; Jekeli and Zhu, 2006), is given by

$$\delta\Gamma_{jj}^{i}(x_1,x_2,0) = -G\rho \tan^{-1}\frac{(x_k - x_k')(x_l - x_l')}{(x_j - x_j')r}\Bigg|_{x_1'=a_i-a/2}^{a_i+a/2}\Bigg|_{x_2'=b_i-b/2}^{b_i+b/2}\Bigg|_{x_3'=0}^{\delta h_i}, \tag{2.12}$$

$$\delta\Gamma_{jk}^{i}(x_1,x_2,0) = G\rho \ln(x_l - x_l' + r)\Big|_{x_1'=a_i-a/2}^{a_i+a/2}\Big|_{x_2'=b_i-b/2}^{b_i+b/2}\Big|_{x_3'=0}^{\delta h_i}. \tag{2.13}$$

where in each case, the index set, $\{j,k,l\}$, is a cyclic permutation of $\{1,2,3\}$ and $x_3 = 0$.

If the terrain height is measured on a regular grid (equal spacing), with a total of N×M points, then the terrain correction can be computed by summing up all these N×M prisms using

$$\delta\Gamma_{jj}^{TC}(x_1,x_2,0)=\sum_{i=1}^{N\times M}\delta\Gamma_{jj}^{i}=-G\rho\sum_{i=1}^{N\times M}\tan^{-1}\frac{(x_k-x_k^{'})(x_l-x_l^{'})}{(x_j-x_j^{'})r}\Bigg|_{x_1^{'}=a_i-a/2}^{a_i+a/2}\Bigg|_{x_2^{'}=b_i-b/2}^{b_i+b/2}\Bigg|_{x_3^{'}=0}^{\delta h_i}, \qquad (2.14)$$

$$\delta\Gamma_{jk}^{TC}(x_1,x_2,0)=\sum_{i=1}^{N\times M}\delta\Gamma_{jk}^{i}=G\rho\sum_{i=1}^{N\times M}\ln(x_l-x_l^{'}+r)\Big|_{x_1^{'}=a_i-a/2}^{a_i+a/2}\Bigg|_{x_2^{'}=b_i-b/2}^{b_i+b/2}\Bigg|_{x_3^{'}=0}^{\delta h_i}. \qquad (2.15)$$

where $r=\sqrt{(x_1-x_1^{'})^2+(x_2-x_2^{'})^2+(x_3^{'})^2}$ (2.16)

and ρ is the constant density of topography;

a and b are spacing of the regular grid in two directions, x_1 and x_2;

$\delta h_i=h_i-h_p$ is the residual terrain height with respect to reference plane passing through observation point, h_p;

N and M are the number of grid points in two directions, x_1 and x_2.

ii. Right rectangular prisms for terrain effect of airborne data

For the case of airborne gravity gradiometry, when the point of computation is not on the topographic surface, we compute the terrain effect (See figure 2.4, the $x_3=0$ plane is the approximately planar geoid) as we mentioned at the end of chapter 2.2.0. From equation (2.6), for the i-th prism, we have

$$\Gamma_{jk}^{i}=G\rho\int_{a_i-a/2}^{a_i+a/2}\int_{b_i-b/2}^{b_i+b/2}\int_{0}^{h_i}\frac{\partial^2}{\partial x_j\partial x_k}\frac{1}{r}dx_1^{'}dx_2^{'}dx_3^{'} \qquad (2.17)$$

Applying the same derivation as for the ground data; we have the terrain effect for the gravitational gradients as

$$\Gamma_{jj}(x_1,x_2,x_3)=\sum_{i=1}^{N\times M}\Gamma_{jj}^{i}=G\rho\sum_{i=1}^{N\times M}\tan^{-1}\frac{(x_k-x_k^{'})(x_l-x_l^{'})}{(x_j-x_j^{'})r}\Bigg|_{x_1^{'}=a_i-a/2}^{a_i+a/2}\Bigg|_{x_2^{'}=b_i-b/2}^{b_i+b/2}\Bigg|_{x_3^{'}=0}^{h_i} \qquad (2.18)$$

$$\Gamma_{jk}(x_1, x_2, x_3) = \sum_{i=1}^{N\times M} \Gamma_{jk}^{i} = -G\rho \sum_{i=1}^{N\times M} \ln(x_l - x_l^{'} + r)\Big|_{x_1^{'}=a_i-a/2}^{a_i+a/2} \Big|_{x_2^{'}=b_i-b/2}^{b_i+b/2} \Big|_{x_3^{'}=0}^{h_i} \tag{2.19}$$

where $r = \sqrt{(x_1 - x_1^{'})^2 + (x_2 - x_2^{'})^2 + (x_3 - x_3^{'})^2}$ (2.20)

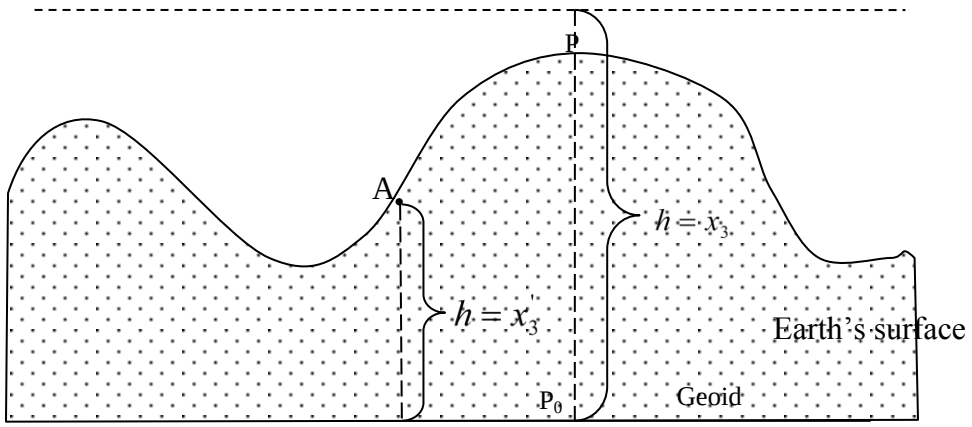

Figure 2.4 Terrain effect for airborne data

For ground observations, we separate the total terrain effect into the Bouguer plate part and the residual terrain part. The terrain correction is computed based on the residual terrain. The formula of Bouguer plate is derived from an infinite plate, for example, $-2\pi G\rho h_p$ for the vertical gravity component; zero for horizontal gravity components.

For airborne observations, we can separate the topography into the residual terrain relative to the mean elevation of the area and the Bouguer plate passing through the mean elevation; also we can use the minimum or maximum elevation of the topography as reference plane. Thus, the vertical gravitational component still is a constant and the horizontal components are zero for such an infinite Bouguer plate. Furthermore, we can even define the residual terrain relative to the higher order reference surface. For this case, the vertical and horizontal gravitational components of the mass between the reference surface and the geoid are complicated, and do not have analytical formulas. For the actual application, our DEM data area is always finite, which will cause the computed effect of the Bouguer plate to be not exactly equal to the analytical value, especially for observation points at the edge of the area. Thus, an error will be included in the total topography effect for a given observation point. In our statistical method, we determine the extent of topography by the variance of the truncation error for observation point, and the observation point is always at the center of the computation area, so this Bouguer plate effect error will not affect our comparison results since it is the same for all

truncation values. It is also noted that x_3 is the height of the observation point and it is not necessary to be constant.

iii. FFT method for ground data

The potential of the residual terrain can be written as

$$\delta V(\mathbf{x}) = G\rho \iint_A \int_0^{h-h_p} \frac{1}{|\mathbf{x}-\mathbf{x}'|} d\mathbf{x}' \tag{2.21}$$

where $\delta h = h - h_p$. (2.22)

Substituting (2.21) into (2.3), we have the following integrals for the residual terrain effect on the gradients evaluated on the reference plane passing through observation point, P, such that $x_3 = 0$:

$$\delta\Gamma_{jk}(\mathbf{x}) = G\rho \iint_A \int_0^{\delta h} \left[\frac{\partial^2}{\partial x_j \partial x_k} \left(\frac{1}{|\mathbf{x}-\mathbf{x}'|} \right) \right]_{x_3=0} d\mathbf{x}' \tag{2.23}$$

Furthermore, (2.23) can be written as

$$\delta\Gamma_{jk}(\mathbf{x}) = G\rho \iint_A \int_0^{\delta h(x_1', x_2')} F_{jk} dx_3' dA \tag{2.24}$$

where $dA = dx_1' dx_2'$; and with

$$|\mathbf{x}-\mathbf{x}'| = r = \sqrt{(x_1 - x_1')^2 + (x_2 - x_2')^2 + (0 - x_3')^2}\,, \tag{2.25}$$

we have

$$\begin{aligned} F_{11} &= -\frac{1}{r^3} + \frac{3(x_1 - x_1')^2}{r^5} & F_{12} &= \frac{3(x_1 - x_1')(x_2 - x_2')}{r^5} & F_{13} &= -\frac{3(x_1 - x_1')(x_3')}{r^5} \\ & & F_{22} &= -\frac{1}{r^3} + \frac{3(x_2 - x_2')^2}{r^5} & F_{23} &= -\frac{3(x_2 - x_2')(x_3')}{r^5} \\ & & & & F_{33} &= -\frac{1}{r^3} + \frac{3(x_3')^2}{r^5} \end{aligned} \tag{2.26}$$

with $F_{jk} = F_{kj}$.

The integrals of F_{jk} with respect to x_3' can be derived using a variable change, and result in (Jekeli and Zhu, 2006, with $x_3 = 0$):

$$T_{11}=\begin{cases}-\dfrac{1}{2(x_3^{'})^2}\Big|_{x_3^{'}=0}^{\delta h}, & \mathrm{s}=0\\ \dfrac{1}{\mathrm{s}^4}((s^2-3(x_1-x_1^{'})^2)\dfrac{(-x_3^{'})}{r}+\dfrac{(x_1-x_1^{'})^2(-x_3^{'})^3}{r^3})\Big|_{x_3^{'}=0}^{\delta h}, & \mathrm{s}\neq 0\end{cases}$$

$$T_{12}=\begin{cases}0, & \mathrm{s}=0\\ \dfrac{(x_1-x_1^{'})(x_2-x_2^{'})}{\mathrm{s}^4}(\dfrac{(-x_3^{'})^3}{r^3}-\dfrac{3(-x_3^{'})}{r})\Big|_{x_3^{'}=0}^{\delta h}, & \mathrm{s}\neq 0\end{cases}$$

$$T_{13}=\frac{x_1-x_1^{'}}{r^3}\Big|_{x_3^{'}=0}^{\delta h}$$

$$T_{22}=\begin{cases}-\dfrac{1}{2(0-x_3^{'})^2}\Big|_{x_3^{'}=0}^{\delta h}, & \mathrm{s}=0\\ \dfrac{1}{\mathrm{s}^4}((s^2-3(x_2-x_2^{'})^2)\dfrac{(-x_3^{'})}{r}+\dfrac{(x_2-x_2^{'})^2(-x_3^{'})^3}{r^3})\Big|_{x_3^{'}=0}^{\delta h}, & \mathrm{s}\neq 0\end{cases}$$

$$T_{23}=\frac{x_2-x_2^{'}}{r^3}\Big|_{x_3^{'}=0}^{\delta h}$$

$$T_{33}=\begin{cases}-\dfrac{1}{(-x_3^{'})^2}\Big|_{x_3^{'}=0}^{\delta h}, & \mathrm{s}=0\\ \dfrac{1}{\mathrm{s}^2}(\dfrac{(-x_3^{'})}{r}-\dfrac{(-x_3^{'})^3}{r^3})\Big|_{x_3^{'}=0}^{\delta h}, & \mathrm{s}\neq 0\end{cases} \tag{2.27}$$

where $s^2=(x_1-x_1^{'})^2+(x_2-x_2^{'})^2$.

Thus $\delta\Gamma_{jk}(\mathbf{x})$ can be computed by using a numerical method of integration, such as the rectangular rule, which approximates eq. (2.24) according to: $\delta\Gamma_{jk}(\mathbf{x})=G\rho\sum_i T_{jk}\Delta A_i$, where for a regular rectangular grid, $\Delta A_i=\Delta x_1^{'}\Delta x_2^{'}$. However, when dealing with a large amount of data on a regular grid, the FFT method can be applied to reduce the computation time.

By following Forsberg's method (Forsberg, 1985), the terrain effect integrals can be expanded into series of convolutions and the convolution can be computed very quickly in the frequency domain by using the convolution theorem. The convolution theorem (Wikipedia, http://en.wikipedia.org/wiki/Convolution_theorem) states that if the signals g and h are finite energy signals, then the Fourier transform of a convolution is the pointwise product of Fourier transforms. The 2-D convolution is defined as

$$c(x_1, x_2) = g(x_1, x_2) * h(x_1, x_2) = \iint_A g(x_1 - x_1', x_2 - x_2') h(x_1', x_2') dx_1' dx_2' \tag{2.28}$$

From the convolution theorem, we have

$$C(f_1, f_2) = \Im(g * h) = \Im(g) \cdot \Im(h) = G(f_1, f_2) H(f_1, f_2) \tag{2.29}$$

and

$$c = g * h = \Im^{-1}(\Im(g) \cdot \Im(h)) \tag{2.30}$$

where

* denotes the convolution operator, (f_1, f_2) is the horizontal frequency pair;

$\Im$ denotes the Fourier transform and $\Im^{-1}$ denotes the inverse Fourier transform;
C, G, H are Fourier transform of c, g, h, respectively.

We expand the functions, $F_{jk}(x_3')$ in equations (2.26) into Taylor series, with respect to zero (corresponding to the reference plane of the residual terrain):

$$F_{jk}\left(x'_3\right) = F_{jk}\left(0\right) + F_{jk}'\left(0\right) x_3' + \cdots + \frac{1}{n!} F_{jk}^{(n)}\left(0\right)\left(x_3'\right)^n + \cdots \tag{2.31}$$

Then, we substitute these into equation (2.24) and integrate with respect to x_3':

$$\delta\Gamma_{jk}\left(\boldsymbol{x}\right) = G\rho \iint_A \left(F_{jk}(0) \cdot \delta h + \frac{1}{2!} F_{jk}'\left(0\right) \delta h^2 + \cdots + \frac{1}{(n+1)!} F_{jk}^{(n)}\left(0\right) \delta h^{n+1} + \cdots \right) dA \tag{2.32}$$

The derivatives of F_{jk} are taken with respect to x_3' and evaluated at $x_3' = 0$.

They are easily derived, for example, for F_{33}:

$$F_{33}(0) = -\frac{1}{s^3},\ F_{33}'(0) = 0,\ F_{33}''(0) = \frac{9}{s^5},\ F_{33}^{(3)}(0) = 0,\ F_{33}^{(4)}(0) = -\frac{225}{s^7} \tag{2.33}$$

When using the FFT method to compute the terrain effect for ground observation positions, the heights of the computation points is not constant, $h_p = h(x_p, y_p) \neq \text{constant}$, i.e., substitute $\delta h = h - h(x_p.y_p)$ into (2.32), we have

$$\begin{aligned}
\delta\Gamma_{jk}(\mathbf{x}) &= G\rho\iint_A (F_{jk}(0)\cdot(h(x',y') - h(x_p,y_p)) + \frac{1}{2!}F'_{jk}(0)\cdot(h(x',y') - h(x_p,y_p))^2 + \cdots)dA \\
&= G\rho\iint_A \begin{bmatrix} F_{jk}(0)\cdot h(x',y') - F'_{jk}(0)h(x',y')h(x_p,y_p) + \frac{1}{2}F'_{jk}(0)\cdot h^2(x',y') \\ -F_{jk}(0)\cdot h(x_p,y_p) + \frac{1}{2}F'_{jk}(0)\cdot h^2(x_p,y_p) + \cdots \end{bmatrix} dA \\
&= G\rho\begin{bmatrix} F_{jk}(0) * h(x_p,y_p) - h(x_p,y_p)\cdot F'_{jk}(0) * h(x_p,y_p) + \frac{1}{2}F'_{jk}(0) * h^2(x_p,y_p) \\ -h(x_p,y_p)\cdot\Im(F_{jk})(0,0) + \frac{1}{2}h^2(x_p,y_p)\cdot\Im(F'_{jk})(0,0) + \cdots \end{bmatrix}
\end{aligned} \tag{2.34}$$

where $\Im(F_{jk})(0,0)$, $\Im(F'_{jk})(0,0)$ are values at zero frequency of the Fourier transforms of F_{jk}, F'_{jk}, respectively.

We neglect the terms in the Taylor expansion (2.32) for derivative orders higher than one (the loss of the accuracy is acceptable for our application of extent determination, see chapter 4.2 analysis), thus (2.34) can be expressed as

$$\delta\Gamma_{jk}(\mathbf{x}) = G\rho[F_{jk}(0) * h - h_p\cdot F'_{jk}(0) * h + \frac{1}{2!}F'_{jk}(0) * h^2 - h_p\cdot\Im(F_{jk})(0,0) + \frac{1}{2}h_p^2\cdot\Im(F'_{jk})(0,0)] \tag{2.35}$$

Next, we use $\delta\Gamma_{33}$ as an example to illustrate how to compute (2.35) for discrete data. The terrain correction for the other gradients can be computed similarly.
We substitute (2.33) into (2.35), and apply the convolution theorem, we have

$$\delta\Gamma_{33}(\mathbf{x}) = G\rho\{\Im^{-1}[\Im(F_{33})\cdot\Im(h)] - h_p\cdot\Im(F_{33})(0,0)\} \tag{2.36}$$

where $\Im(F_{33})(0,0)$ is value at zero frequency of of the Fourier transform of F_{33}.

A numerical implementation of equation (2.36) requires using the discrete Fourier transform, or equivalently the Fast Fourier Transform (FFT). This transform operates only on discrete and periodic functions. Let g_{m_1,m_2} and h_{m_1,m_2} be the discrete kernel

function F_{33} and the terrain elevation on a regularly spaced grid, respectively. The FFT and its inverse are defined as follows:

(with $m_1, p_1, n_1 = 0, \cdots, N-1; m_2, p_2, n_2 = 0, \cdots, M-1$):

$$FFT(g_{m_1,m_2}) = G_{p_1,p_2} = \Delta x_1^{'} \Delta x_2^{'} \sum_{m_1=0}^{N-1} \sum_{m_2=0}^{M-1} g_{m_1,m_2} e^{-i2\pi(\frac{p_1 m_1}{N} + \frac{p_2 m_2}{M})} \tag{2.37}$$

$$FFT^{-1}(G_{p_1,p_2}) = g_{m_1,m_2} = \frac{1}{N\Delta x_1^{'} M \Delta x_2^{'}} \sum_{p_1=0}^{N-1} \sum_{p_2=0}^{M-1} G_{p_1,p_2} e^{i2\pi(\frac{p_1 m_1}{N} + \frac{p_2 m_2}{M})} \tag{2.38}$$

The discrete convolution of g_{m_1,m_2} and h_{m_1,m_2} is defined as

$$c_{n_1,n_2} = \sum_{m_1=0}^{N-1} \sum_{m_2=0}^{M-1} g_{m_1-n_1,m_2-n_2} h_{m_1,m_2} \Delta x_1^{'} \Delta x_2^{'} . \tag{2.39}$$

and the convolution theorem yields:

$$c_{m_1,m_2} = FFT^{-1}(FFT(g)_{p_1,p_2} FFT(h)_{p_1,p_2}) . \tag{2.40}$$

Thus the numerical equivalent of eq.(2.36) is

$$\delta\Gamma_{33}(n_1,n_2) = G\rho\{FFT^{-1}\left(FFT(F_{33})_{p_1,p_2} FFT(h)_{p_1,p_2}\right)_{n_1,n_2} - h_{n_1,n_2} FFT(F_{33})_{0,0}\} . \tag{2.41}$$

It is noted that the terrain effect computed here is for every observation point on the topographic surface and so the observation point's height, h_{n_{11},n_2}, is not constant. In other words, the reference plane of the residual terrain which passes through the observation point is changing for every observation point. However, the convolution theorem is applied only to the convolutions of the total topographic height.

Also from equation (2.9), we know the gravitational gradients of the Bouguer plate can be computed as $\Gamma_{jk}^{Bouguer} = G\iint_A \int_0^{h_p} \frac{\partial^2}{\partial x_j \partial x_k}\left(\frac{\rho(\mathbf{x}')}{|\mathbf{x}-\mathbf{x}'|}\right) d\mathbf{x}'$. For an infinite Bouguer plate, the gravitational gradients should be zero since the vertical component of gravitational acceleration for a Bouguer plate is constant: $-2\pi G\rho h_p$, while the horizontal components of gravitational acceleration for a Bouguer plate are zero. Actually, if we do the computations for a finite area using prisms (formulas (2.12) and (2.13)) for the total effect, then the gravitational gradients are not exactly zero. And the gravitational

gradients of the finite Bouguer plate will not only be non-zero but also they are different for each observation point since each observation point has a different elevation height. Thus when we want to do the Bouguer reduction, each observation point needs to remove its corresponding gravitational gradients of Bouguer plates. Also as we mentioned previously for the right rectangular prism method, the finite Bouguer plate errors can not be neglected, but it can be neglected since our statistical method always does the computation for a center point. Also we determine the extent of topography based on the variance of the truncation error using the residual terrain before the Bouguer plate correction is involved, i.e., the finite Bouguer plate error will affect the total topography effect but not affect our extent determination.

iv. FFT method for airborne data

When dealing with airborne gravity gradient data, we compute the terrain effect for the topography above the geoid (see figure 2.4). Tziavos et al. (1988) computes the terrain effect for airborne gravity and gradiometry using the residual terrain referring to the reference plane which is the average height of the topography in the area. Thus their total terrain effect is the sum of the gravitational effect of a Bouguer plate associated with the average height of the topography and the effect of the residual terrain relative to that height. The advantage of using an average height is faster convergence of their binomial series expansion comparing to the series expansion with respect to the zero plane, as done by Sideris (1984). Here, we do not separate the topography into a Bouguer plate plus the residual terrain in order to make our results consistent with the terrain effect computed by Bell Geospace at Vinton Dome, LA and Parkfield, CA.

The residual height δh in (2.21), (2.22), (2.23), (2.24), (2.32) should be changed to topographic height, h, which will result in

$$V(\mathbf{x}) = G\rho \iint_A \int_0^h \frac{1}{|\mathbf{x}-\mathbf{x}'|} d\mathbf{x}' \tag{2.42}$$

$$\Gamma_{jk}(\mathbf{x}) = G\rho \iint_A \int_0^h \frac{\partial^2}{\partial x_j \partial x_k}\left(\frac{1}{|\mathbf{x}-\mathbf{x}'|}\right) d\mathbf{x}' \tag{2.43}$$

$$\Gamma_{jk}(\mathbf{x}) = G\rho \iint_A \int_0^{h(x_1',x_2')} F_{jk}\, dx_3' dA \tag{2.44}$$

$$\text{where } |\mathbf{x}-\mathbf{x}'| = r = \sqrt{(x_1-x_1')^2 + (x_2-x_2')^2 + (x_3-x_3')^2}\,, \tag{2.45}$$

and

$$F_{11} = -\frac{1}{r^3} + \frac{3(x_1 - x_1')^2}{r^5} \quad F_{12} = \frac{3(x_1 - x_1')(x_2 - x_2')}{r^5} \quad F_{13} = \frac{3(x_1 - x_1')(x_3 - x_3')}{r^5}$$
$$F_{22} = -\frac{1}{r^3} + \frac{3(x_2 - x_2')^2}{r^5} \quad F_{23} = \frac{3(x_2 - x_2')(x_3 - x_3')}{r^5} \tag{2.46}$$
$$F_{33} = -\frac{1}{r^3} + \frac{3(x_3 - x_3')^2}{r^5}$$

with $F_{jk} = F_{kj}$.

Similar to the derivation for the residual terrain of ground data, the functions, $F_{jk}(x_3^{'})$ were expanded into Taylor series and after the integration with respect to $x_3^{'}$, it can be expressed as convolution form, provided that $x_3 = \text{constant}$:

$$\Gamma_{jk}(\mathbf{x}) = G\rho \sum_{n=1}^{\infty} \frac{1}{n!} F_{jk}^{(n-1)}(0) * h^n \tag{2.47}$$

Thus the terrain effect of the topography can be derived as

$$\Gamma_{jk}(\mathbf{x}) = G\rho \cdot \Im^{-1} \sum_{n=1}^{\infty} \frac{1}{n!} \Im(F_{jk}^{(n-1)}) \cdot \Im(h^n) \tag{2.48}$$

Here, $F_{jk}^{(n-1)}$ is the (n-1)th derivative of $F_{jk}(x_3^{'})$ and evaluated at $x_3^{'} = 0$, however $x_3 \neq 0$ but it should be constant.

They are easily derived, for example, for F_{33}:

$$F_{33}(0) = -\frac{1}{r_0^3} + \frac{3x_3^2}{r_0^5}, \; F_{33}^{'}(0) = -\frac{9x_3}{r_0^5} + \frac{15x_3^3}{r_0^7},$$
$$F_{33}^{''}(0) = \frac{9}{r_0^5} - \frac{90x_3^2}{r_0^7} + \frac{105x_3^4}{r_0^9}, F_{33}^{(3)}(0) = \frac{225x_3}{r_0^7} - \frac{1050x_3^3}{r_0^9} + \frac{945x_3^5}{r_0^{11}}, \tag{2.49}$$
$$F_{33}^{(4)}(0) = -\frac{225}{r_0^7} + \frac{4725x_3^2}{r_0^9} - \frac{14175x_3^4}{r_0^{11}} + \frac{10395x_3^6}{r_0^{13}}$$

where $r_0 = \sqrt{(x_1 - x_1^{'})^2 + (x_2 - x_2^{'})^2 + x_3^2}$ (2.50)

We neglect the terms in the Taylor expansion for orders of height higher than one, thus the terrain effect for gradients can be expressed as

$$\Gamma_{jk}(\mathbf{x}) = G\rho \cdot \Im^{-1}[\Im(F_{jk}(0) \cdot \Im(h) + \frac{1}{2}\Im(F_{jk}^{'}(0) \cdot \Im(h^2)] \tag{2.51}$$

where $F_{jk}(0), F_{jk}^{'}(0)$ come from (2.49).

Also, a numerical implementation of equation (2.51) requires using the discrete Fourier transform, or equivalently the Fast Fourier Transform (FFT) which is described in method iii. It should be pointed out that when computing the terrain effect for the airborne observation points, the computation height, x_3 , in equation (2.50) should be constant for all $(x_1^{'}, x_2^{'})$ in order to express equation (2.32) as a series of convolution and such that we can use the FFT technique for fast computations.

v. FFT method combined with right rectangular prism model method

When we expand the kernel functions $F_{jk}(x_3^{'})$ into Taylor series using equation (2.31), we need to be careful about the convergence of the series especially for dense topography grids or in rough areas. Tsoulis (1998) expanded the terrain effect integral for gravity into a binomial series and thus formed the convolution. He also pointed out that the degrees of expansion as well as the convergence condition for the validity of the series affect the final result.

Tsoulis (1998) divided the total terrain effect of the topography into the effect of a Bouguer plate of a height equal to h_p minus the deviation of the actual terrain from this plate, i.e., the terrain correction of the residual terrain. We also applied the same procedure for the gravitational gradients, see equation (2.10). The vertical component of the residual topographic attraction at P is equal to the vertical derivative of equation (2.21),

$$\delta g_z(x_1, x_2, 0) = G\rho \iint_A \int_0^{h(x,y)-h_p} \frac{\partial}{\partial x_3}\left(\frac{1}{|\mathbf{x}-\mathbf{x}'|}\right) d\mathbf{x}' = G\rho \iint_A \int_0^{h(x,y)-h_p} \frac{-x_3^{'}}{|\mathbf{x}-\mathbf{x}'|^3} dx_3^{'} dA\,. \tag{2.52}$$

It is easy to integrate (2.52) with respect to $x_3^{'}$ first and one obtains after a few steps (Tsoulis,1998)

$$\delta g_z(x_1, x_2, 0) = G\rho \iint_A \left(-\frac{1}{|\mathbf{x}-\mathbf{x}'|}\Big|_{x_3^{'}=0}^{h(x,y)-h_p}\right) dA = G\rho \iint_A \left(\frac{1}{s}\left[1-\left[1+\left(\frac{h_p-h}{s}\right)^2\right]^{-1/2}\right]\right) dA \tag{2.53}$$

Let $x = (\frac{h_p - h}{s})^2$, Tsoulis (1998) expands equation (2.53) into a series which involves the convolution by using the binomial expansion of $(1+x)^{-1/2}$ according to

$$(1+x)^{-1/2} = 1 - \frac{1}{2}x + \frac{1\cdot 3}{2\cdot 4}x^2 - \frac{1\cdot 3\cdot 5}{2\cdot 4\cdot 6}x^3 + \cdots \tag{2.54}$$

under the precondition that $-1 < x \le 1$. This convergence condition means the slope of the terrain surrounding the computation point should not exceed 45^0 (Forsberg, 1985; Tsoulis, 1998; Tsoulis, 2001). After substituting (2.54) into (2.53), we have

$$\delta g_z(x_1, x_2, 0) = G\rho \iint_A [\frac{(h_p - h)^2}{2s^3} - \frac{3(h_p - h)^4}{8s^5} + \frac{5(h_p - h)^6}{16s^7} - \cdots] dA \tag{2.55}$$

After expanding the numerators in (2.55) into polynomials, h_p can be moved outside the integral and equation (2.58) can be expressed as a series of convolutions between powers of $\frac{1}{s}$ and powers of h. Thus these convolutions can be computed using the convolution theorem and the FFT methods. When the source point is close to the observation point, the binomial series may not converge, so the FFT method will not give an accurate result. Tsoulis (1998) solved this problem for the gravity terrain correction by combining the FFT method and the right rectangular prism method, thus both the computational efficiency and the accuracy of results are obtained. Tsoulis (2001) proposed a combination method which applied the FFT method to all DEM data except for a small zone surrounding the computation point which, where the analytical right rectangular prism formula was used. He tested this combination method for a DEM area with extent of 15 km by 20 km and resolution of 50 m. His results showed that the combination method overcomes the convergence problem, which will happen for the rough terrain area. At the same time, the results still maintain the computation efficiency of FFT method, while keeping satisfactory agreement with the prism summation method. We also use this combination method to solve our Taylor series converge problem, where the FFT method is applied for the outer area where the series convergence holds; while the prism summation method is applied for inner area.

Studies in the published literature seldom discussed the convergence problem for gradient terrain correction. Their computation using the FFT method starts from the spectrum of the vertical gravitational components, where they assume the convergence problem is solved for the gravity terrain correction, for example, using the method of Tsoulis (1998, 2001). Based on their previous computations for the gravity terrain

correction, Tziavos et al. (1988) also computed the terrain corrections for the gradient tensor using the formulas from (2.56) to (2.61). Since V is a harmonic function and satisfies Laplace's equation, it can be proved (Tziavos et al., 1988) that the spectra of the gradients and the spectrum of the vertical gravitational component have the following relationships

$$\Im(\delta\Gamma_{zx}) = \Im(\delta\Gamma_{xz}) = 2\pi i f_1 \cdot \Im(\delta g_z) \tag{2.56}$$

$$\Im(\delta\Gamma_{zy}) = \Im(\delta\Gamma_{yz}) = 2\pi i f_2 \cdot \Im(\delta g_z) \tag{2.57}$$

$$\Im(\delta\Gamma_{zz}) = 2\pi f \cdot \Im(\delta g_z) \tag{2.58}$$

$$\Im(\delta\Gamma_{xx}) = \frac{-2\pi f_1^{\,2}}{f} \cdot \Im(\delta g_z) \tag{2.59}$$

$$\Im(\delta\Gamma_{xy}) = \Im(\delta\Gamma_{yx}) = \frac{-2\pi f_1 f_2}{f} \cdot \Im(\delta g_z) \tag{2.60}$$

$$\Im(\delta\Gamma_{yy}) = \frac{-2\pi f_2^{\,2}}{f} \cdot \Im(\delta g_z) \tag{2.61}$$

where $f = (f_1^{\,2} + f_2^{\,2})^{1/2}$.

However, we do not use this method to compute the terrain correction for gravitational gradients. Jekeli and Zhu (2006) provide and compare other methods to compute the terrain correction for gravitational. One method is the numerical integration method (see equations (7), (9), (13), (14)); another method is the same as we described in previous section (iv: FFT method for airborne data). But, the convergence problem is not well discussed, so now we solve the convergence problem by using a combination method similar to the method of Tsoulis (1998).

Tsoulis (1998) used the binomial series expansion to express the terrain correction for vertical gravitational components as convolutions, whereas, we use the Taylor series expansion. We can show that the convergence condition of the Taylor series is the same as that of the binomial series by showing that the two series are the same. The function, F_{jk}, is expanded into a Taylor series with respect to variable $x_3^{'}$, and the different orders of derivatives of F_{jk} are evaluated at $x_3^{'} = 0$. Thus, the function F_{jk} can be expressed as

a series of different powers of $x_3^{'}$ (2.31). At the same time, the function, F_{jk}, can also be expanded into a series of different powers of $x_3^{'}$ using the binomial expansion as shown below. First, since F_{jk} has the expression (2.46) for airborne data, we express the term, $\frac{1}{r}$, as:

$$\frac{1}{r} = \frac{1}{\sqrt{s^2 + (x_3 - x_3^{'})^2}} = \frac{1}{s}(1 + (\frac{x_3 - x_3^{'}}{s})^2)^{-\frac{1}{2}} \tag{2.62}$$

Let $x = (\frac{x_3 - x_3^{'}}{s})^2$, (2.63)

thus $\frac{1}{r} = \frac{1}{s}(1+x)^{-1/2}$, so it can be expanded into series of different powers of x by using the binomial expansion of (2.54). The result has the expression

$$\frac{1}{r} = \frac{1}{s}(1 - \frac{1}{2}x + \frac{1\cdot 3}{2\cdot 4}x^2 - \frac{1\cdot 3\cdot 5}{2\cdot 4\cdot 6}x^3 + \cdots). \tag{2.64}$$

Thus, the terms, $\frac{1}{r^3}$ and $\frac{1}{r^5}$ in equation (2.46) can also be expanded into series of different powers of x by using the series expression of $\frac{1}{r}$, we derived above, as:

$$\frac{1}{r^3} = \frac{1}{s^3}(1 - \frac{1}{2}x + \frac{1\cdot 3}{2\cdot 4}x^2 - \frac{1\cdot 3\cdot 5}{2\cdot 4\cdot 6}x^3 + \cdots)^3; \tag{2.65}$$

$$\frac{1}{r^5} = \frac{1}{s^5}(1 - \frac{1}{2}x + \frac{1\cdot 3}{2\cdot 4}x^2 - \frac{1\cdot 3\cdot 5}{2\cdot 4\cdot 6}x^3 + \cdots)^5. \tag{2.66}$$

Substitute (2.63), (2.65) and (2.66) into (2.46) and compute the powers 3, 5 of the series in (2.65), (2.66); then compute all terms, rearrange and merge the terms which have the same power of $x_3^{'}$. At last, we can express F_{jk}, as a general series with respect to different powers of $x_3^{'}$:

$$F_{jk} = A_1 + A_2 x_3^{'} + A_3 (x_3^{'})^2 + A_4 (x_3^{'})^3 + \cdots \tag{2.67}$$

where $A_1, A_2, A_3, A_4, \cdots$ are the coefficients.

The convergence condition of (2.67) can be obtained from the convergence condition of (2.64), which is $(\frac{x_3 - x_3^{'}}{s})^2 \le 1$.

By comparing (2.31) and (2.67), we are expanding the same function F_{jk} into two series of powers of $x_3^{'}$, thus the two series are the same and share convergence conditions. So it is easy to see that the convergence condition is $(\frac{x_3 - x_3^{'}}{s})^2 \le 1$ for our Taylor series.

So when the integration point is close to the computation point, or the terrain between the integration point and the computation point has the ratio of height difference to horizontal distance greater than one, there exist the dangers that the Taylor series does not converge in theory. In order to avoid this kind of convergence problem, we modify our FFT method and divide the terrain around the computation point into an inner zone and an outer zone. The inner zone was selected to include the terrain where the convergence condition does not hold, and its effect was computed using the prism summation method. While the outer zone was selected to include the terrain where the convergence condition holds (i.e., the slopes between the source point and the computation point are less than 45^o) and its effect was determined using the FFT method with a modified kernel function (Tsoulis, 1998; Tsoulis, 2001).

The above method was applied to our terrain correction computations for the gradients on the ground or for airborne data. First, we modified our kernel functions $F_{jk}^{(n-1)}$ in (2.33) for ground data or (2.49) for airborne data as follows:

$$\hat{F}_{jk}^{(n-1)} = \begin{cases} 0 & \left|x_1 - x_1^{'}\right| \le R_1/2 \text{ and } \left|x_2 - x_2^{'}\right| \le R_2/2 \\ F_{jk}^{(n-1)} & \textit{otherwise} \end{cases} \tag{2.68}$$

where R_1, R_2 are the selected horizontal distances of the inner zone.

The terrain correction or terrain effect within the inner zone is computed using the right rectangular prism method by (2.14), (2.15), (2.16) for ground gradients, or (2.18), (2.19), (2.20) for airborne gradients. Next, we combine the inner zone result with the outer zone result for each observation point. So, finally our formula for the terrain correction of the residual terrain at ground is

$$\begin{aligned}\delta\Gamma_{jj}(\mathbf{x}) &= \delta\Gamma_{jj}^{outer}(\mathbf{x}) + \delta\Gamma_{jj}^{inner}(\mathbf{x}) \\ &= G\rho[\Im^{-1}(\Im(\hat{F}_{jj})\cdot\Im(h)) - h_p\cdot\Im^{-1}(\Im(\hat{F}_{jj}^{'})\cdot\Im(h)) + \frac{1}{2!}\Im^{-1}(\Im(\hat{F}_{jj}^{'})\cdot\Im(h^2)) \\ &\quad - h_p\cdot\Im(\hat{F}_{jj})(0,0) + \frac{1}{2}h_p^2\cdot\Im(\hat{F}_{jj}^{'})(0,0)] \\ &\quad - G\rho\sum_{i=1}^{N_{inner}\times M_{inner}}\tan^{-1}\frac{(x_k - x_k^{'})(x_l - x_l^{'})}{(x_j - x_j^{'})r}\Bigg|_{x_1^{'}=a_i-a/2}^{a_i+a/2}\Bigg|_{x_2^{'}=b_i-b/2}^{b_i+b/2}\Bigg|_{x_3^{'}=0}^{h_i-h_{p_i}}\end{aligned} \tag{2.69}$$

$$\begin{aligned}\delta\Gamma_{jk}(\mathbf{x}) &= \delta\Gamma_{jk}^{outer}(\mathbf{x}) + \delta\Gamma_{jk}^{inner}(\mathbf{x}) \\ &= G\rho[\Im^{-1}(\Im(\hat{F}_{jj})\cdot\Im(h)) - h_p\cdot\Im^{-1}(\Im(\hat{F}_{jj}^{'})\cdot\Im(h)) + \frac{1}{2!}\Im^{-1}(\Im(\hat{F}_{jj}^{'})\cdot\Im(h^2)) \\ &\quad - h_p\cdot\Im(\hat{F}_{jk})(0,0) + \frac{1}{2}h_p^2\cdot\Im(\hat{F}_{jk}^{'})(0,0)] \\ &\quad + G\rho\sum_{i=1}^{N_{inner}\times M_{inner}}\ln(x_l - x_l^{'} + r)\Big|_{x_1^{'}=a_i-a/2}^{a_i+a/2}\Bigg|_{x_2^{'}=b_i-b/2}^{b_i+b/2}\Bigg|_{x_3^{'}=0}^{h_i-h_p}\end{aligned} \tag{2.70}$$

And the formula for the terrain effect of gradients at airborne altitude is

$$\begin{aligned}\Gamma_{jj}(\mathbf{x}) &= \Gamma_{jj}^{outer}(\mathbf{x}) + \Gamma_{jj}^{inner}(\mathbf{x}) \\ &= G\rho\cdot\Im^{-1}[\Im(\hat{F}_{jk}(0)\cdot\Im(h) + \frac{1}{2}\Im(\hat{F}_{jk}^{'}(0)\cdot\Im(h)] - \\ &\quad G\rho\sum_{i=1}^{N_{inner}\times M_{inner}}\tan^{-1}\frac{(x_k - x_k^{'})(x_l - x_l^{'})}{(x_j - x_j^{'})r}\Bigg|_{x_1^{'}=a_i-a/2}^{a_i+a/2}\Bigg|_{x_2^{'}=b_i-b/2}^{b_i+b/2}\Bigg|_{x_3^{'}=0}^{h_i}\end{aligned} \tag{2.71}$$

$$\Gamma_{jk}(\mathbf{x}) = \Gamma_{jk}^{outer}(\mathbf{x}) + \Gamma_{jk}^{inner}(\mathbf{x})$$
$$= G\rho \cdot \Im^{-1}[\Im(\hat{F}_{jk}(0) \cdot \Im(h) + \frac{1}{2}\Im(\hat{F}_{jk}^{'}(0) \cdot \Im(h)] +$$
$$G\rho \sum_{i=1}^{N_{inner} \times M_{inner}} \ln(x_l - x_l^{'} + r)\Big|_{x_1^{'}=a_i-a/2}^{a_i+a/2}\Big|_{x_2^{'}=b_i-b/2}^{b_i+b/2}\Big|_{x_3^{'}=0}^{h_i} \tag{2.72}$$

The DEM we used for our analysis comes from the 3″ SRTM data (around 90 m resolution) in an area defined by latitude: 29.977°~30.323°; and longitude: -93.753°~-93.437° , which is also the terrain correction area for the Air-FTG at Vinton Dome, LA; see Chapter 4.3, Figure 4.17. We selected the 3 x 3 grid points around the observation point as the inner zone. Thus the minimum horizontal distance between a source point in outer zone and the observation point is 1.5 times the grid resolution, which is about $1.5 \cdot R \cdot \frac{3''}{3600} \cdot \frac{\pi}{180} \approx 139\,\mathrm{m}$ in x_2 direction, and about $1.5 \cdot R \cdot \cos(30^o) \cdot \frac{3''}{3600} \cdot \frac{\pi}{180} \approx 120\,\mathrm{m}$ in x_1 direction. At the same time, the maximum height difference between the observation point and the source point is about 80 m which can be seen from Table 4.4. Thus, both these two horizontal distances are greater than 80 m, which ensures that the convergence condition holds in outer zone. Also in our computations, the observation point height is selected at constant flight altitude of 80 m. The topography density is set to 1 gm/cc in order to compare our results with those of Bell Geospace, who used this density value (as a scale factor). We make an assumption that the result from the right rectangular prism method is the true value. The two differences between the normal FFT (method iv) and the true value, and between the modified FFT (method v) and the true value are computed, respectively, and shown in Figure 2.5 for a W-E profile (Γ_{33}, for example), together with the contribution of the topography outside the inner zone. It is shown that the normal FFT method has an error of about 10 E, while the modified FFT method only has an error of about 0.1 E. This means that the difference of these two errors is caused by the inner zone topography, because the Taylor series does not converge within the inner zone. It also shows that the modified FFT method reduces the effect of the inner zone errors significantly, leaving only sub-Eötvös error.

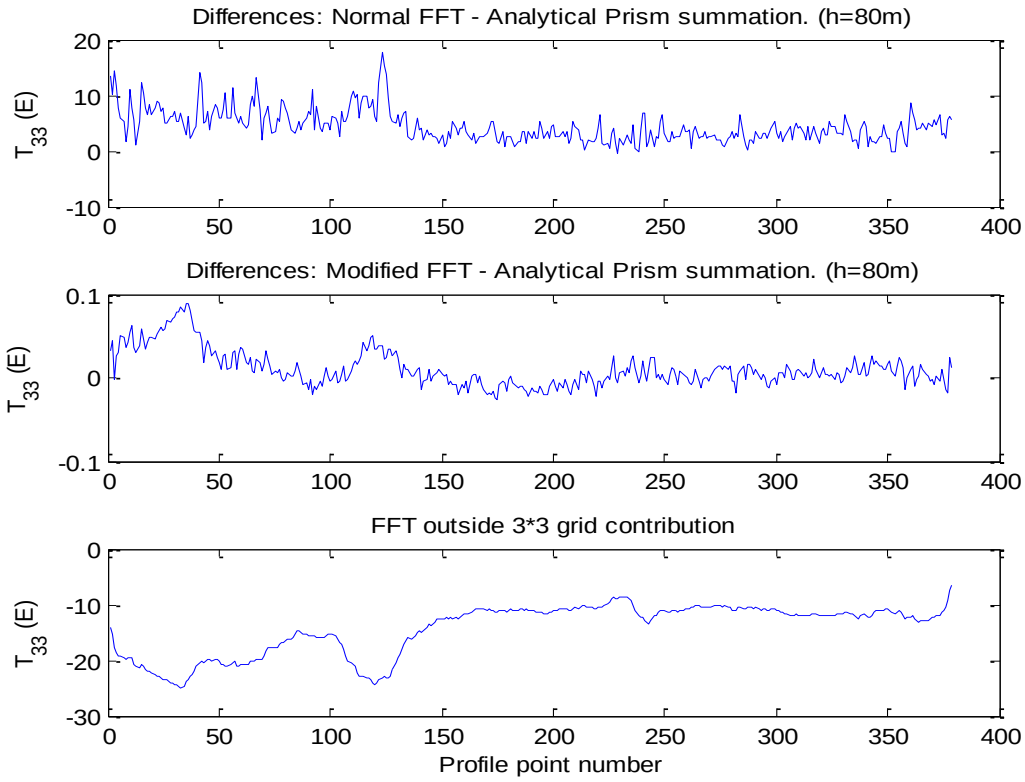

Figure 2.5 Normal FFT method comparing with the combination method and its outer zone contribution

2.2.2 Extent determination by Geostatistical methods

One common problem of the terrain correction for gravity or gravity gradients is how much terrain should be included, and furthermore the extent used should be based on our application of gravity gradiometry. For example, for the application of subsurface exploration, the grid spacing error, the instrument error, the size of observation area, the signal of the subsurface object, and the noise of the background etc., should all have an influence on the determination of the required topographic data extent. The more area of terrain is included, the more computation effort and cost of exploration will be needed, so our purpose is to find an efficient way to determine the extent of the topographic data based on the actual need of our application. One direct method is to compute the terrain correction for gradients at a certain extent based on given DEM data, then increase the extent and repeat the computation until we can see that the latter topography we included no longer has a significant contribution compared to the previously included topography. Such a method has the problem that it needs great computational effort in order to analyze the problem for a given regional terrain, as detailed in the previous sections. Also

this method needs a large area DEM data around the observation area which may not be available for every situation. In order to learn how much contribution the remote topography will have on our observations; an alternative method is developed by applying classical truncation theory and a geostatistical analysis. The geostatistical analysis method is an efficient method based on a stochastic representation of the topography that can quantify the errors in truncating the terrain effect.

Sprenke (1989) used this method for optimizing the distance to which terrain corrections are made. His method is similar to ours, but differs in three ways. First, the topography simulation method is different although both are based on the geostatistical method. He only used statistics from a profile of the area to simulate the radial zone elevation around the observation station, and then the elevations in the subarea of the radial zone are simulated by a uniform distribution of elevations. However we simulate the whole topography by extending the covariance model to higher frequencies and our covariance model is based on the statistics of all points within an area. Second, the truncation error computation method is different; Sprenke used the direct numerical integration, while we use the spectrum method. The difference of these two methods was discussed by Jekeli and Zhu (2006). Third, Sprenke computed the truncation error for gravity, while we compute the variance of truncation error for gravity gradients. Also his extent determination is based on the error while ours based on the variance of error. Furthermore, we also consider the error in the differences of terrain effect at two neighboring points. This is important because usually the remote terrain has similar gravitational effect on a pair of observation points, which are separated by a short distance. That is, in this case the effect is like a bias and can be neglected under certain situations; and, thus the required extent maybe significantly smaller.

i. PSD of terrain correction (effects)

The 2-D convolution of our signals g, h can be computed in the frequency domain by using equation (2.29) according to the convolution theorem, assuming the signals g, h are finite power signals. Then the power spectral density of the function, c, is given by

$$\Phi_c(f_1, f_2) = C^*(f_1, f_2)C(f_1, f_2), \tag{2.73}$$

where $*$ denotes the complex conjugate.

Apply (2.73) to our terrain effect of the residual terrain, $\delta\Gamma_{jk}(\mathbf{x})$, calculated in equation (2.34), we can apply the periodogram method to compute the power spectral density of the terrain effect of the gradients for ground data, as

$$\Phi_{\delta\Gamma_{jk}}(f_1, f_2) = [\Im(\delta\Gamma_{jk})]^* \cdot \Im(\delta\Gamma_{jk}) \tag{2.74}$$

Also by applying (2.73) to our terrain effect of the topography, $\Gamma_{jk}(\mathbf{x})$, calculated in equation (2.48), we have the power spectral density of the terrain effect of the gradients at altitude,

$$\begin{aligned}\Phi_{\Gamma_{jk}}(f_1, f_2) &= [\Im(\Gamma_{jk})]^* \cdot \Im(\Gamma_{jk}) \\ &= (G\rho)^2 [\sum_{n=1}^{\infty} \frac{1}{n!} \Im(F_{jk}^{(n-1)}) \cdot \Im(h^n)]^* \cdot [\sum_{n=1}^{\infty} \frac{1}{n!} \Im(F_{jk}^{(n-1)}) \cdot \Im(h^n)]\end{aligned} \tag{2.75}$$

ii. Truncation theory applied to geostatistical analysis

We assume a planar approximation since the terrain correction for gravity gradiometry is presumed to be a very local phenomenon. Although for the extent determination of the terrain effect, we are interested in the distant zone effect, we still can take the planar approximation for the purpose of a comparative analysis. Also, it is anticipated that the gradient effect decreases very fast when the distance enlarges, since the function, F_{jk}, involves the high orders (order 3 and 5) of inverse distance (see (2.26), (2.46)). Nevertheless, the effect of mountainous terrain can still be large at large distances; then if larger areas are analyzed, the spherical approximation may need to be used instead. However, we confine our analysis to the planar case and also assume that the terrain of the distant zone is a stochastic process and is a stationary, ergodic process. For terrain that involves rapid changes from one kind of topography (i.e., mountainous area) to another (i.e., flat plains), the above assumption may not be suitable and will cause the geostatistical analysis to be inapplicable. Therefore, our analysis is somewhat restricted to cases where the assumptions of stationarity hold over the area of our geostatistical analysis. Equations (2.34) or (2.47) show that the terrain effect can be expanded in a series of convolutions of different powers of topography, h (or residual terrain, δh) and the corresponding kernel functions $F_{jk}^{(n-1)}(0)$. These functions depend on the distance between the integration point and the evaluation point; they are singular at the origin and yield strongly singular integrals for ground gravity gradiometry observations. However we don't need to worry about their behavior at zero distance since our analysis concerns the truncation error in restricting the terrain correction area A to a finite region where the distance in this error expression is always greater than zero. The truncation theory is

developed below in general terms for a single convolution (2.28), and it can be applied to as many of the terms in equation (2.34) or (2.47) as needed.

Equation (2.28) is analogous to one convolution term in equation (2.34), or (2.47), where c corresponds to a contribution to the terrain effect, g corresponds to the kernel function F_{jk} (or a higher order derivative of F_{jk}), and h corresponds to a power of the terrain. If h is used only in some finite domain around the computation point, (x_1, x_2), that is, $-\frac{T_1}{2} \le x_1 - x_1' \le \frac{T_1}{2}$, $-\frac{T_2}{2} \le x_2 - x_2' \le \frac{T_2}{2}$, then the error in c is the truncation error:

$$\varepsilon(x_1, x_2) = \int\limits_{|x_1 - x_1'| > T_1/2} \int\limits_{|x_2 - x_2'| > T_2/2} h(x_1', x_2') g(x_1 - x_1', x_2 - x_2') dx_1' dx_2' , \tag{2.76}$$

We define a new kernel:

$$\hat{g}(x_1 - x_1', x_2 - x_2') = \begin{cases} g(x_1 - x_1', x_2 - x_2'), & |x_1 - x_1'| > T_1/2 \text{ or } |x_2 - x_2'| > T_2/2 \\ 0, & |x_1 - x_1'| \le T_1/2 \text{ and } |x_2 - x_2'| \le T_2/2 \end{cases} \tag{2.77}$$

so that the truncation error can be expressed as a convolution over the plane:

$$\varepsilon(x_1, x_2) = \int\limits_{-\infty}^{\infty} \int\limits_{-\infty}^{\infty} h(x_1', x_2') \hat{g}(x_1 - x_1', x_2 - x_2') dx_1' dx_2' . \tag{2.78}$$

Applying this to the series of convolutions in equations (2.34) or (2.47), we get the truncation error of the terrain effect of gradients on the ground beyond the finite extent:

$$\varepsilon_{\delta\Gamma_{jk}}(x_1, x_2) = G\rho[\hat{F}_{jk} * h - h_p \cdot \hat{F}_{jk}' * h + \frac{1}{2!} \hat{F}_{jk}' * h^2 - h_p \cdot \Im(\hat{F}_{jk})(0,0) + \frac{1}{2} h_p^2 \cdot \Im(\hat{F}_{jk}')(0,0) + \cdots] \tag{2.79}$$

Also, the truncation error in the terrain effect of gradients at altitude is:

$$\varepsilon_{\Gamma_{jk}}(x_1, x_2) = G\rho \sum_{n=1}^{\infty} \frac{1}{n!} \hat{F}_{jk}^{(n-1)}(0) * h^n , \tag{2.80}$$

where

$$\hat{F}_{jk}^{(n-1)}(0) = \begin{cases} F_{jk}^{(n-1)}(0), & |x_1 - x_1'| > T_1/2 \text{ or } |x_2 - x_2'| > T_2/2 \\ 0, & |x_1 - x_1'| \le T_1/2 \text{ and } |x_2 - x_2'| \le T_2/2 \end{cases} . \tag{2.81}$$

The spectrum of the truncation error can be computed by the convolution theorem, such as for (2.80):

$$E_{\Gamma_{jk}}(f_1, f_2) = G\rho\sum_{n=1}^{\infty}\Im(\frac{1}{n!}\hat{F}_{jk}^{(n-1)})\cdot\Im(h^n), \tag{2.82}$$

The above first Fourier transform holds for any topography but it has to be computed for each extent (T_1, T_2).

Thus the power spectral density of the truncation error can be computed by:

$$\Phi_{\varepsilon}(f_1, f_2) = E^*(f_1, f_2)E(f_1, f_2), \tag{2.83}$$

And the covariance function of the error is just the inverse Fourier transform of $\Phi_{\varepsilon}(f_1, f_2)$, given by

$$\phi_{\varepsilon}(s_1, s_2) = \Im^{-1}(E^*(f_1, f_2)E(f_1, f_2)). \tag{2.84}$$

where s_1, s_2 are the horizontal distances along x_1, x_2 directions between a pair of observation points.

The value of the covariance function at zero distance ($s_1 = 0, s_2 = 0$) gives the variance of the truncation error for the observation point at the center of the computation area, due to the neglect of the remote zone beyond the limited extent. The variance of the truncation error represents the statistical variation of the errors for an observation point always centered within its data area. The needed extent of the terrain correction can be determined by evaluating the variance for the (T_1, T_2) that is less than some threshold value, such as the variance of the gradient measurement error, typical values of 10^{-2} E^2.

Furthermore, for a pair of points separated by a specified distance, s , we can formulate the variance of the error difference as a function of the size of the limited extent, (T_1, T_2). Since the effect of the remote zone will be nearly the same for two neighboring points of interest, it behaves like a bias among many points within a smaller area of computation and could be calibrated by other methods. Therefore, for such points in a limited area, the determined values of (T_1, T_2) may be smaller if the bias is not a concern. For points further apart, the effect of the remote zone will have a larger difference and it will not behave like a bias. In this case, we need to increase the values of (T_1, T_2) further in order to reduce the truncation effect until it behaves like a bias.

We define the error difference as

$$\Delta\varepsilon(s) = \varepsilon(x_1^{(1)}, x_2^{(1)}) - \varepsilon(x_1^{(2)}, x_2^{(2)}) = \varepsilon_1 - \varepsilon_2, \tag{2.85}$$

at two points, $(x_1^{(1)}, x_2^{(1)})$ and $(x_1^{(2)}, x_2^{(2)})$, separated by distance s. Again, with the assumption of a stationary stochastic process, its variance is:

$$\text{var}(\Delta\varepsilon) = E((\Delta\varepsilon)^2) = E(\varepsilon_1^2 + \varepsilon_2^2 - 2\varepsilon_1\varepsilon_2) = 2\phi_\varepsilon(0,0) - 2\phi_\varepsilon(s_1, s_2). \tag{2.86}$$

We make the assumption that all errors have zero mean in order to derive (2.86), and here E is expectation operator. If this is not the case, we can redefine the error to satisfy this requirement, since we are only interested in the variance of the error. For a particular distance, (s_1, s_2), the covariance of the difference of errors depends on (T_1, T_2). It is the covariance for the effect of the remote zone beyond (T_1, T_2) computed for all pairs of points with distance (s_1, s_2), where each point of a pair theoretically is centered within the same size data area. Thus, we find the specific value of (T_1, T_2) which yields a chosen variance of the difference of the errors; again, e.g., less than the variance of the measurement error. Usually, we determine the extent (T_1, T_2) only for the distance $s = \sqrt{s_1^2 + s_2^2}$, and then it has the limitation that we need to assume the difference of errors is isotropic, which is not always the case. Another limitation is that our error estimation is for the points centered within the survey area, so when the observation points are actually near the edge, the result will be biased by the different geometry of the correction; and this will be left for future research.

Chapter 3

Topography Simulation

3.1 Reciprocal distance covariance model

In the previous chapter, we developed a method to determine the extent of terrain correction for gravity gradients by applying the truncation theory and a geo-statistical analysis. However such an analysis, the results of which are given in Chapter 4, should also be confirmed by simulations using traditional terrain correction calculations. Although we have very good topographic data already, such as SRTM 1" DEM for the entire US, we may still need higher resolution data for terrain correction applications using very local gravity gradiometry, which is sensitive to very local mass distributions. For example, a ground gravity gradiometry observation area may extend only about a few hundred meters in length and width. In order to determine the extent of terrain correction for such a local area, we need high resolution DEM, higher than 30m, even up to a few meters. By developing a method of simulating different spectra and resolution of the topography, we have complete control of every element to see how they affect our results of extent determination.

The simulation procedure is as follows. In chapter 3.1, based on the reciprocal distance covariance model (Moritz, 1980), we use its high frequency part as the PSD model of high frequency topography. Jekeli (2003) used the model to study the gravity field from the terrain and thus the low frequency part of the model is fitted with gravity field. Here, we only simulate the high frequency topography by extending the PSD model of low frequency topography to higher frequencies. Thus, the parameters of the low frequency part of the model are not needed in our application. However, it is also noted that sometimes when people study the ocean bottom topography, the satellite radar altimetry is used and thus the topography or the bathymetry is modeled from gravity field. In our application, by fitting an isotropic empirical PSD of DEM data with the PSD model of topography, we find appropriate parameters of the covariance model at high frequencies. By using the high frequency information of the fitted PSD model, we simulate the very high frequency part of topography (i.e., higher than 30 m resolution), and combine this with the part up to 30m resolution (which comes from the DEM data). The spectrum of the topography can be derived from the PSD of the topography where they are related with each other by the periodogram method. After we have the spectrum of the topography, the inverse Fourier transform can be applied to produce the realized topography. Thus we obtain the simulated topography with an arbitrarily high resolution.

Although modeling the PSD of the topography does not explicitly depend on a model for the gravitation, the forms of the two models are similar due to the fact that in many cases gravitation and topography are linearly correlated at the higher frequencies. Therefore, the following development is based on potential and gravitation, which are the original quantities for which the reciprocal distance model was designed. Later, we simply interpret the gravitation PSD model with appropriate scaling as a model for the topography. We assume that both the disturbing potential, T, and the topography in a region are stationary, isotropic stochastic processes on the plane. Under such an assumption, a standard model for the covariance function of T, called the reciprocal distance model (Moritz, 1980), is

$$\phi_T(\Delta x_1, \Delta x_2; x_3, x_3^{'}) = \sum_{j=1}^{J} \frac{\sigma_j^2}{\sqrt{(1+\alpha_j(x_3+x_3^{'}))^2 + \alpha_j^2 s^2}}\,, \tag{3.1}$$

where

$\Delta x_1 = x_1 - x_1^{'}$, $\Delta x_2 = x_2 - x_2^{'}$, $s = \sqrt{\Delta x_1^{\,2} + \Delta x_2^{\,2}}$, and where J, σ_j, α_j are parameters whose values are selected to fit an empirical determination of the covariance or power spectral density (PSD) of the disturbing potential or one of its derivatives.

The PSD model corresponding to equation (3.1) is given by:

$$\Phi_T(f_1, f_2; x_3, x_3^{'}) = \sum_{j=1}^{J} \frac{\sigma_j^2 e^{-2\pi f \alpha_j^{-1}}}{\alpha_j f} e^{-2\pi f (x_3 + x_3^{'})}\,, \tag{3.2}$$

where the magnitude of the spatial frequencies, f_1 and f_2 is given by

$$f = \sqrt{f_1^2 + f_2^2}\,, \tag{3.3}$$

That Φ_T depends only on f is a consequence of ϕ_T depending only on s, which means that the potential field is assumed to be statistically isotropic.

The gravity anomaly is defined as $\Delta g_P = g_P - \gamma_Q$, where g_P is the gravity at a point P of the geoid, γ_Q is the normal gravity at a point Q of the reference ellipsoid, and P is projected onto the point of Q by means of the ellipsoidal normal. With the planar approximation of the earth, the auto-covariance function for gravity anomalies, according to the rules of propagation of covariance (Moritz, 1980), is given by

$$\phi_{\Delta g,\Delta g} = \frac{\partial^2 \phi_T}{\partial x_3 \partial x_3^{'}} \,. \tag{3.4}$$

The corresponding PSD relationships in the frequency domain between the potential and its vertical derivatives are given by (Jekeli 2003):

$$\Phi_{\Delta g,\Delta g} = (2\pi f)^2 \Phi_T \,. \tag{3.5}$$

3.2 Topography simulation using covariance model

In order to relate the gravity field with topography, it is a reasonable assumption that the high frequency anomalies of the gravity field are generated principally by the terrain variations. For example, Wang and Rapp (1990) applied the assumption of linear relationship between free-air gravity anomalies and topographical heights in geoid undulation computations. Voigt (2006) also points out that local gravity field effects are strongly correlated with the topography and the case of high frequency terrain effects in gravity field modeling was studied using 1"×1" DEM. However, Vanicek and Kleusberg (1987) did not make such an assumption for the effects of terrain in Helmert's 2nd condensation method. Martinec et al. (1993) also pointed out that both methods, Vanicek and Kleusberg (1987) as well as Wang and Rapp (1990), are approximate for different reasons and there are cases when the mass distribution in the earth creates the gravity field which behaves opposite to the above assumption. Here we apply the assumption of Wang and Rapp (1990) to our application, realizing also that it is particularly applicable to the higher frequencies representing the local features of the topography and gravitation (Jekeli, 2006). To simplify the relationship between the gravitational field and the topographic heights, we approximate the topography by its Helmert condensation (Heiskanen and Moritz, 1967) onto the geoid. The topographic masses thus are modeled as a two-dimensional mass layer on the geoid with density equal to ρh at any point, where ρ is the crustal density (constant) and h is the terrain elevation at this point. From the equation (2.1), we have the potential V at a point P, due to such a layer is given by

$$V(\mathbf{x}) = G\rho \iint_A \frac{h}{r} dA \,, \tag{3.6}$$

where G is Newton's gravitational constant, A represents the integration area and r is the distance between the computation point and the integration point. With planar coordinates, we have $r = \sqrt{(x_1 - x_1')^2 + (x_2 - x_2')^2 + x_3^2}$ and $(x_1^{'}, x_2^{'})$ are coordinates of the integration points on the geoid.

Equation (3.6) is a convolution of h with the inverse distance, r^{-1} and can be written as $V(\mathbf{x}) = G\rho h \cdot r^{-1}$. We can apply the convolution theorem (2.30), (2.31) to (3.7) and also we have the 2-D Fourier transform of $\frac{1}{\sqrt{x_1^2 + x_2^2 + x_3^2}}$ as $\frac{1}{f} e^{-2\pi x_3 f}$ which is a Hankel transform. Thus it is shown that the Fourier transform of the potential at the level $x_3 \geq 0$ is given by

$$\Im(V) = \frac{G\rho}{f} \Im(h) e^{-2\pi f x_3}, \tag{3.7}$$

Equation (2.70) gives the relationship between power spectral density and spectra. Therefore, we obtain the (cross-) PSD of the potential at two levels, x_3 and $x_3^{'}$, by substituting (3.7) into (2.70)

$$\Phi_V(f; x_3, x_3^{'}) = (\Im(V))^* \Im(V) = (\frac{G\rho}{f})^2 \Phi_h(f) e^{-2\pi f (x_3 + x_3^{'})}. \tag{3.8}$$

From equations (3.5) and (3.8) we can get the PSD of the vertical derivative of V by

$$\Phi_{\Delta g}(f; x_3, x_3^{'}) = (2\pi G\rho)^2 \Phi_h(f) e^{-2\pi f (x_3 + x_3^{'})}. \tag{3.9}$$

Equation (3.9) gives the relationship between the PSD of gravity anomaly with PSD of topography which is based on our assumption that gravity anomaly is linearly related with the topography elevation.

The next step is to synthesize the topography in space domain from the discrete PSD.

We assume that the topography height signal is a finite power signal and that it is truncated at T_1, T_2 along the two directions of a region and so can be treated as a finite energy signal; and we apply the Fourier transform to it. From equation (2.70), we have:

$$\Phi_h(f_1, f_2) = \lim_{T_1, T_2 \to \infty} (\varepsilon(\frac{1}{T_1 T_2} H^*_{T_1, T_2}(f_1, f_2) H_{T_1, T_2}(f_1, f_2))). \tag{3.10}$$

Therefore, the PSD of the topography can be estimated from its spectrum by the periodogram. We want to synthesize the topography on a 2-D grid, h_{k_1, k_2} (evenly spaced, $\Delta x_1, \Delta x_2$) where $k_1 = 0, \ldots, N_1 - 1; k_2 = 0, \ldots, N_2 - 1$. We use discrete Fourier transforms and estimate the PSD by ignoring the limit and the expectation in (3.10):

$$\hat{\Phi}_h(f_1, f_2) = \frac{1}{N_1 \Delta x_1 N_2 \Delta x_2} H^*_{T_1,T_2}(f_1, f_2) H_{T_1,T_2}(f_1, f_2). \quad (3.11)$$

where $f_1 = -\frac{N_1/2}{N_1 \Delta x_1}, \ldots 0, \ldots, \frac{N_1/2-1}{N_1 \Delta x_1}; f_2 = -\frac{N_2/2}{N_2 \Delta x_2}, \ldots 0, \ldots, \frac{N_2/2-1}{N_2 \Delta x_2}$

and $H_{T_1,T_2}(f_1, f_2)$ is the discrete spectrum of topography height for the interval T_1, T_2.

So the spectrum of topography, $H_{T_1,T_2}(f_1, f_2)$, on our synthesized grid can be computed according to:

$$H_{n_1,n_2} = (b_{n_1,n_2} + ic_{n_1,n_2}) \sqrt{N_1 \Delta x_1 N_2 \Delta x_2} \sqrt{\Phi_h(n_1, n_2)}, \quad (3.12)$$

where b_{n_1,n_2}, c_{n_1,n_2} are assumed to be normally distributed random variables:

$$b_{n_1,n_2} \sim N(0, (1/\sqrt{2})^2), c_{n_1,n_2} \sim N(0, (1/\sqrt{2})^2). \quad (3.13)$$

By substituting (3.12) back into (3.11), the square-root of the periodogram of H_{n_1,n_2} is

$\sqrt{\Phi_h(n_1, n_2)} \cdot \sqrt{b^2_{n_1,n_2} + c^2_{n_1,n_2}}$.

Since b_{n_1,n_2}, c_{n_1,n_2} are normally distributed and independent, we have

$$\sqrt{\left(\frac{b_{n_1,n_2} - 0}{1/\sqrt{2}}\right)^2 + \left(\frac{c_{n_1,n_2} - 0}{1/\sqrt{2}}\right)^2} = \sqrt{2} \cdot \sqrt{b^2_{n_1,n_2} + c^2_{n_1,n_2}} \quad (3.14)$$

And by using the law of propagation of variances, (3.14) has the variance $\sigma^2 = 2$, thus we can derive that the standard deviation of $\sqrt{b^2_{n_1,n_2} + c^2_{n_1,n_2}}$ is 1. Therefore, the standard deviation of the square-root of $\hat{\Phi}_h$ is $\sqrt{\Phi_h(n_1, n_2)}$, for all n_1, n_2.

Thus, the inverse discrete Fourier transform of H_{n_1,n_2} yields a realization of the corresponding topography.

3.3 Simulation results

The topographies in two areas (Figure 3.1) were selected to compute the empirical PSD and thus to select the proper parameters in (3.1) to make the PSD of the reciprocal

distance covariance model fit the empirical model. Area 1 represents relatively smooth terrain, and Area 2 is a rough mountainous terrain. The topographies simulated in smaller Area 1_a (using the PSD of Area 1) and Area 2_a (using the PSD of Area 2) are based on DTM2006 5′ data; while the topographies simulated in smaller Area 1_b (using the PSD of Area 1) and Area 2_b (using the PSD of Area 2) are based on SRTM 30″ data.

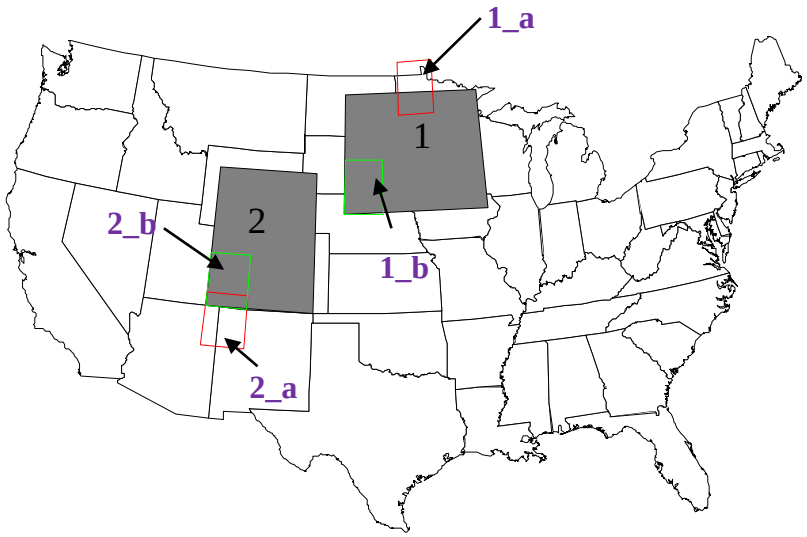

Figure 3.1 Four Areas (1_a, 1_b; 2_a, 2_b) of Simulated Topography.

Two kinds of low frequency terrain data were used for the simulation. Dataset1 is coming from the DTM2006 model which uses spherical harmonic expansion (to harmonic degree 2160) of Earth's topography made available by the EGM2008 development team (Pavlis et al., 2007). Dataset1 has resolution 5′ and is computed for large Area 1 (Latitude: 42^{o}~48^{o}, Longitude: 259^{o}~269^{o}) and large Area 2 (Latitude: 37^{o}~44^{o}, Longitude: 250^{o}~257^{o}), respectively, for the purpose of empirical PSD computation. The software we used is NGA's harmonic synthesis program; both it and the spherical harmonic coefficients of the topographic elevation, are downloaded from the NGA website: http://earth-info.nga.mil/GandG/wgs84/gravitymod/egm2008/first_release.html. Dataset2 is the SRTM (Shuttle Radar Topographic Mission) global dataset (Farr et al., 2007) and its resolution is 30″. Dataset2 is downloaded for large Area 1 and large Area 2, respectively, also for the purpose of empirical PSD computation; and, it is downloaded from website: http://webmap.ornl.gov/wcsdown/wcsdown.jsp?dg_id=10008_1.

The dataset1 (5′ resolution) for large Area 1 has 72×120 grid points, while for large Area 2 has 84×84 grid points. The dataset2 (30″ resolution) for large Area 1 has 720×1200 grid points, while for large Area 2 has 840×840 grid points.

Dataset1, Dataset 2 were also used to model the low-frequency terrain data in our simulation sub-Areas, i.e., Dataset 1 for Area 1_a (latitudes: $47^o \sim 49.7^o$, longitudes: $263^o \sim 265.7^o$) and Area 2_a (latitudes: $35^o \sim 37.7^o$, longitudes: $250^o \sim 252.7^o$); Dataset2 for Area 1_b (latitudes: $42^o \sim 44.7^o$, longitudes: $259^o \sim 261.7^o$) and Area 2_b (latitudes: $37^o \sim 39.7^o$, longitudes: $250^o \sim 252.7^o$), respectively.

First, the empirical PSD, $(\hat{\Phi}_h)_{k_1,k_2}$ of topography data was computed using the periodogram method, i.e., equation (3.11) evaluated for our two-dimensional grid dataset of Area1 and Area2. Next, the isotropic empirical PSD was computed by averaging the 2-D discrete PSD values within each radial frequency band using following equations

$$\hat{\Phi}_h^{isotropic}(f_r) = \frac{1}{N}\sum_{i=1}^{N}(\hat{\Phi}_h(f_r))_i \tag{3.15}$$

where $f_r = \sqrt{f_1^2 + f_2^2}$, is radial frequency; $\Delta f = \min(\frac{1}{N_1\Delta x_1}, \frac{1}{N_2\Delta x_2})$ and $r = Interg(\frac{f_r}{\Delta f})$ is the radial frequency band number, N is the total number of $(\hat{\Phi}_h)_{k_1,k_2}$ whose radial frequency is located between the frequency band $[f_r, f_{r+\Delta f})$.

The angular units for the downloaded grid data of Area 1 and 2 have been converted to horizontal distance units using $\Delta x_1 = R\cos\phi d\lambda; \Delta x_2 = Rd\phi$, where R is the radius of the earth, ϕ is the average latitude of the area. Also the horizontal frequency units can be obtained from the units of $\Delta x_1, \Delta x_2$. The fitted reciprocal distance covariance model, especially the lower frequency parameters were obtained such that the various components of the reciprocal distance model are tangent to (osculating) the empirical power law PSD, as described in section 28 of Freeden et al. (2010). The following figures (Figure 3.2; Figure 3.3) show the isotropic empirical PSD of two datasets (blue line: DTM2006 5′ grid; green line: SRTM 30″ grid), the global DTM2006 degree variances (black line) and the PSD of the fitted reciprocal distance covariance model (red line) in Area 1 and Area 2 respectively. For Area 1, the global DTM2006 degree variances up-shift with respect to the local empirical PSD, indicating that the topographic features of Area 1 are not represented well by the global topographic PSD. On the other hand, Area 2 is a relatively mountainous area and the local topographic feature is more consistent with the degree variances of the global topography (and bathymetry). Also the low frequencies

of DTM2006 degree variances do not fit well with the covariance model because the low frequencies of the covariance model come from the gravity potential, which means that the low frequencies of DTM2006 are not consistent with that of the gravity field. However, this will not affect our topography simulation since we only use the high frequency part of the covariance model. The PSD magnitude jump (for blue line and green line) occurs where the radial frequency, f_r exceeds the Nyquist frequencies $(f_1)_N = \frac{1}{2\Delta x_1}, (f_2)_N = \frac{1}{2\Delta x_2}$. The reason is that not enough data information exists along the radial direction when reaching the boundaries of the square.

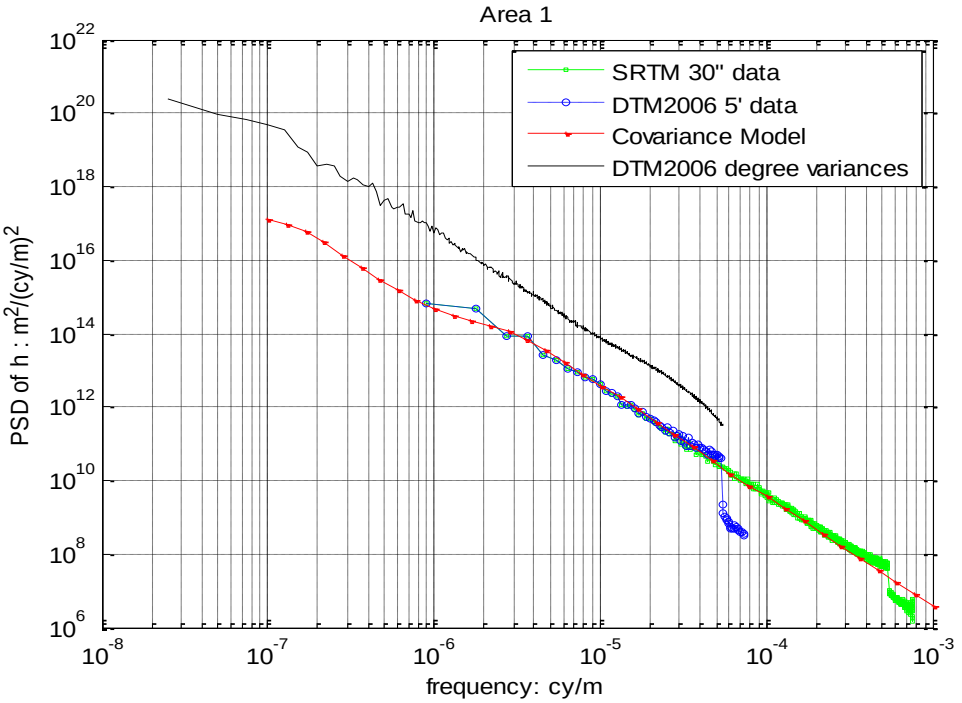

Figure 3.2 Empirical PSD and Reciprocal Distance model PSD in Area 1.

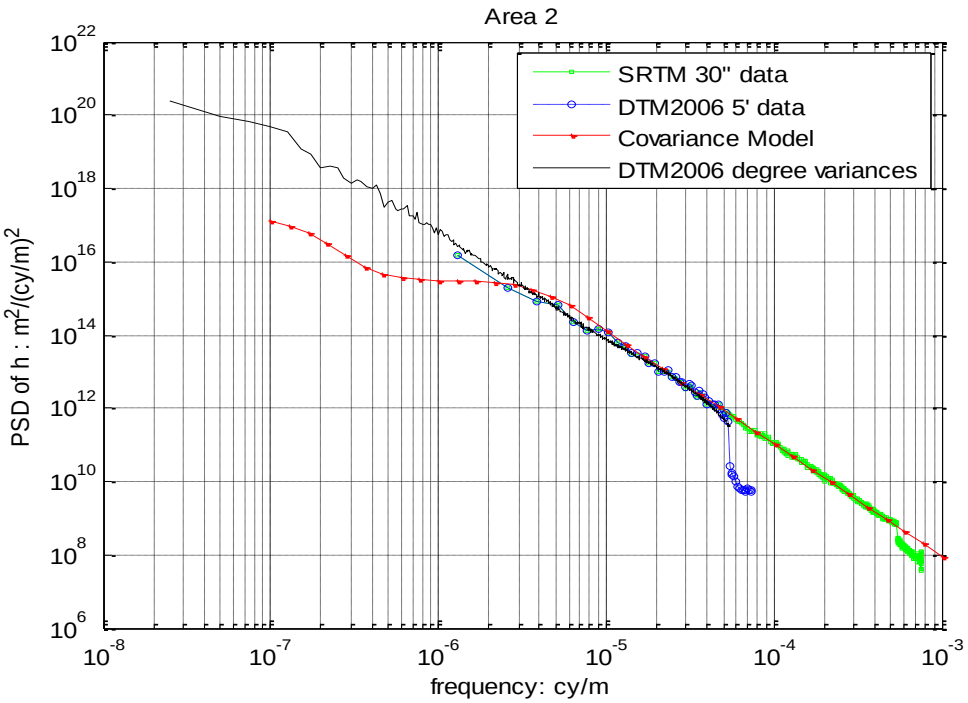

Figure 3.3 Empirical PSD and Reciprocal Distance model PSD in Area 2.

The parameters σ_j^2 and α_j in equation (3.1) that are the selected values to fit empirical PSD's are shown in Table 3.1. Although the table gives the all parameters corresponding to whole frequencies, we only use the parameters representing the high frequency part of the covariance model to simulate the topography.

Table 3.1 Reciprocal Distance Model Parameters

Area 1			Area 2		
j	σ^2 (m^4/s^4)	α (1/m)	j	σ^2 (m^4/s^4)	α (1/m)
1	10^5	3×10^{-7}	1	10^5	3×10^{-7}
2	3300	9.69×10^{-7}	2	3300	9.69×10^{-7}
3	130	4.76×10^{-6}	3	640	7.56×10^{-6}
4	32.4	8.94×10^{-6}	4	951	9.73×10^{-6}
5	3.4	2×10^{-5}	5	79.9	2.18×10^{-5}
6	0.3205	4.48×10^{-5}	6	6.71	4.88×10^{-5}
7	2.01×10^{-2}	1×10^{-4}	7	0.564	1.09×10^{-4}
8	2.53×10^{-3}	2.25×10^{-4}	8	4.74×10^{-2}	2.44×10^{-4}
9	1.59×10^{-4}	5.03×10^{-4}	9	3.98×10^{-3}	5.47×10^{-4}
10	1.994×10^{-5}	1.13×10^{-3}	10	3.34×10^{-4}	1.23×10^{-3}
11	1.565×10^{-6}	2.52×10^{-3}	11	2.81×10^{-5}	2.74×10^{-3}
12	3.93×10^{-8}	5.64×10^{-3}	12	2.36×10^{-6}	6.14×10^{-3}
13	2.47×10^{-9}	1.26×10^{-2}	13	1.98×10^{-7}	1.37×10^{-2}
14	1.55×10^{-10}	2.83×10^{-2}	14	1.66×10^{-8}	3.08×10^{-2}
15	9.74×10^{-12}	6.33×10^{-2}	15	1.4×10^{-9}	6.89×10^{-2}

The DTM2006.0 5′ dataset (approximate 9.2 km resolution) has largest Nyquist frequency about 5.4×10^{-5} cy/m. If we need to simulate the topography with 20m resolution, which has Nyquist frequency 2.5×10^{-2} cy/m, then the PSD models with the parameters of Table 3.1 are suitable to simulate the topography with frequencies between

5.4×10^{-5} cy/m and 2.5×10^{-2} cy/m within Area 1 or Area 2. The reason is that those parameters in the reciprocal distance model of potential include the high frequency information of the empirical PSD of topography which indicates a power law, consistent with the known properties of the Earth's topography. Therefore, we can extend it to the higher frequencies for our simulated topography. This extension of our PSD of topography from the 5′ resolution empirical DTM2006 data up to frequency of 10^{-3} cy/m is reasonable and was verified by the empirical PSD of real SRTM 30″ data (Figure 3.2, and Figure 3.3). We assume that this extension also holds for topography with even higher frequency, i.e., the Nyquist frequency of our simulated topography. This is combined with the DTM2006 5′ topography to obtain the total simulated topography. For the SRTM 30″ dataset (approximate 920m resolution), the simulation is for frequencies approximately between 5.4×10^{-4} cy/m and 2.5×10^{-2} cy/m. Four topographies were simulated for smaller Areas 1_a, 1_b, 2_a, 2_b, respectively; each area covers about 300 km by 300 km with 20 m resolution.

Figure 3.4 shows the simulation result for Area 1_a using the PSD of Area 1 and the DTM 2006 5′ dataset; Figure 3.5 shows two W-E profiles of Figure 3.4.

The similar figures for the simulated topography of Areas 1_b, 2_a, 2_b are shown in Figure 3.6~3.10.

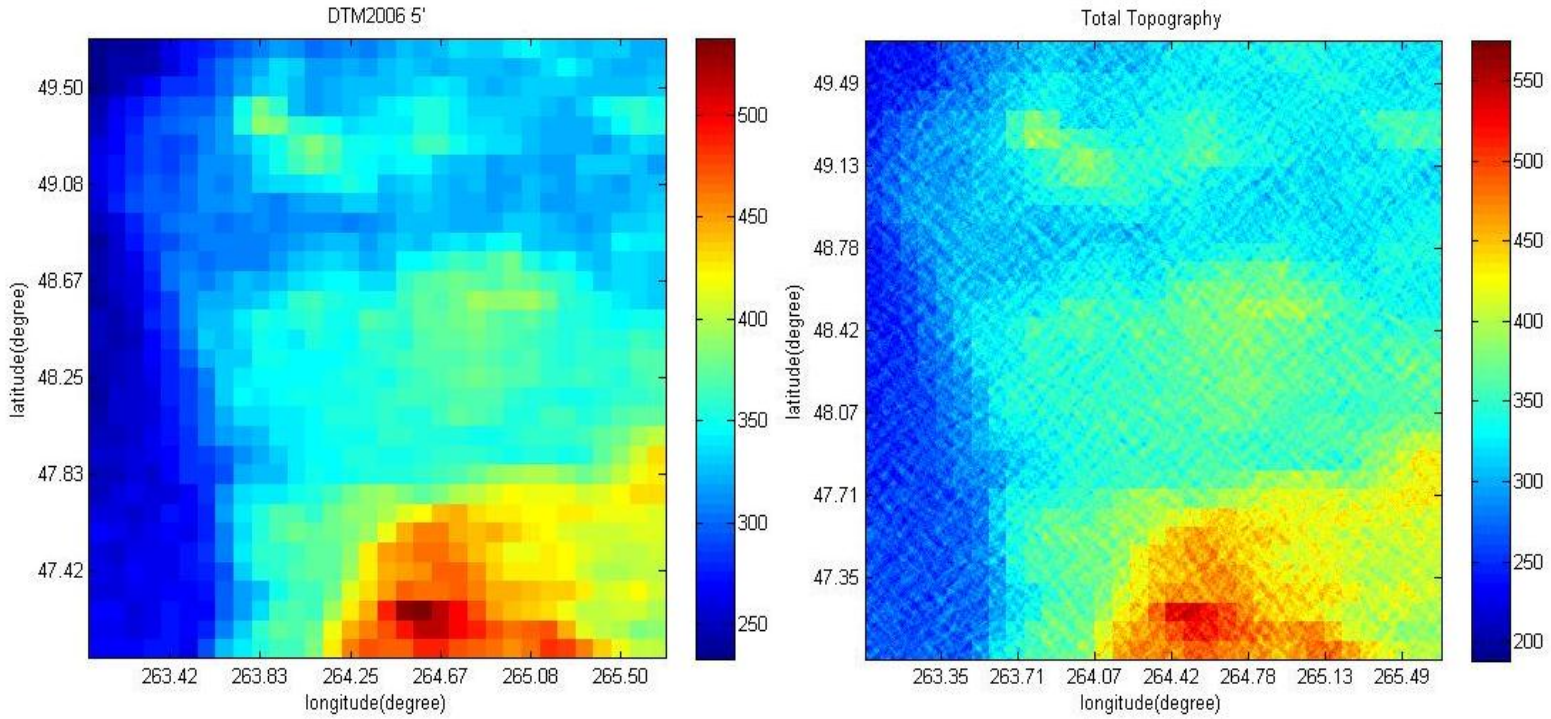

Figure 3.4 DTM 2006 5′ topography and simulated 20 m resolution topography for Area 1_a using PSD of Area 1

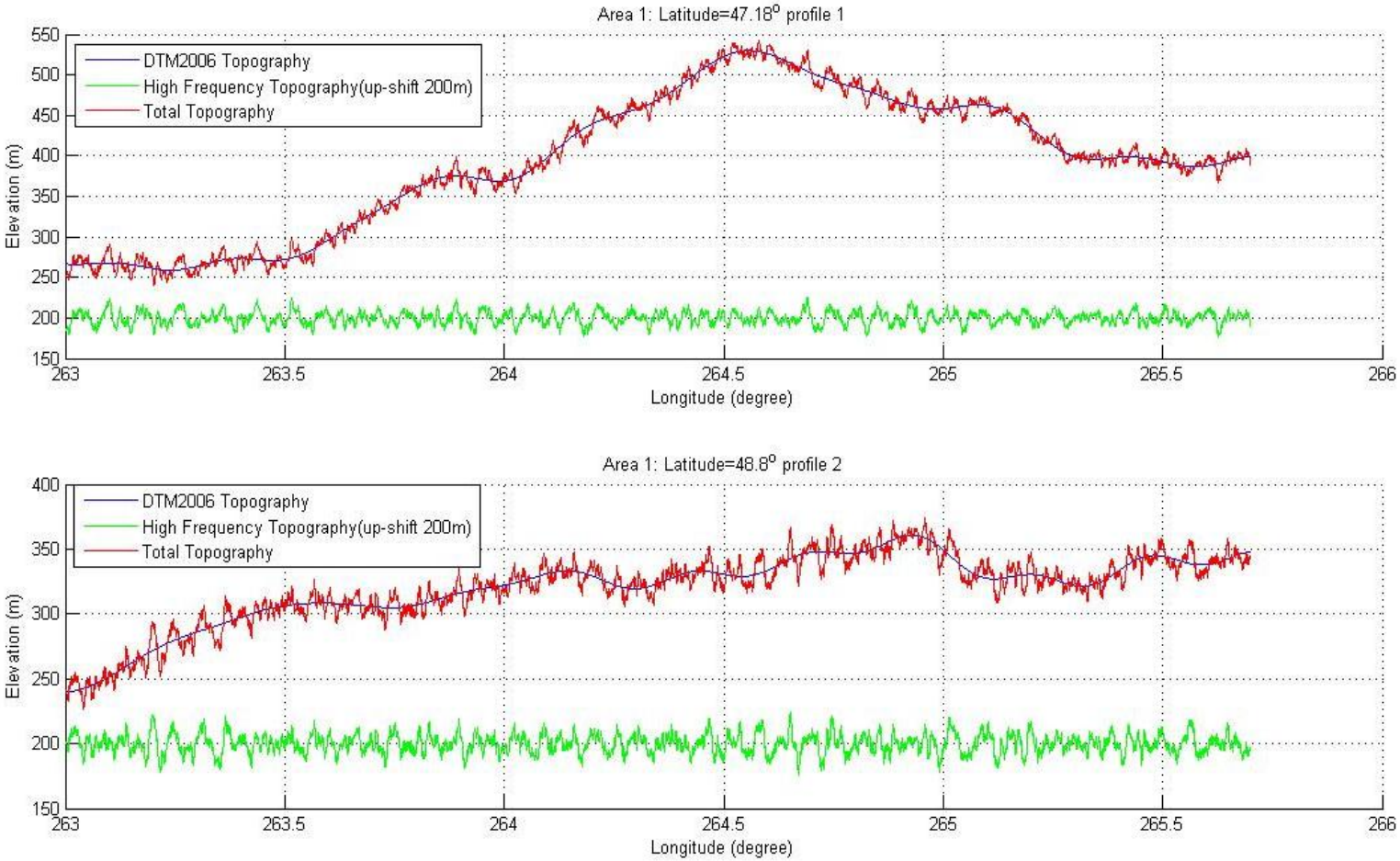

Figure 3.5 Two profiles for DTM 2006 5′ topography and simulated 20 m resolution topography for Area 1_a using PSD of Area 1

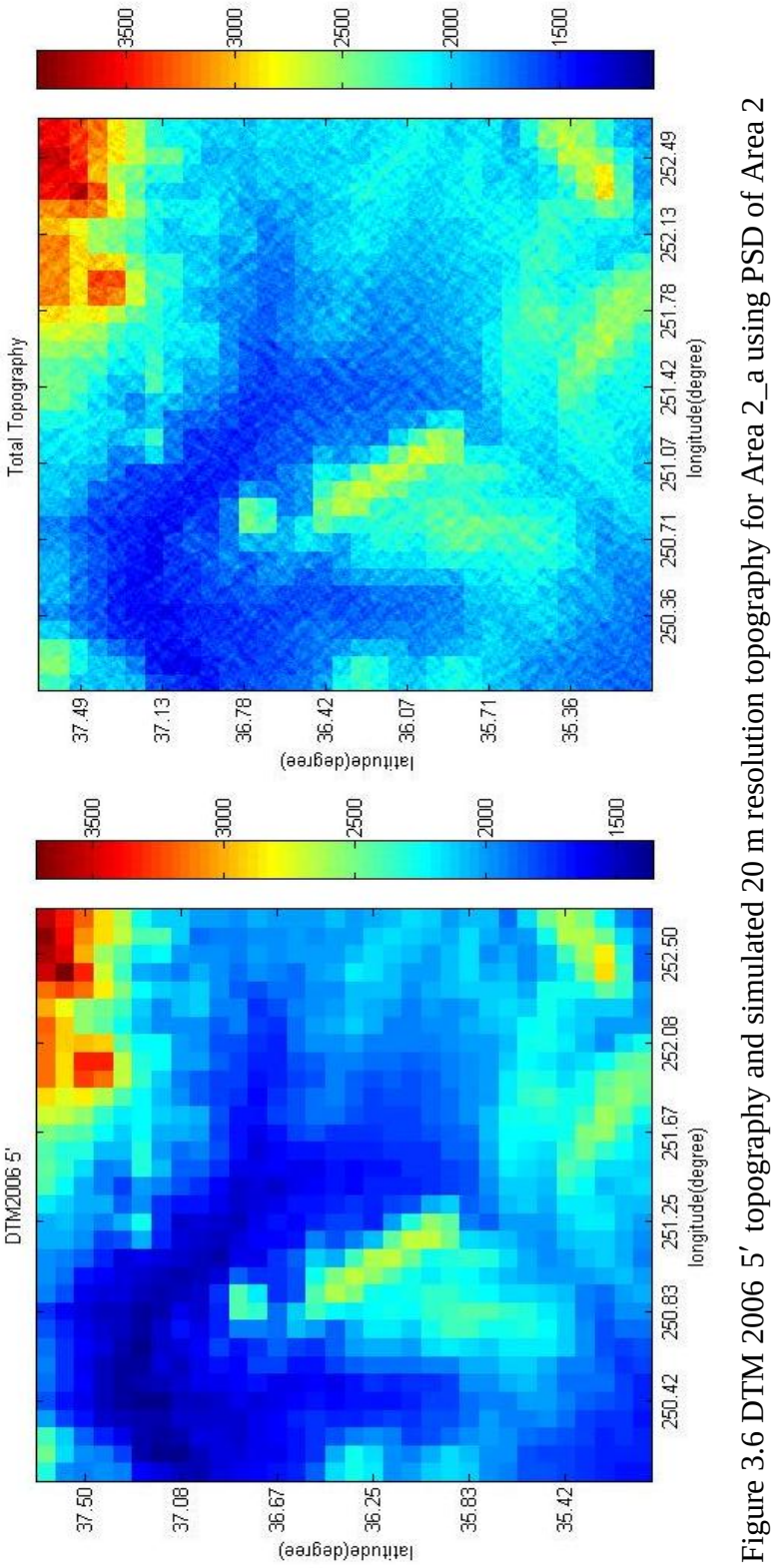

Figure 3.6 DTM 2006 5′ topography and simulated 20 m resolution topography for Area 2_a using PSD of Area 2

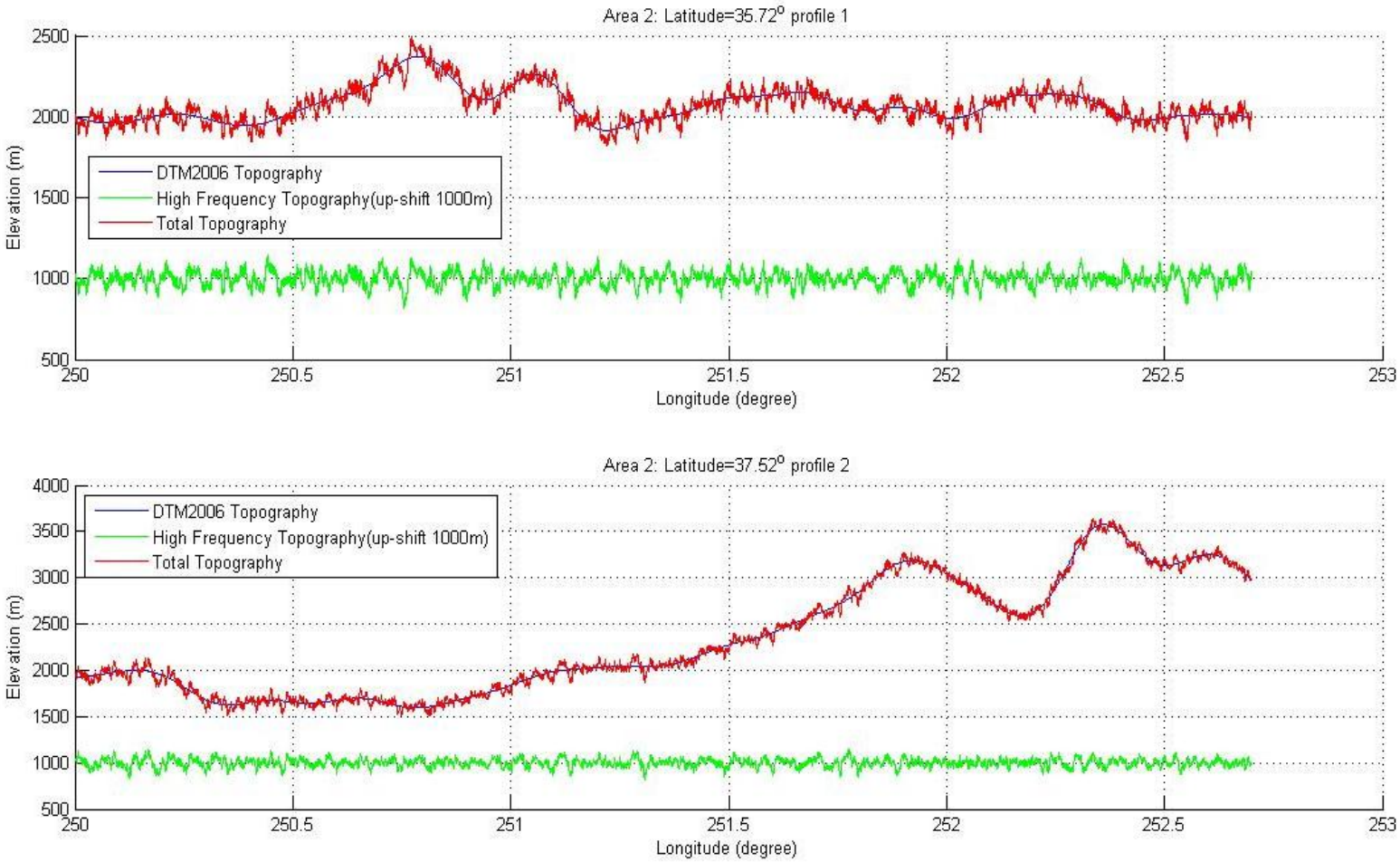

Figure 3.7 Two profiles for DTM 2006 5′ topography and simulated 20 m resolution topography for Area 2_a using PSD of Area 2

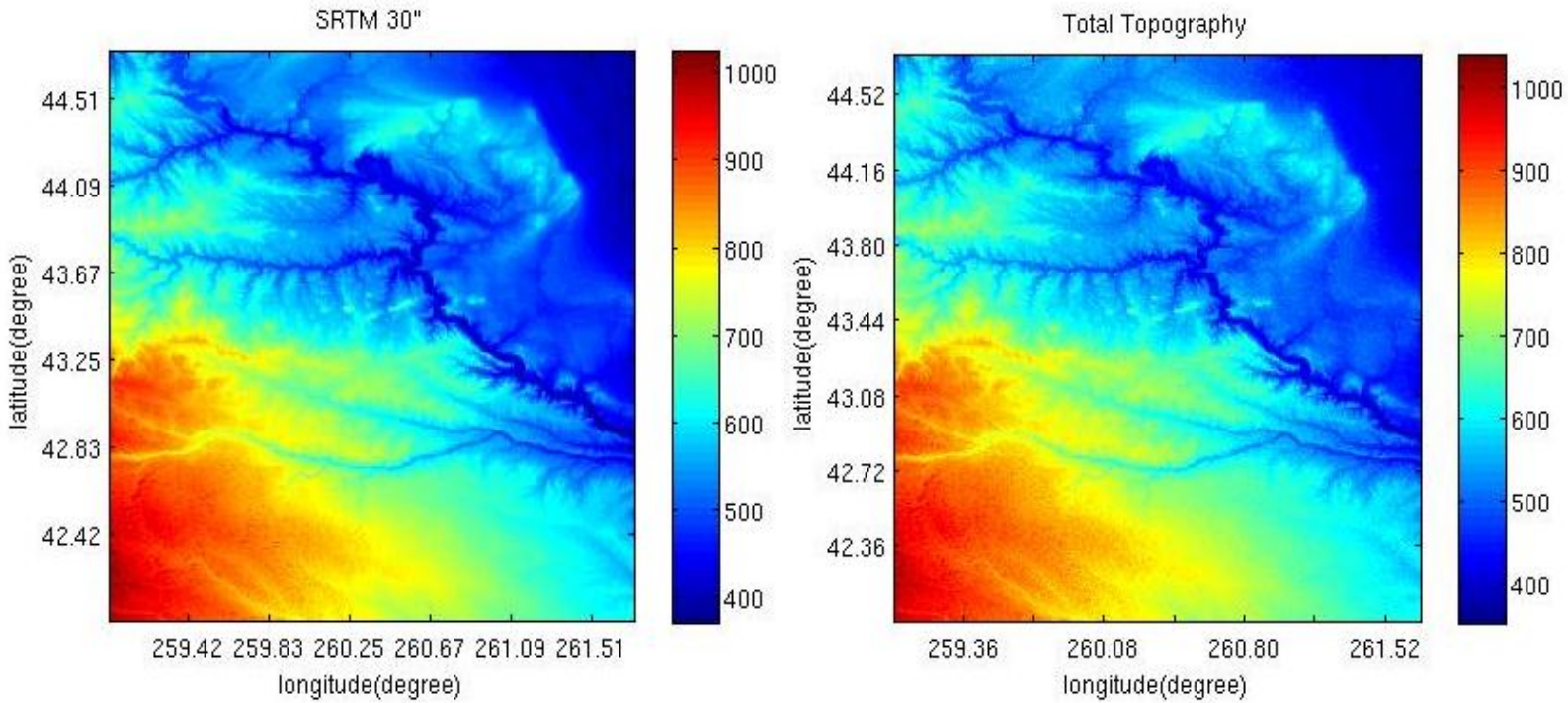

Figure 3.8 SRTM 30" topography and simulated 20 m resolution topography for Area 1_b using PSD of Area 1

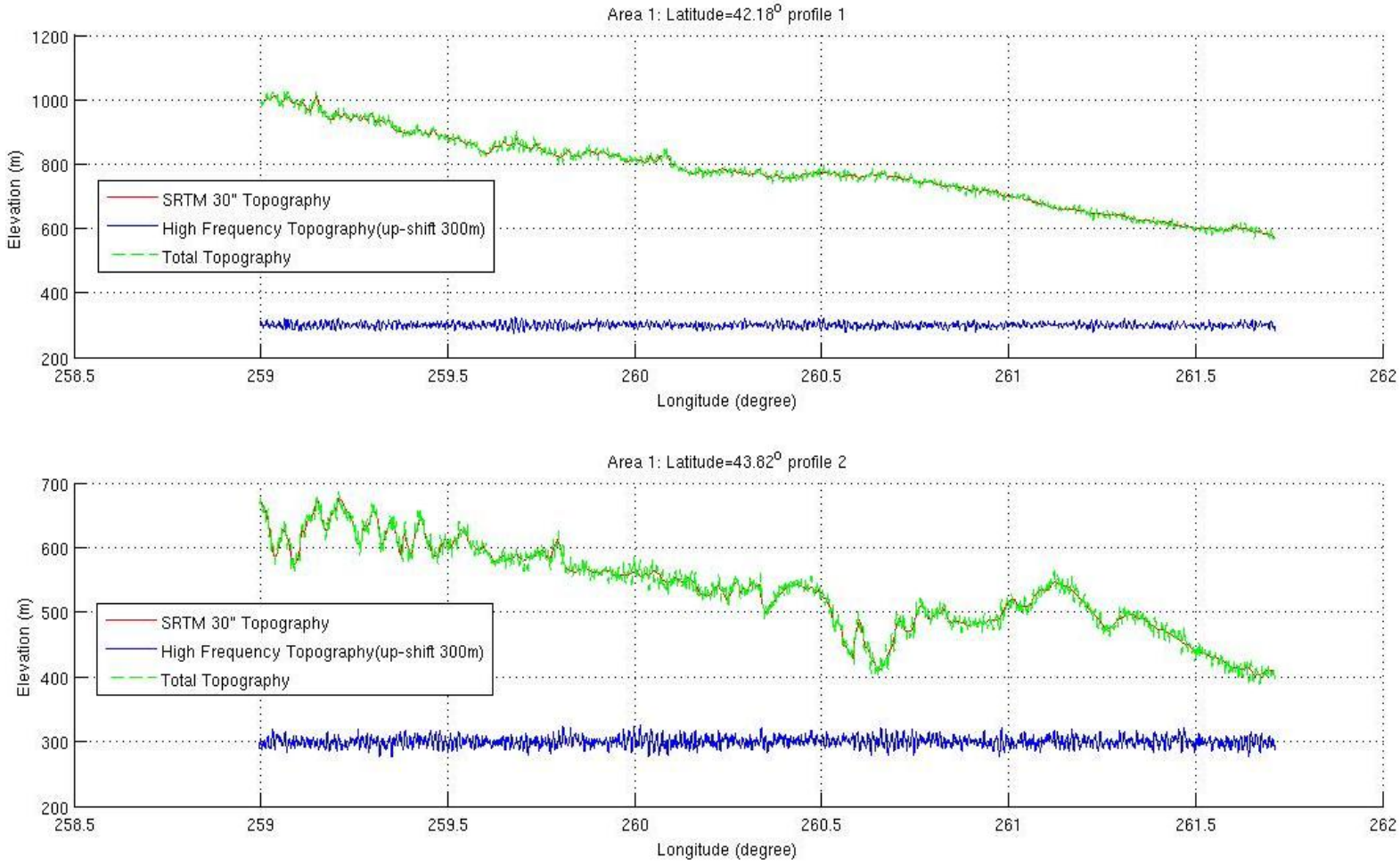

Figure 3.9 Two profiles for SRTM 30" topography and simulated 20 m resolution topography for Area 1_b using PSD of Area 1

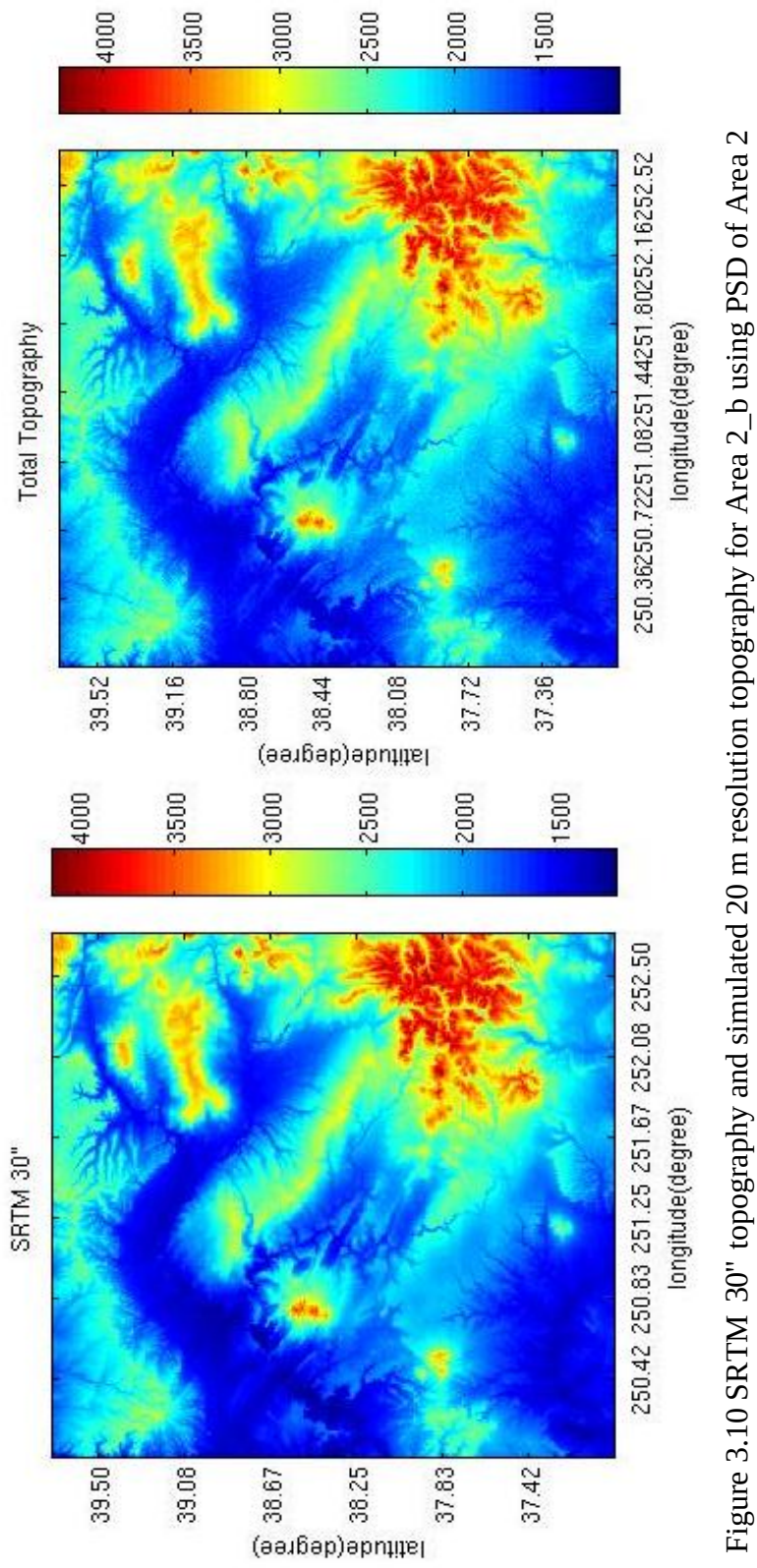

Figure 3.10 SRTM 30" topography and simulated 20 m resolution topography for Area 2_b using PSD of Area 2

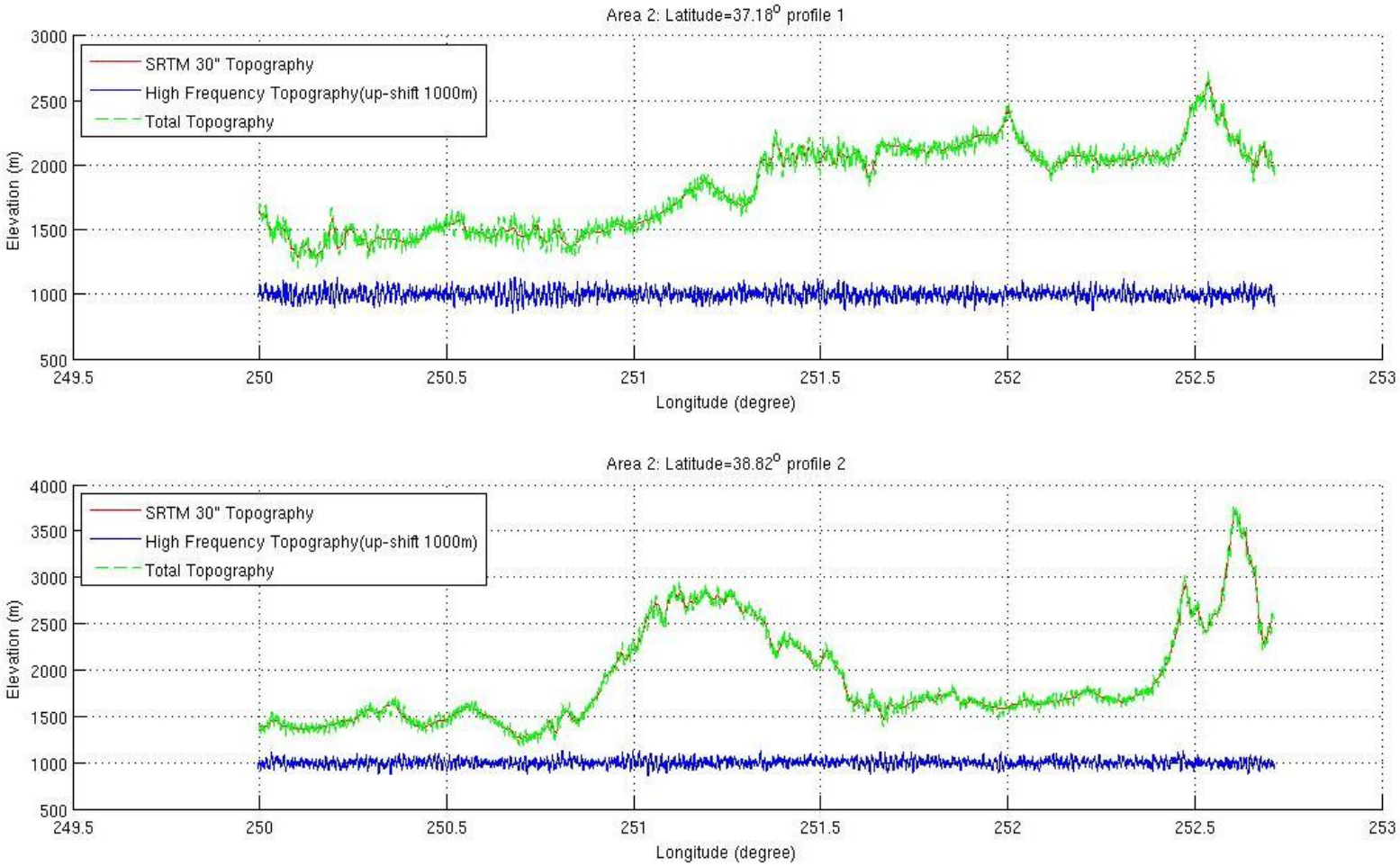

Figure 3.11 Two profiles for SRTM 30" topography and simulated 20 m resolution topography for Area 2_b using PSD of Area 2

It can be seen from the above figures that the data (low frequency part of topography) provide the information needed to determine the PSD model and act as the smooth part of topography in the simulated results. If the data include higher frequency information (which also means less simulated topography), the better is the total simulated topography. This explains why the topography simulated from the SRTM 30″ DEM data looks much better than from the DTM 2006 5′ data. Also it can be seen that the rough Area 2 has larger magnitude for high frequency topography than the smooth Area 1 because the PSD of h for high frequency has larger magnitude in rough Area 2 than in planar Area 1.

In order to know how reasonable our simulated topography is, for our selected Area 1_a, we simulated the topography up to resolution 30" on top of the DTM2006 5' data; also we simulated the topography up to resolution 3" on top of the SRTM 30" data. Then we compared these to the real SRTM data which has the same resolution as our simulated topography. These comparisons for Area 1_a are shown in Figures 3.12, and 3.13. A West-East profile at latitude 47.33^{o} of Figure 3.12, 3.13 is shown in Figures 3.14, and 3.15. It can be seen that our simulation is closer to real data when simulation starts with higher frequency data, i.e., simulated topography based on SRTM 30" data is better than based on DTM2006 5" data. Also the topography simulated in relatively rough areas is better than in flat areas. It is because our simulation is based on the stationary property of the high frequency topography signal, whereas, from the actual data we can see that the topography signal at high frequencies is not stationary, especially at the boundary between rough area, flat area and lake area. To improve the simulation results, two kinds of methods can be applied. In the first method we can smooth the simulated topographic signal for different subareas thus further simulating a kind of non-stationarity. In the second method we can divide the large simulation area into several subareas based on the topographic characteristics of flatness, such as flat or mountainous. Each subarea includes only one kind of topography and the stationarity can be assumed to hold within each subarea, while the stationarity between these subareas does not hold. The covariance models of PSD are fitted with the empirical data of each subarea, respectively, and then we simulate the topography for each subarea, respectively. Finally, the total topography is obtained by combining the simulation results of these subareas. However we did not apply such methods in our truncation error computations by geostatistical analysis, which may affect the validity of the results in applications where significant non-stationarity exists.

By using this latter method, we can simulate ultra-high frequency topography (e.g., resolution up to 10 m) based on a model implied by the spectral attenuation of the prior low frequency DEM data. We use this simulated topography to test and verify the

method described in chapter 2 which determines the extent of terrain correction needed for specific applications. This part will be described in the next chapter.

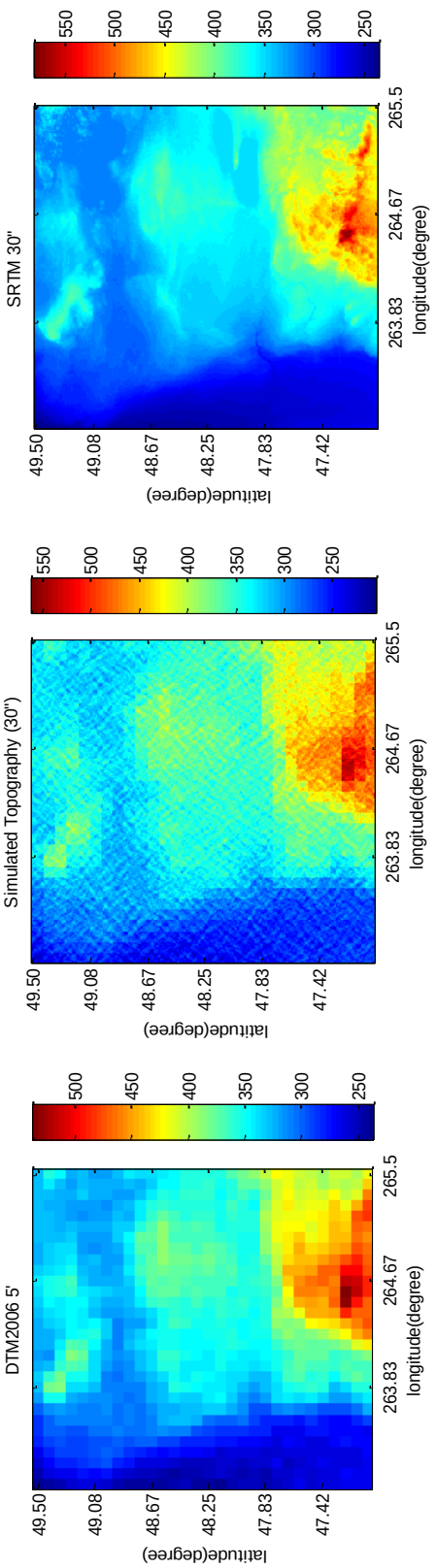

Figure 3.12 DTM2006 5' data, simulated topography and the SRTM 30" DEM in Area 1_a

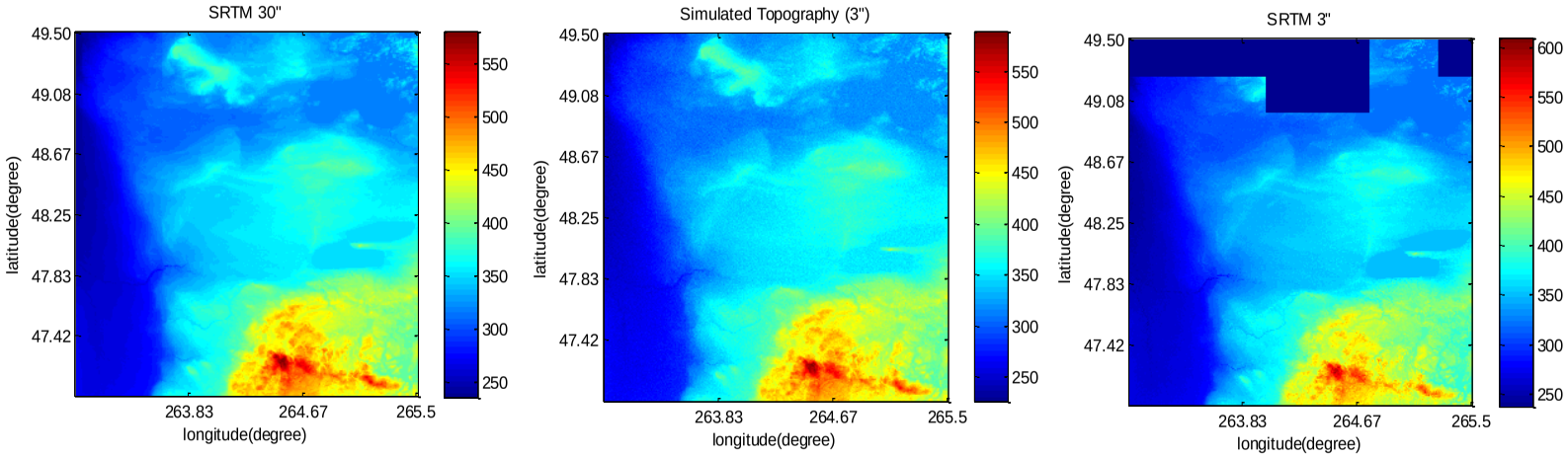

Figure 3.13 SRTM 30" data, simulated topography and the SRTM 3" DEM in Area 1_a

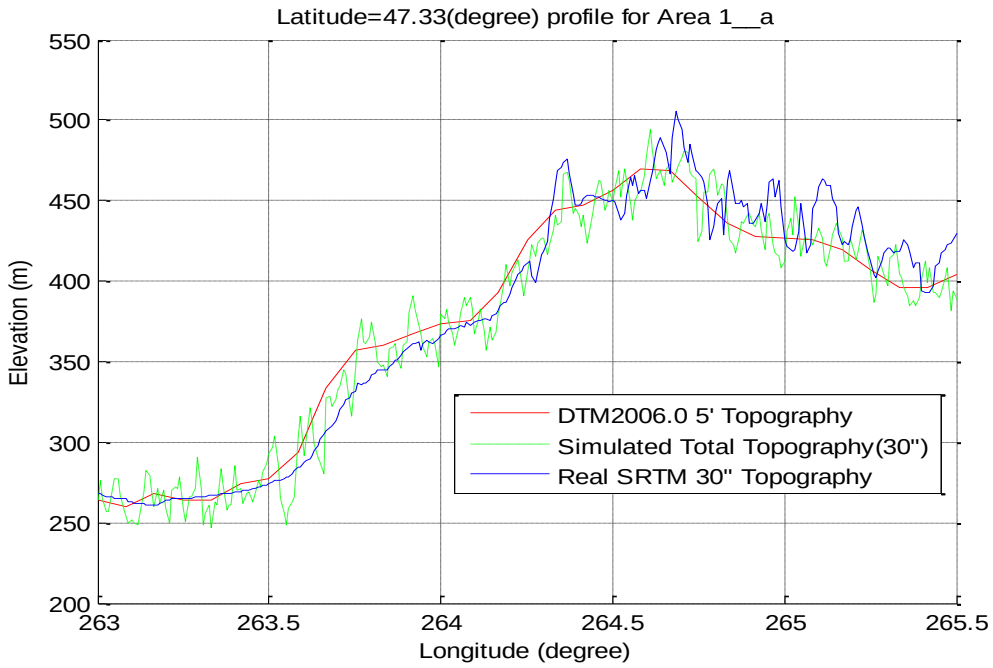

Figure 3.14 Profile of low frequency data, simulated topography, and real topography

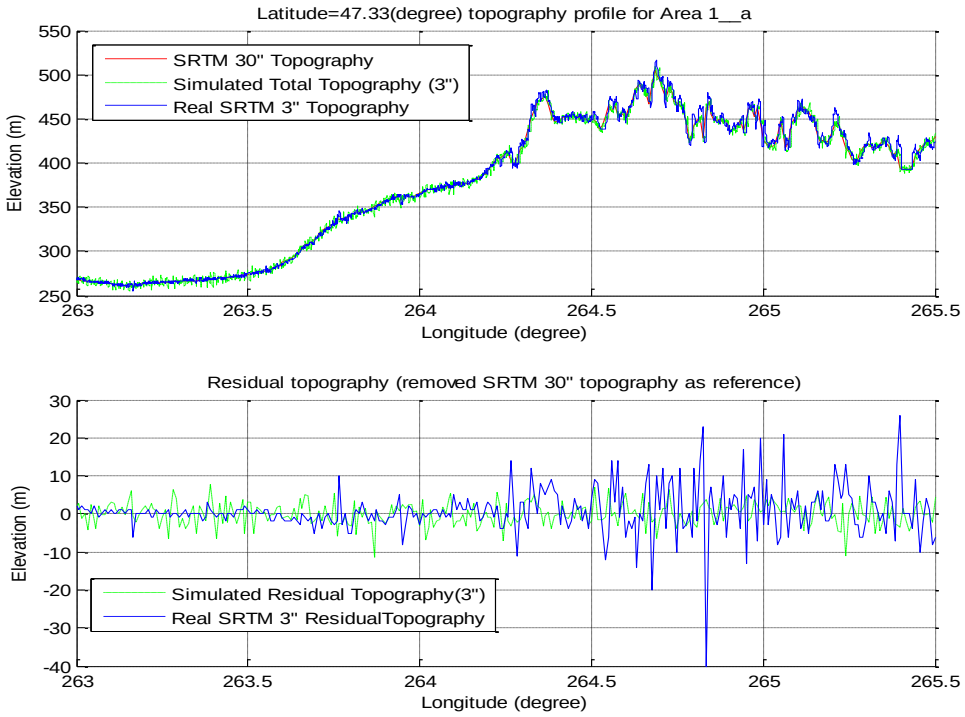

Figure 3.15 Profile of low frequency data, simulated topography, and real topography

Chapter 4

Terrain Correction for Ground-based and Airborne Gravity Gradiometry

4.1 Truncation error verification by deterministic method

In this section, we will verify the geostatistical methods by comparing with the deterministic method. The geostatistical method which we described in chapter 2.2.2 uses the statistics of the residual topography data or the geostatistics of our simulated topography to compute the variance of the truncation error. The deterministic method applies the analytical right rectangular prism method to the topography directly and computes the truncation error in space domain. Then by applying a Monte Carlo analysis, that is, by repeating the computation many times (such as, 1000 times) to get a large sample. Thus the variance of the truncation error is computed statistically based on the sample. In chapter two, we developed the geostatistical method where the data extent of the terrain correction can be determined by setting the criterion such that the truncation error is smaller than the typical gravity gradiometry instrument error, provided that we neglect other errors first. Since gravity gradients are very local signals, also for our application of subsurface detection, we need to quantify the extent of needed topographic data for the terrain correction of gravity gradients for a small observation area, say several hundred meters or a few kilometers. To aid in this investigation we also developed a method to simulate the ultra-high resolution topography based on the reciprocal distance covariance model that is constructed from given low, as well as high resolution data. In order to verify the procedure of extent determination using the geo-statistical method for local gravity gradiometry, i.e., to verify the variance of truncation error, we need to compare it with the actual error variance determined by the deterministic method using the simulated topography.

First, we use the method described in chapter three to simulate topography with the resolution of 1 meter. The PSD covariance model was fitted to the low resolution SRTM 30″ and high resolution SRTM 1″ DEM data in Area 1 (Figure 4.1) and the parameters used for the reciprocal distance covariance model are listed in Table 4.1. Although the table gives the all parameters corresponding to whole frequencies, we only use the parameters which represent the high frequency part (higher frequency than 1″ DEM) of the covariance model to simulate the topography. The simulated 1 m resolution

topography (over an area, 3 km by 3 km) is shown in Figure 4.2 together with the SRTM 1″ DEM and also two profiles are shown in Figure 4.3, respectively.

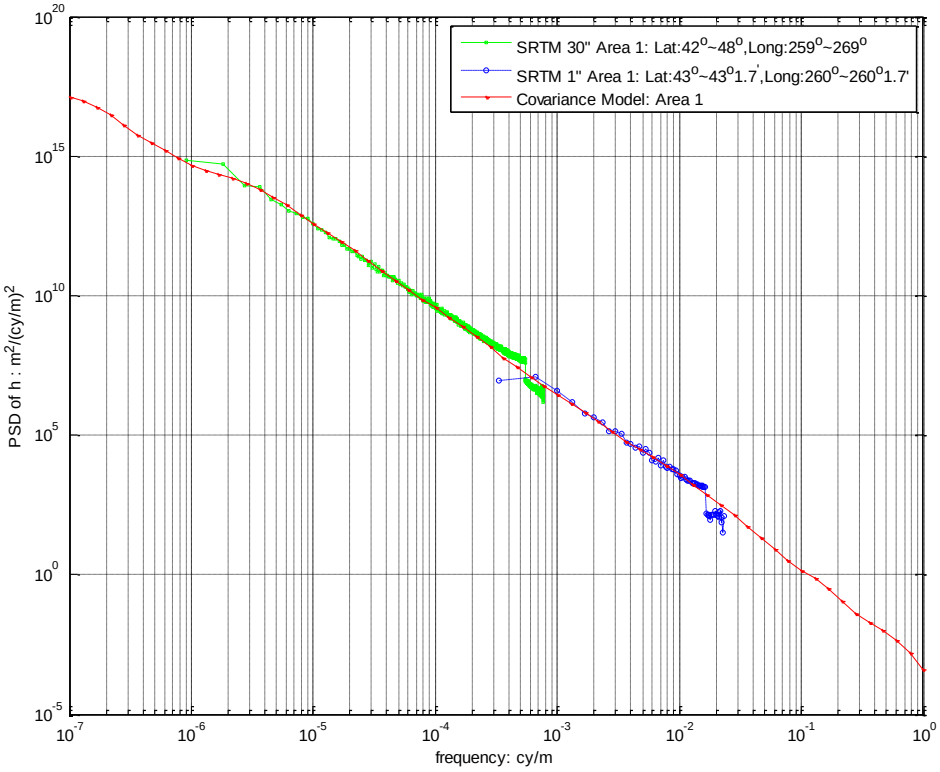

Figure 4.1 PSD covariance model with empirical PSD

Table 4.1 Parameters of Reciprocal Distance Covariance model for Area 1

j	σ^2 (m^4/s^4)	α (1/m)
1	1×10^{5}	3×10^{-7}
2	3.3×10^{3}	9.69×10^{-7}
3	1.3×10^{2}	4.76×10^{-6}
4	3.24×10^{1}	8.94×10^{-6}
5	3.4	2×10^{-5}
6	3.205×10^{-1}	4.48×10^{-5}
7	2.01×10^{-2}	1×10^{-4}
8	2.53×10^{-3}	2.25×10^{-4}
9	1.59×10^{-4}	5.03×10^{-4}
10	9.97×10^{-5}	1.13×10^{-3}
11	1.565×10^{-6}	2.52×10^{-3}
12	7.86×10^{-8}	5.64×10^{-3}
13	1.482×10^{-8}	1.26×10^{-2}
14	9.3×10^{-10}	2.83×10^{-2}
15	9.74×10^{-11}	5.93×10^{-2}
16	1.74×10^{-12}	2.08×10^{-1}
17	1.8×10^{-14}	8.48×10^{-1}

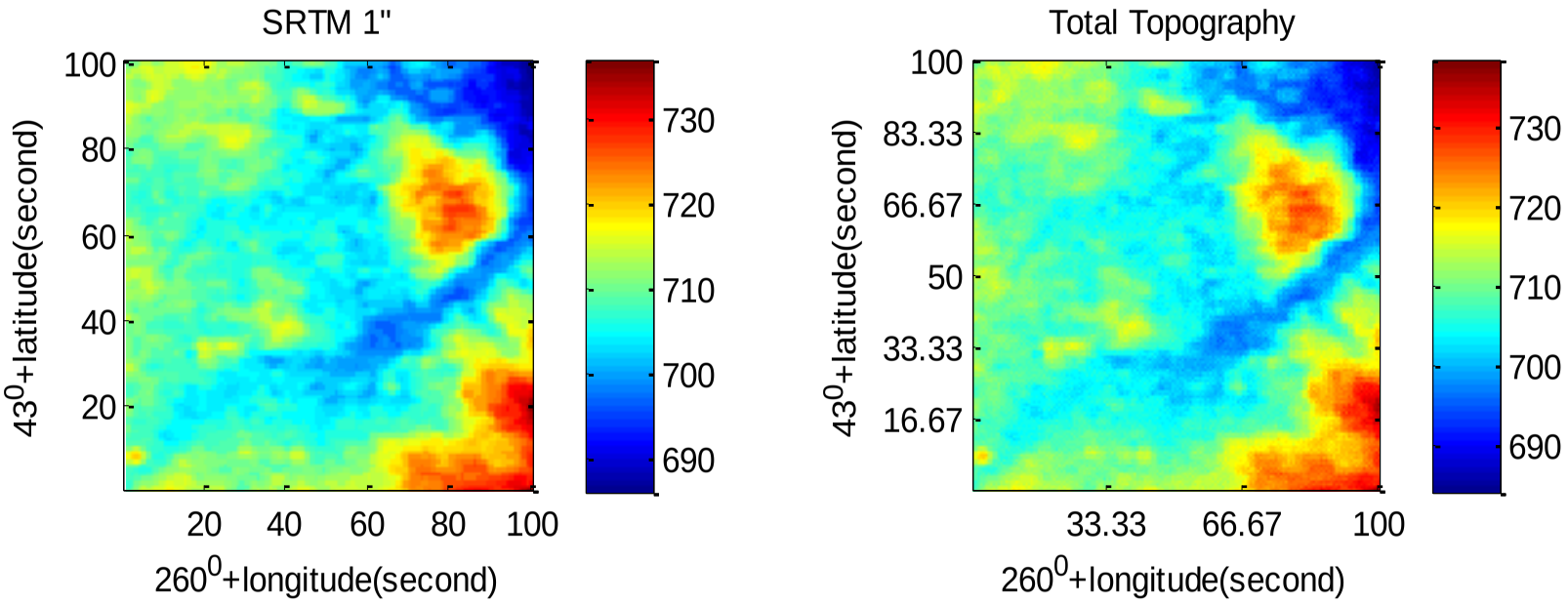

Figure 4.2 SRTM 1″ DEM and simulated 1 m resolution topography

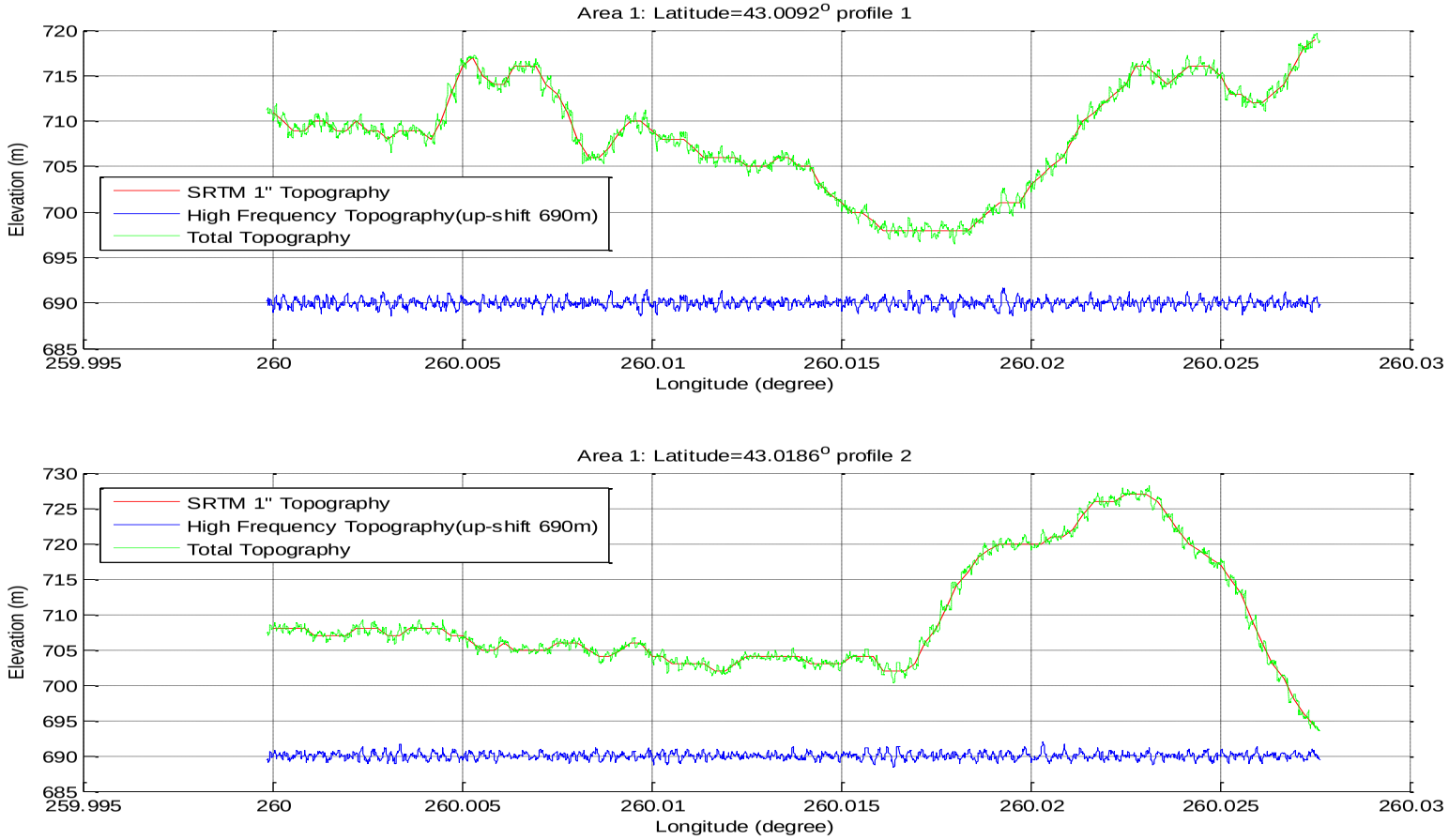

Figure 4.3 Two profiles for SRTM 1″ DEM and the simulated 1 m resolution topography

We apply the geostatistical procedure of Chapter 2 to compute the truncation error variance on the basis of this simulated topography. This means that we determine the covariance model for the truncation error for each truncated area according to equation (2.84). Then, the variance of the error is the covariance at zero distance, and the variance of the error difference between two neighboring points is given by equation (2.86). The results of the truncation error variance on the basis of this simulated topography are listed in Table 4.2, 4.3. In this way, we determine the extent of topographic data needed to make sure the variance of truncation error is smaller than the variance of instrument error, for example, 0.01 E^2. Also we can determine the needed extent of topography data for a pair of points through the variance of truncation error difference.

Through the analysis in section 4.2, we will find that the extent determined for the truncation error of one point is much larger than the extent determined for the truncation error difference of a pair of points, provided the same criterion is used where the variance of instrument error is 0.01 E^2. Since our simulated topography has only a 3 km by 3 km area, the variance of truncation error for one point will not reach the criterion even if the topography within the whole simulation area is included.

So for these simulated data, we only determine the extent of data for a pair of points separated by a certain distance, for example, up to 500 m, for local gradient observations. That is, in a local gradiometer survey over an area of about 500 m, only the variations in the gradients relative to the mean would be of interest.

The above describes the procedure of using the geostatistical method to compute the variance of truncation error difference (2.86). In this procedure, the FFT method was used to compute the convolution in (2.76) or (2.77) which means that the data are assumed to be periodic with period 3 km. For the observation point near the edge of the simulated area, the correction area is still 3 km by 3 km (determined by the kernel function area) and centered on the observation point. In effect, this will make the total topography area 6 km by 6 km which is achieved by the periodicity.

On the other hand, the deterministic method was also used to compute the the truncation error difference for a pair of points using the prism summation model described in chapter 2.2.1 in order to verify the above geostatistical method. Then the variance of the error difference was computed using the Monte Carlo method. We first compute the truncation error for one observation point using the simulated topography centered on this observation point, and then the computation was repeated for another observation point. The truncation error difference was obtained by subtracting one truncation error from the other. These two observation points should have the distance of 500 m which is the same as that in the geostatistical method; also the direction along the pair of points should be random. The computation was repeated one thousand times for such a pair of points and then the variance was computed.

It should be pointed out that for the deterministic method, the pair of points selected at random should appear in an area that is consistent with the area of data used in the geostatistical method. Since the simulated 3 km by 3 km topography used in the latter in effect covers an area 6 km by 6 km due to the periodicity assumption of FFT, also the pair of observation points for the deterministic method should be at the center of 3 km by 3 km area extended periodically to cover 6 km by 6 km. Another case is that if real instead of simulated data are used for the computations, they usually will be padded with zeros in order to reduce the cyclic convolution error. To be consistent with the geostatistical method, the errors should also be computed using data in a zero-padded area. Figure 4.4 shows the diagrams of these two cases. For the above two cases, the actual computation area is four times larger than the simulated topography area. So, due to the computation capability and speed of our computer, we set our simulated topography with ultra-high resolution of 1 m to cover only a small area of 3 km by 3 km.

For our verification of the geostatistical method by using the deterministic method, we first select the data area as 1 km by 1 km, and then increase this with steps of 0.5 km until it reaches the whole simulated area of 3 km by 3 km.

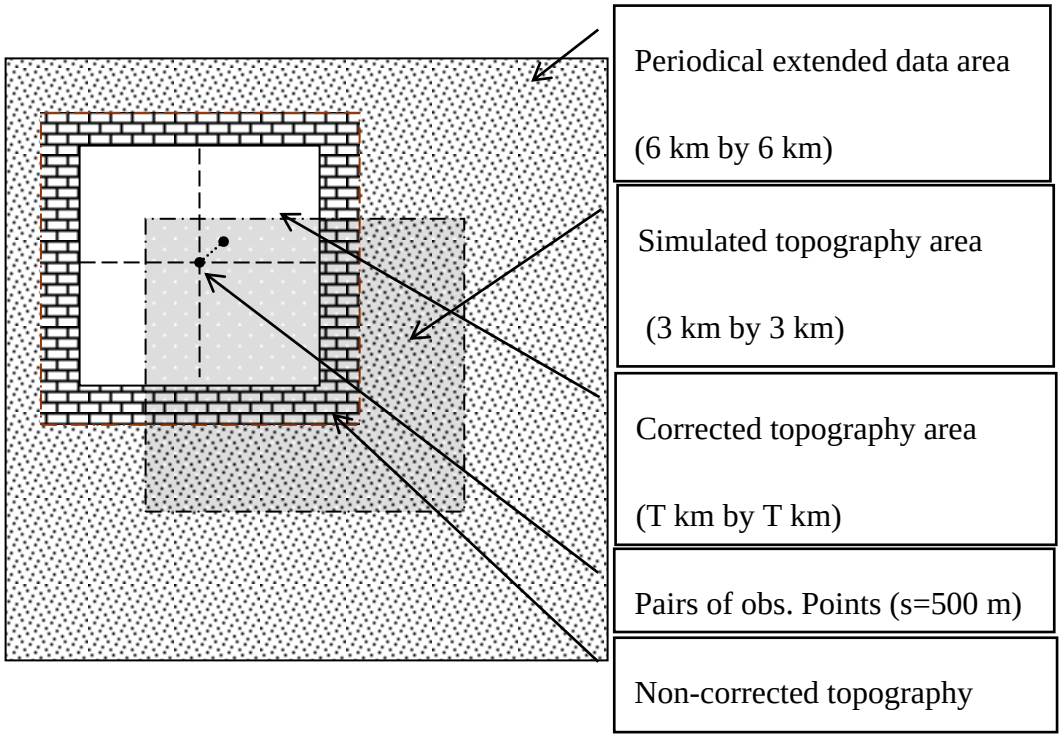

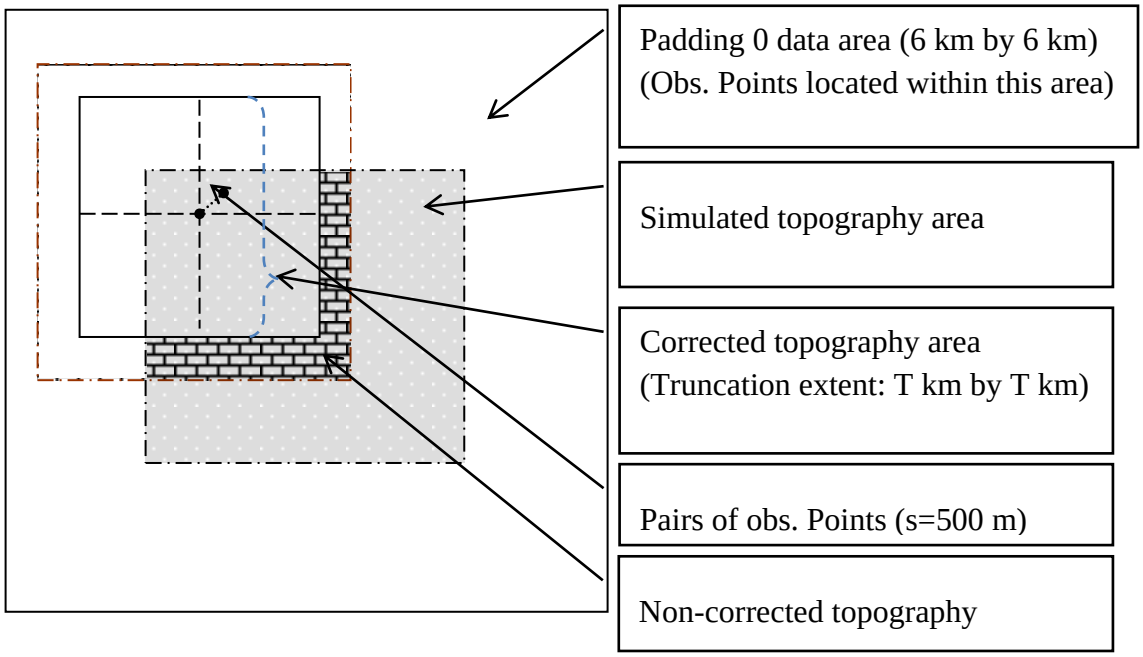

Figure 4.4 Diagram of deterministic method to compute variance of error difference.

The variance of truncation error differences coming from the geostatistical method in section ii of chapter 2.2.2 was compared with that from the deterministic

method described above. Table 4.2 shows results for the case of padding beyond the 3 km x 3 km area by zeros; Table 4.3 shows results for the alternative case of padding data periodically. Both results use the terrain correction for T_{11} as an example.

Data padded by zeros

Extent (km)	Variance (E^2) (truncation error difference)	Variance (E^2)* (actual error difference)
1	3.430	3.638
1.5	0.662	0.700
2	0.156	0.163
2.5	0.0265	0.0256
3	0	0

Table 4.2 Case 1: Variance of geostatistical method VS deterministic method

Data padded periodically

Extent (km)	Variance (E^2) (truncation error difference)	Variance (E^2)* (actual error difference)
1	8.875	8.730
1.5	0.9798	0.9776
2	0.2502	0.2562
2.5	0.1004	0.1069
3	0	0

Table 4.3 Case 2: Variance of geostatistical method VS deterministic method

* denote the results based on 1000 random Monte Carlo samples

From the above results, it can be seen that the truncation error variances from the geostatistical analysis are consistent with those from the deterministic method. Here the good agreement is due to the fact that we compute the variance of truncation error using topography that is simulated with the same PSD that is used for the geostatistical method. Also it is confirmed that the two methods yield consistent results for other distances between points. Therefore we confirm that our method of determining the extent of terrain correction is correct by using the geo-statistical method and the corresponding procedure described in chapter two. Also, if we pad data periodically instead of with zeros, the variance we get is larger due to the extra signal that contributes to the truncation error beyond the data area. As the extent increases, the excluded area becomes smaller, so the variance will also be smaller correspondingly. If we wish the variance of the truncation error for a pair of points with distance separated by 500 m to be smaller than 1 E^2 as our criterion, then the minimum extent for this simulated case should be 1.5 km. The truncation effect of the topography beyond this extent is larger for a single

observation point, but most of this just act like a bias, when considering a pair of points. The above conclusions are obtained for the topography we simulated in Area 1, which is a relatively smooth area; if the topography has another character, the consistency between the two methods still holds; however the values of the variances would be different.

4.2 Extent of terrain correction for ground-based gravity gradiometry

Now we apply the geostatistical method described in chapter 2.2.2 to determine the extent of terrain correction required for a possible set of ground-based gravity gradiometry observations. Since we compute only the truncation error or its variance, the integration area excludes a certain area around the observation points; and thus, since the integration source point will not approach the computation point, there are no convergence issue for the series developments in chapter 2, specifically (2.31), (2.32).

The DEM we select to compute the terrain is the SRTM 3″ DEM (about 90 m resolution) within an area of latitude: 35°N~40°N and longitude: 110°W~105°W. The terrain elevation data were downloaded from website "http://srtm.csi.cgiar.org/SELECTION/inputCoord.asp". The location and image of the DEM data are shown in Figure 4.5. The residual topography is computed for the ground reference plane at altitude of 2317.2 m which is the average altitude of the DEM area.

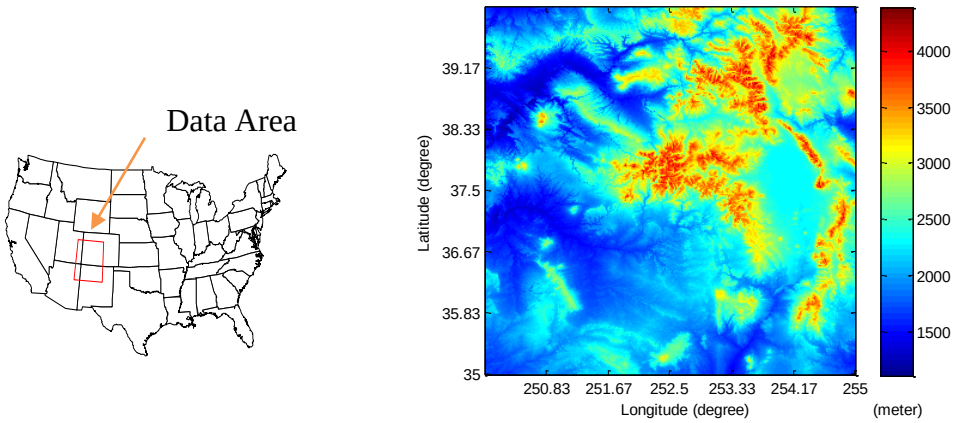

Figure 4.5 SRTM 3″ DEM data for ground gravity gradiometry

When we compute the truncation error variance for the terrain correction using the geostatistical method, we expand the integral kernel using the Taylor series (2.31) in order to form the convolution and then apply the convolution theorem. Thus we need to evaluate which order of expansion is needed, i.e., determine the maximum n in (2.34). We did a test for T_{33} at one point, as well as for a pair of points separated by 0.9 km, 4.5 km, 9 km, 18 km, 45 km, 90 km, 180 km, 270 km, and 360 km, respectively. The results

were computed for expansions of order one and order four and are shown in Figures 4.6, 4.7. Figure 4.6 for the variances at one point shows that the difference between these two orders is only 10^{-2} E^2 for the extent beyond 80 km; and it is even smaller for pairs of points, as shown in Figure 4.7. Therefore, the Taylor series expansion up to order one is enough for the extent determination. It should be pointed out that neglecting terms in Taylor expansion of order higher than one is only reasonable for the determination of the terrain correction extent. If we also want to compute the terrain correction using Taylor expansion of order one, then the method (v) in chapter 2.2.2 must be used, i.e., the inner zone must be computed separately using the prism summation method.

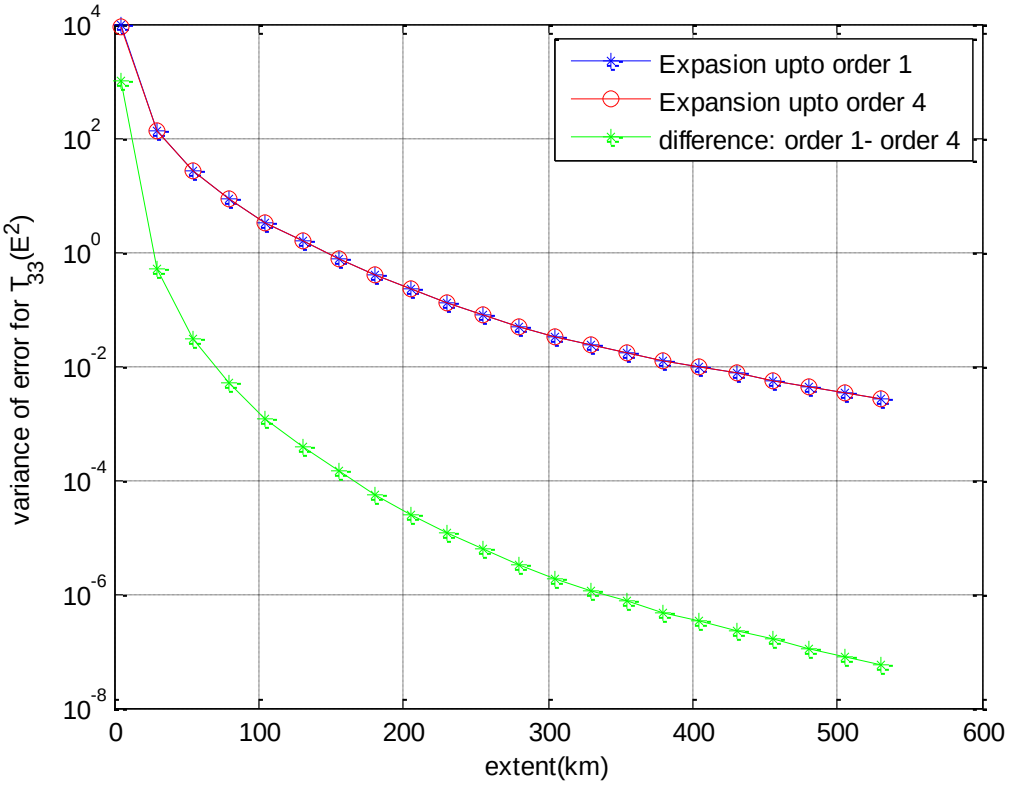

Figure 4.6 Differences of truncation error variances between Taylor expansion order 1 and order 4 for one observation point

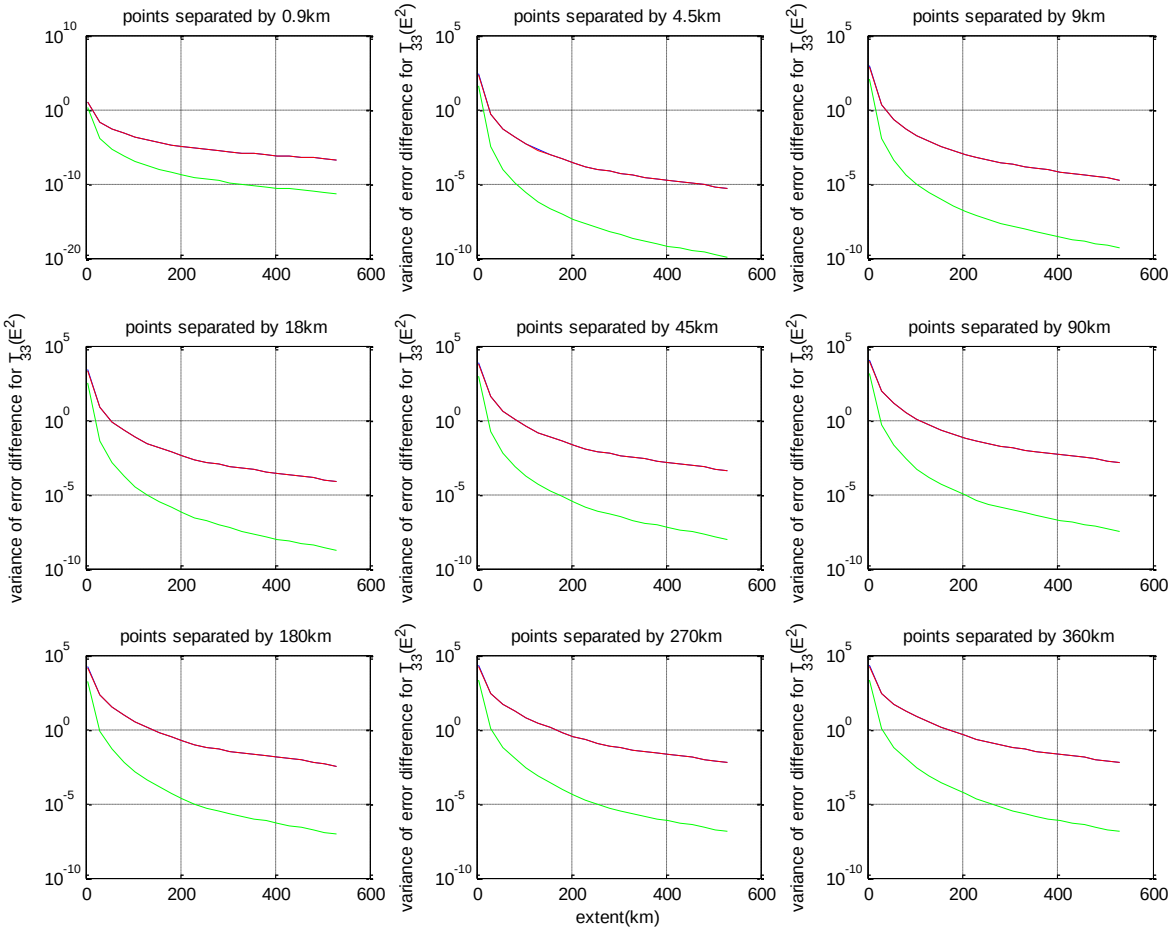

Figure 4.7 Differences of truncation error difference variances between Taylor expansions order 1 and order 4 for pairs of points separated by different distances

Next, the $5^o \times 5^o$ DEM area was divided into 5 concentric sub-areas with side arc lengths $0.4167^o, 0.8333^o, 2.5^o, 4.1667^o, 5^o$, respectively. Then the variance of the truncation error was computed using the given DEM data within each sub-area by applying equations (2.81), (2.82), (2.83), (2.84). The results were plotted versus the extent of terrain correction in the same Figure 4.8 for all 5 sub-areas (T_{33}, for example). The variance of the error is not exactly equal to zero when the truncation extent is equal to the total sub-area. The reason is that we extend the area of the kernel function, $\hat{F}_{jk}^{(n-1)}$, to four times larger than the data area, which means we are assuming there is always terrain outside the data area. If we truncate the kernel function outside the original data area to be zero (which means there is no extra terrain outside the data area), then the variance of truncation error will be very close to zero (see right plot of Figure 4.8).

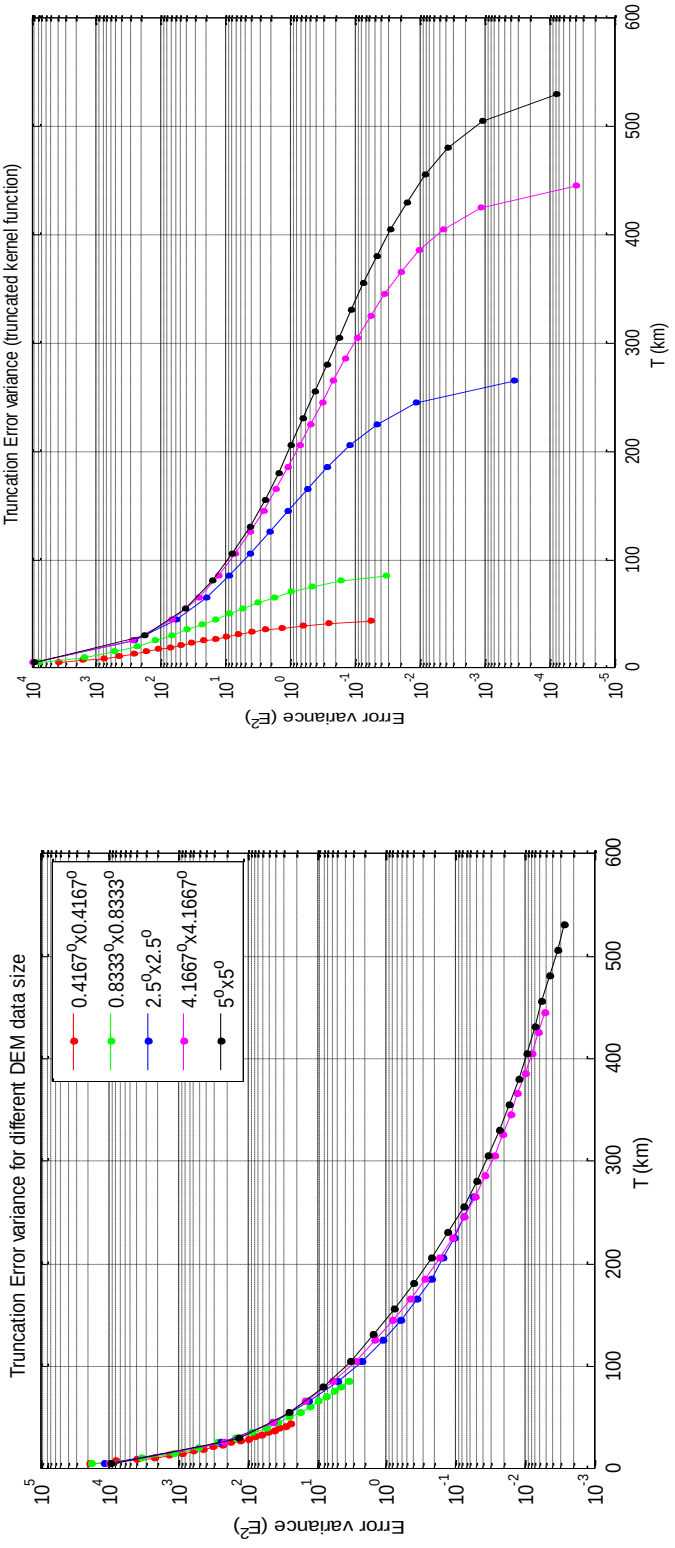

Figure 4.8 Truncation error variance versus extent for different DEM data sizes

It is shown that the extent of the terrain correction needs to reach 400 km in order that the truncation error variance is smaller than 10^{-2} E^2, or 230 km for variance to be smaller than 10^{-1} E^2. It should be noted that these results are obtained for a single observation point. For a pair of points separated by a certain distance the terrain effect mostly cancels, even if the surrounding topography would generate a large terrain effect for one observation point. So if we consider the truncation error difference for a pair of points, then the extent needed will decrease significantly. The variance of the truncation error difference for a pair of points, separated by 0.9 km, 4.5 km, 9 km, 18 km, 45 km, 90 km, 180 km, 270 km, and 360 km was computed and is shown in Figure 4.9, which also shows the variance of the absolute truncation error for one point. It can be seen that the extent needed on the basis of the error difference variance is dramatically smaller than the extent determined from the variance of the total error, especially for points separated by a short distance.

With the separation increasing, the required extent also becomes larger. For example, if we want the variance of the error difference to be smaller than 10^{-2} E^2, then the extent only needs to be 35 km for points separated by 0.9 km, or 85 km for points separated by 4.5 km, etc. These results are obtained for the gravity gradient T_{33}. The results for gravity gradients T_{11}, T_{12}, T_{13}, T_{22}, T_{23} are shown in Figure 4.10 ~4.14, respectively. It is noted that the required extent of the terrain correction for gravity gradients T_{13}, T_{23} are much less than for the other gravity gradient components. It is because in the Taylor expansion of (2.32), $F_{jk}(0) = 0, F_{jk}^{'}(0) \neq 0$ for T_{13}, T_{23} considering (2.26); while $F_{jk}(0) \neq 0, F_{jk}^{'}(0) = 0$ for the other gravity gradient components. $F_{jk}(0)$ is associated with the residual terrain, δh; but $F_{jk}^{'}(0)$ is associated with the higher-order residual terrain, δh^2. Also, from Figure 4.9 ~4.14, it is noted that the error variance for a single point is not always greater than the variance for a pair of points separated by large distance. The reason is that the covariance in (2.86) for a pair of points separated by large distance may be negative in certain cases.

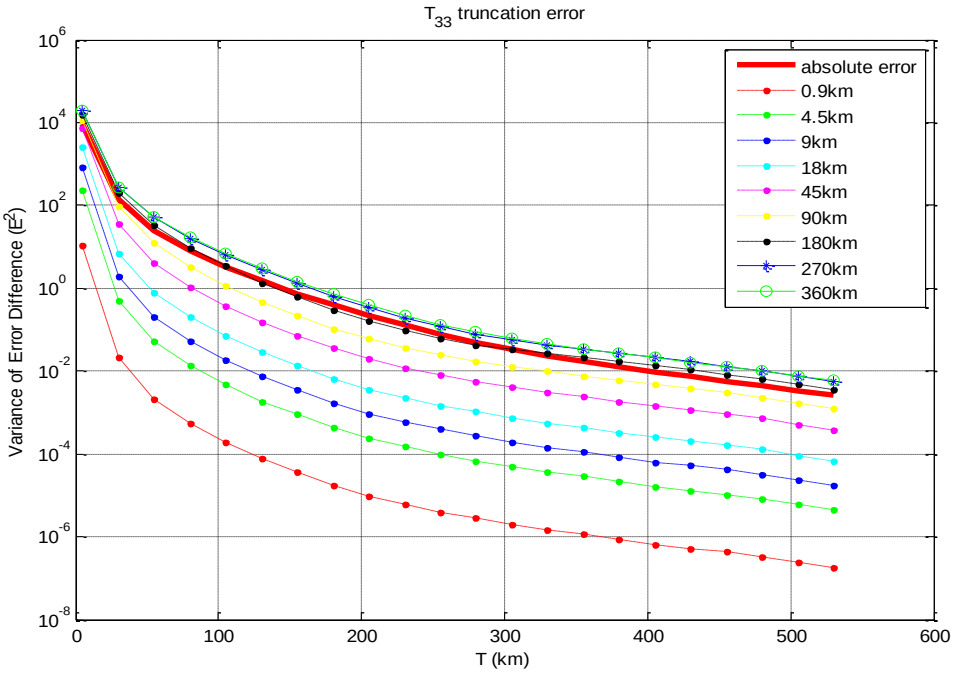

Figure 4.9 T_{33}: Variance of truncation error and error difference for different distance

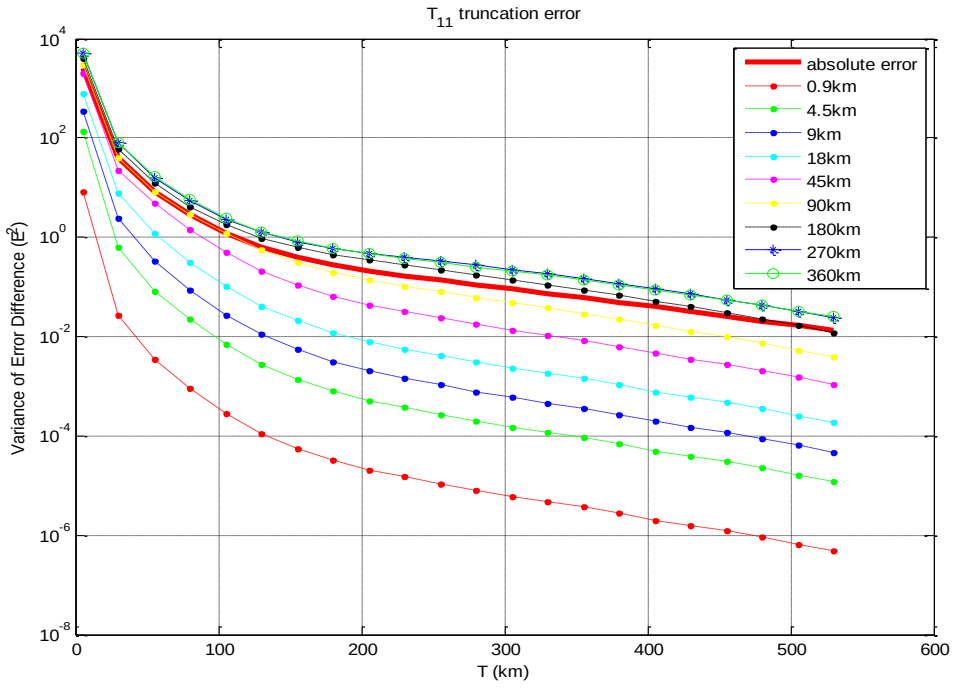

Figure 4.10 T_{11}: Variance of truncation error and error difference for different distance

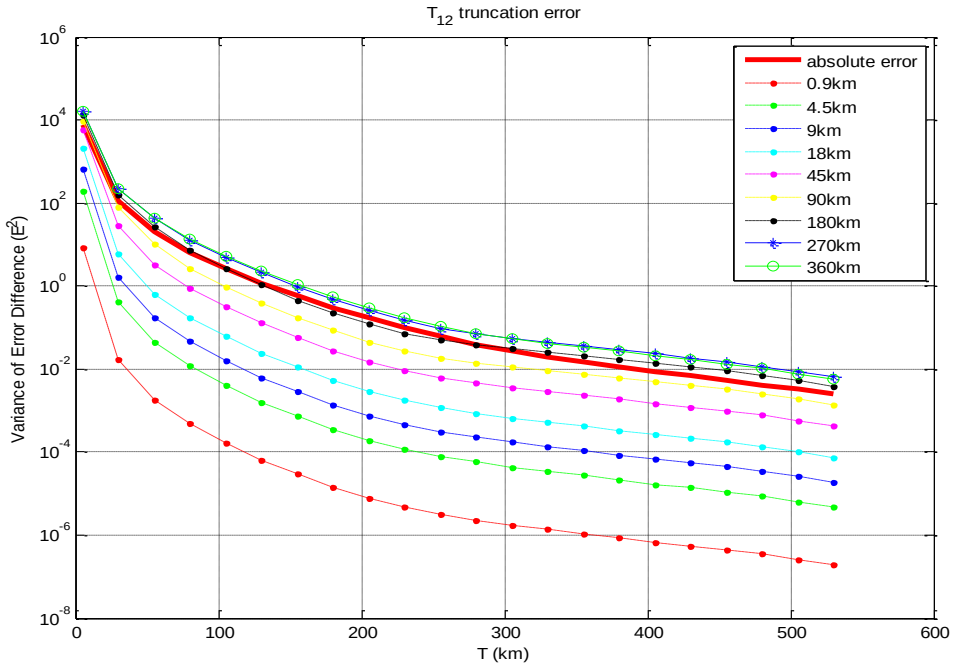

Figure 4.11 T_{12}: Variance of truncation error and error difference for different distance

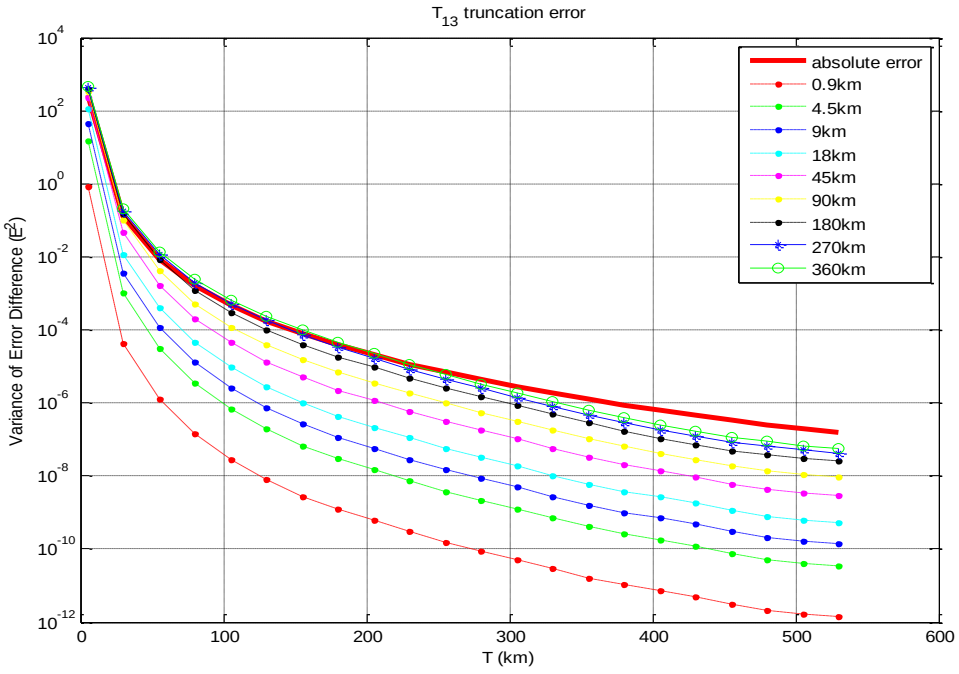

Figure 4.12 T_{13}: Variance of truncation error and error difference for different distance

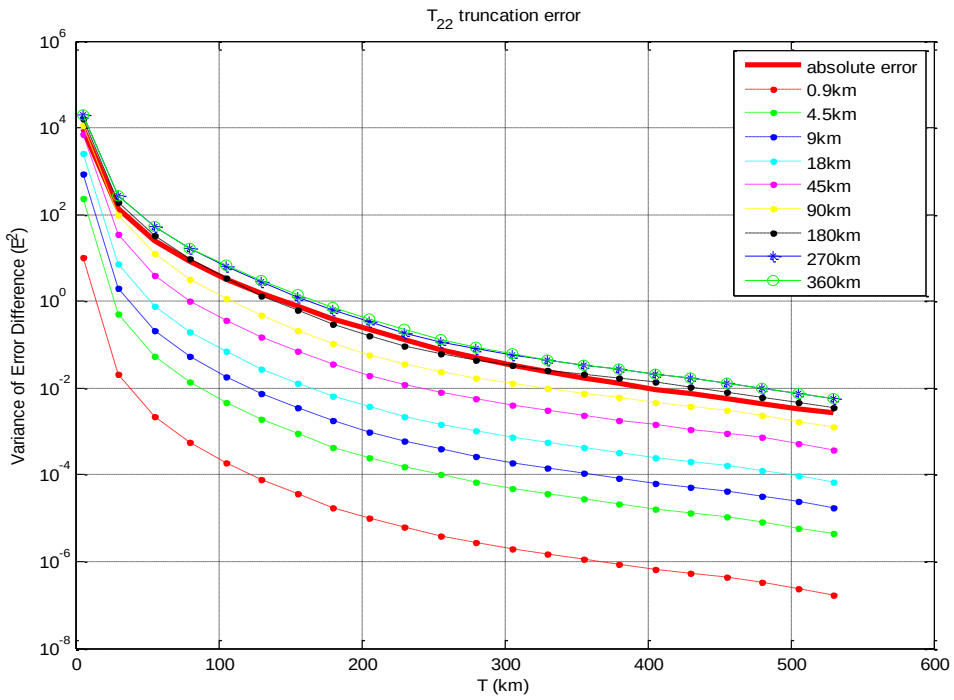

Figure 4.13 T_{22}: Variance of truncation error and error difference for different distance

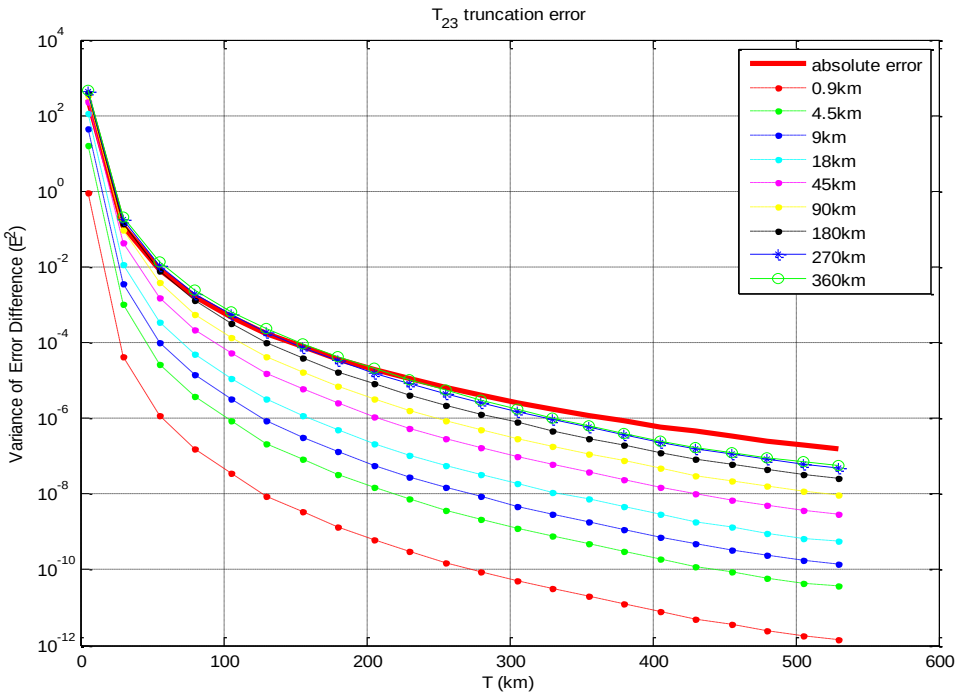

Figure 4.14 T_{23}: Variance of truncation error and error difference for different distance

4.3 Terrain correction for airborne gravity gradiometry

4.3.1 Terrain correction of Air-FTG at Vinton Dome, LA

A survey was done by Bell Geospace Inc. (BGI) using the Air-FTG (Full Tensor Gravity Gradiometry) installed on a BT67 fixed wing airplane in 2008 over the Vinton Dome located in the south-west of Louisiana close to the Texas boarder (Figure 4.15). The flight lines are between latitudes 30.07^{o} ~ 30.23^{o}, and longitudes -93.66^{o} ~ -93.53^{o}.

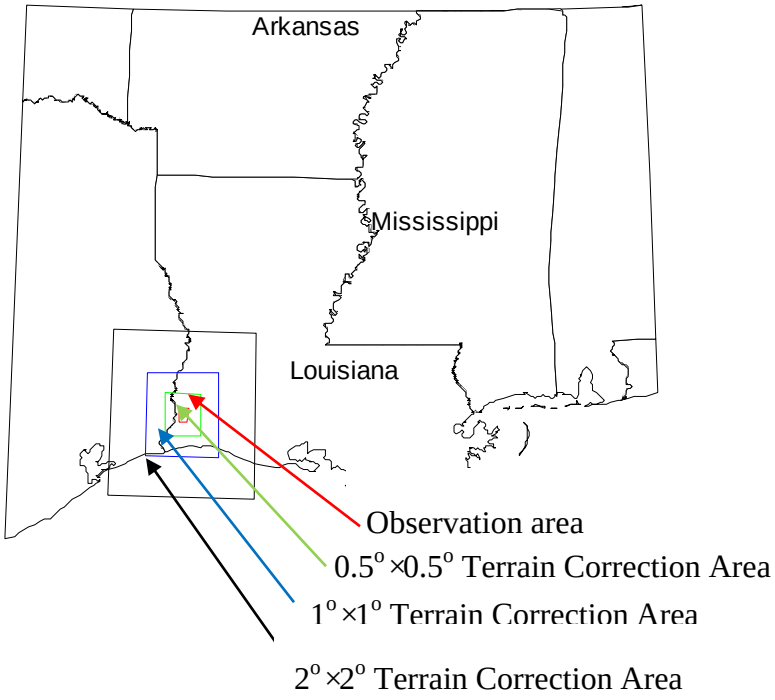

Figure 4.15 Vinton Dome Air-FTG survey locations and terrain correction areas

Figure 4.16 shows the location of the survey lines (South-North flight lines) and tie lines (West-East flight lines). There are a total of 53 survey lines separated by 250 meters and the center 18 survey lines are separated by 125 meters. Each survey line is about 16.7 km long. There are 17 tie lines separated by 1000 meters. Each tie line is about 11.7 km long. The survey area is a relative flat area, so the flight clearance does not vary much. The statistics of the terrain and flight altitude of the survey area are listed in Table 4.4.

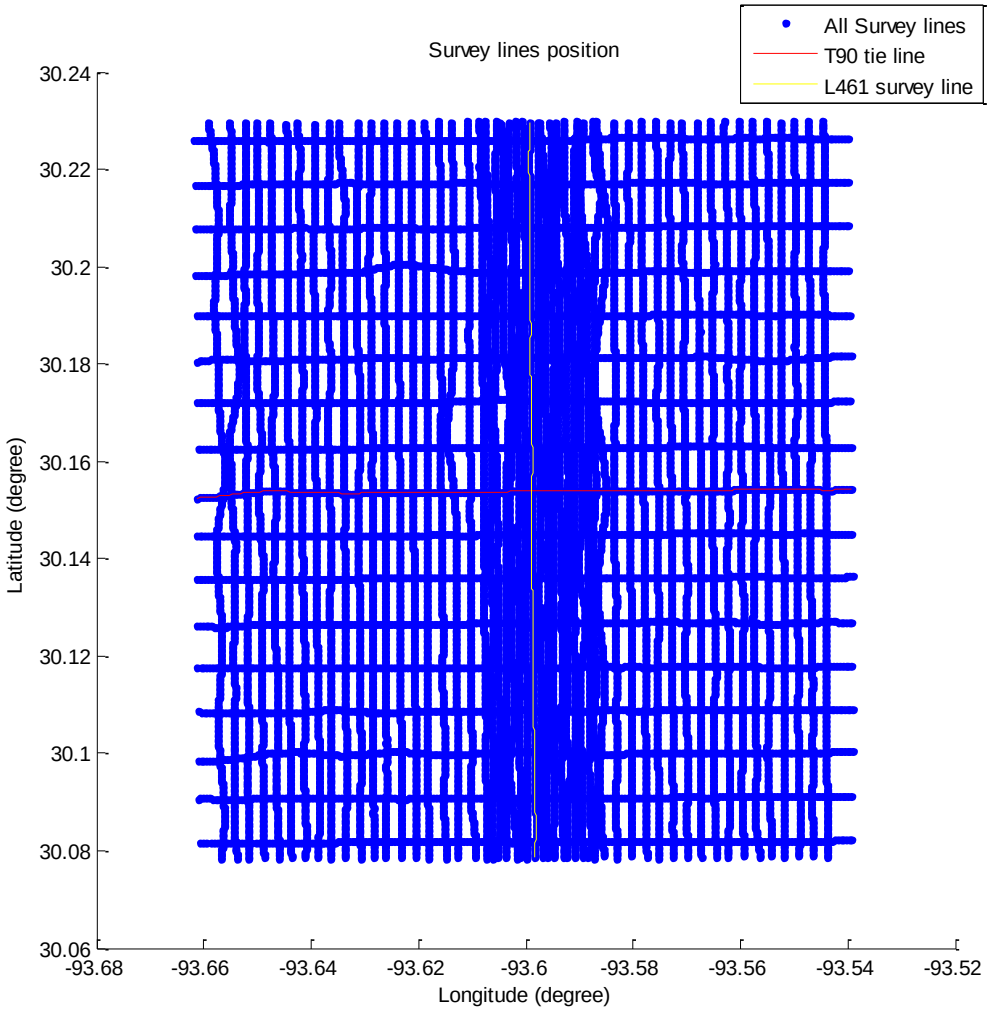

Figure 4.16 Survey line position and two center lines as profile

Bell Geospace computed the terrain correction based on a modeling package that uses 3-D prism to represent the topography. Their computation assumes a density of 1.0 gm/cc, so the true value (assuming constant density) is simply a scaled version of their result. The terrain corrections for gravity and gravity gradients were computed using the topographic mass above the geoid. The terrain data they use is the SRTM 90 m DEM which extends 10 km in all directions beyond the survey area.

	Min	Max	Std. Dev.	Mean
Terrain	-1.81	24.40	4.18	7.30
Altitude	53.55	116.34	8.26	85.17
Clearance	43.88	108.76	7.40	77.87

Table 4.4 Flight altitude statistics (m)

It is of interest to compare our terrain corrections with Bell Geospace's and also to check if the extent of terrain that Bell Geospace used for their terrain correction is reasonable or not under the criterion that the variance of truncation error should be smaller than the variance of instrument error. First, a SRTM 3″ DEM dataset (Figure 4.17) was downloaded from http://srtm.csi.cgiar.org/SELECTION/inputCoord.asp within latitudes: 29.977^{o}~30.323^{o} and longitudes: -93.753^{o}~-93.437^{o}. Then the method (ii) (i.e., space prism summation) in chapter 2.2.1 was used to compute the terrain corrections at the observation positions on the flight line. Figure 4.18 shows the terrain corrections of all gravity gradients for the T90 tie line profile using Bell Geospace's and our results; while Figure 4.19 shows their differences. Figure 4.20 shows the terrain corrections of all gravity gradients for the L461 survey line profile using Bell Geospace's and our results; while Figure 4.21 shows their differences.

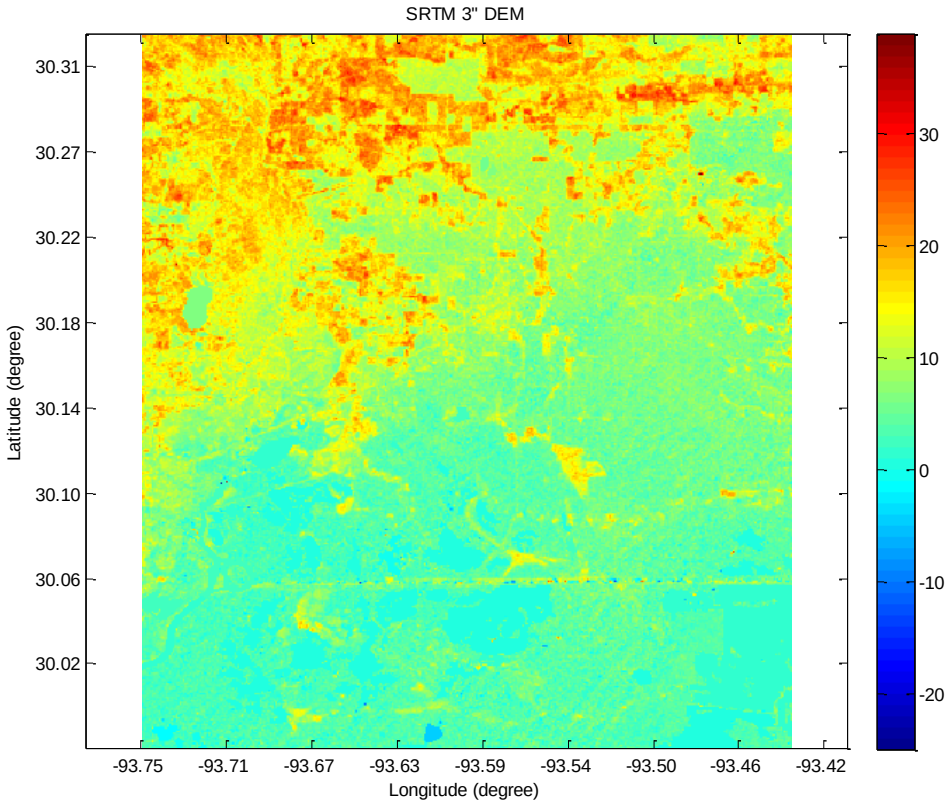

Figure 4.17 SRTM 3″ DEM used for the terrain correction

It can be seen from these figures that the two results are basically consistent with each other and have a difference of about ±5 E for all gradients except for T_{12}, where the differences are smaller. It should be noted that Bell Geospace's corrections are the result of de-noising (using a 150 meter cut-off wavelength) and represent a line leveled result, which means the long wavelength noise was removed for inline and cross line observations, including the terrain correction. Using the wavelength filter to the terrain correction is equal to assume there is no actual topography outside their terrain correction area; furthermore it is similar to assume that the outer topography have similar effect on pair of points and can be neglected. This is what causes the differences between the two results. Bell Geospace extended 10 km (0.09^o for latitude, 0.104^o for longitude considering the Earth's curvature) along all direction of their observation area which result in their terrain correction area between latitudes 29.980^o ~ 30.320^o, and longitudes -93.764^o ~ -93.426^o; while our area is between latitudes 29.977^o ~ 30.323^o, and

longitudes -93.753^{o}~-93.437^{o}. The DEM data within these two areas are not exactly same and this is the another reason that cause the difference.

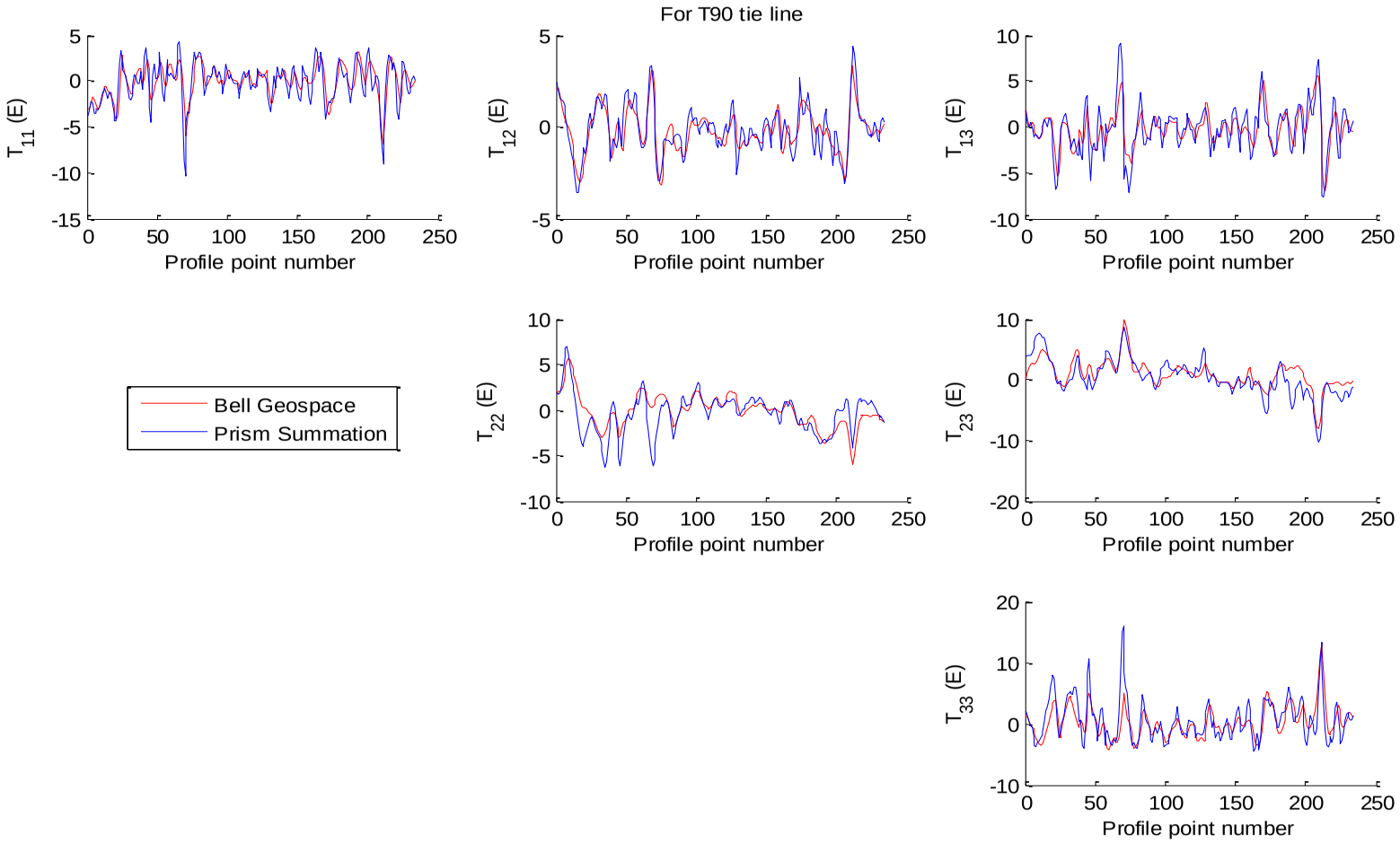

Figure 4.18 Terrain corrections of all gradients between two methods for T90 tie line

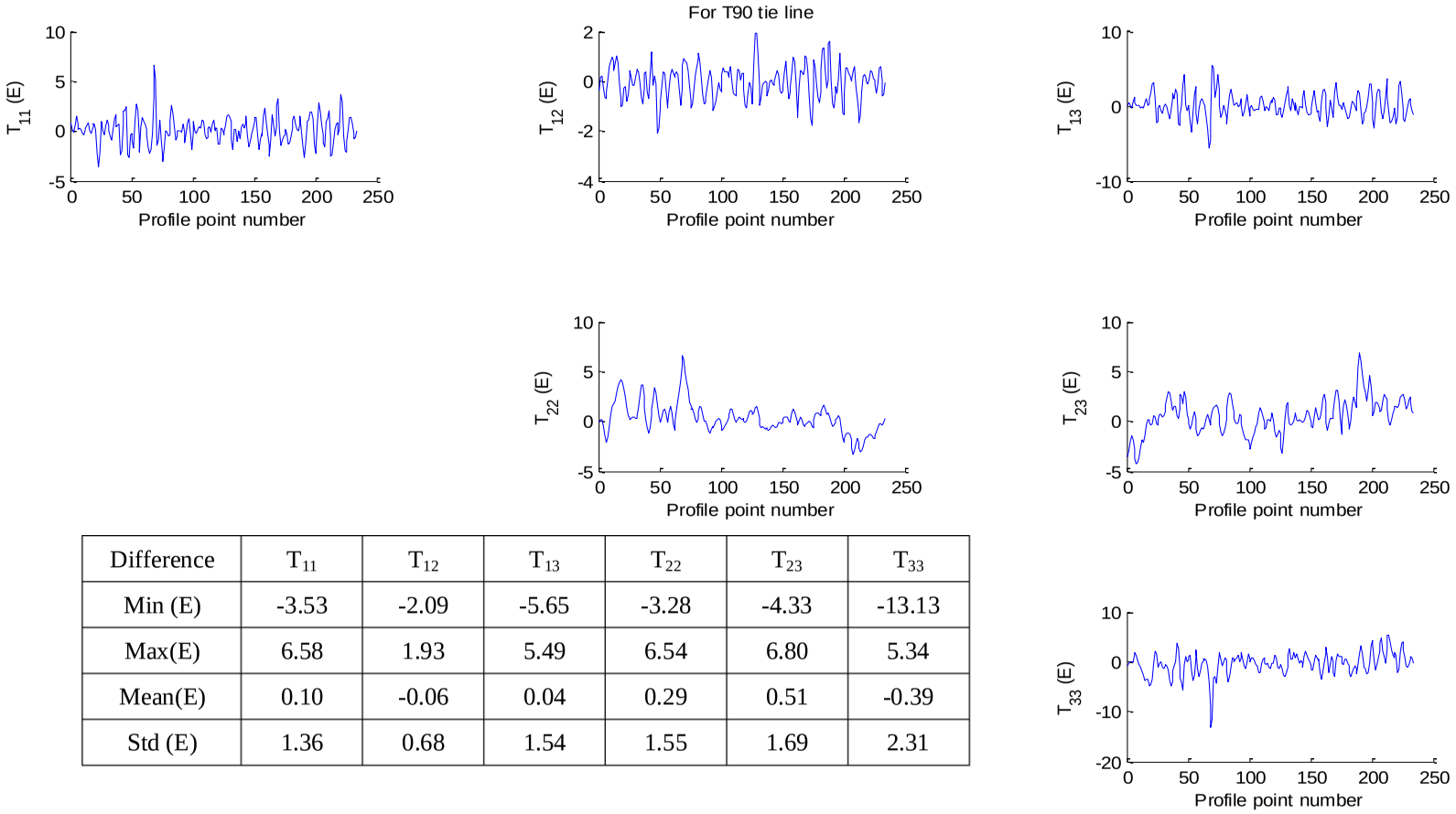

Difference	T_{11}	T_{12}	T_{13}	T_{22}	T_{23}	T_{33}
Min (E)	-3.53	-2.09	-5.65	-3.28	-4.33	-13.13
Max(E)	6.58	1.93	5.49	6.54	6.80	5.34
Mean(E)	0.10	-0.06	0.04	0.29	0.51	-0.39
Std (E)	1.36	0.68	1.54	1.55	1.69	2.31

Figure 4.19 Differences of terrain corrections of all gradients between two methods for T90 tie line

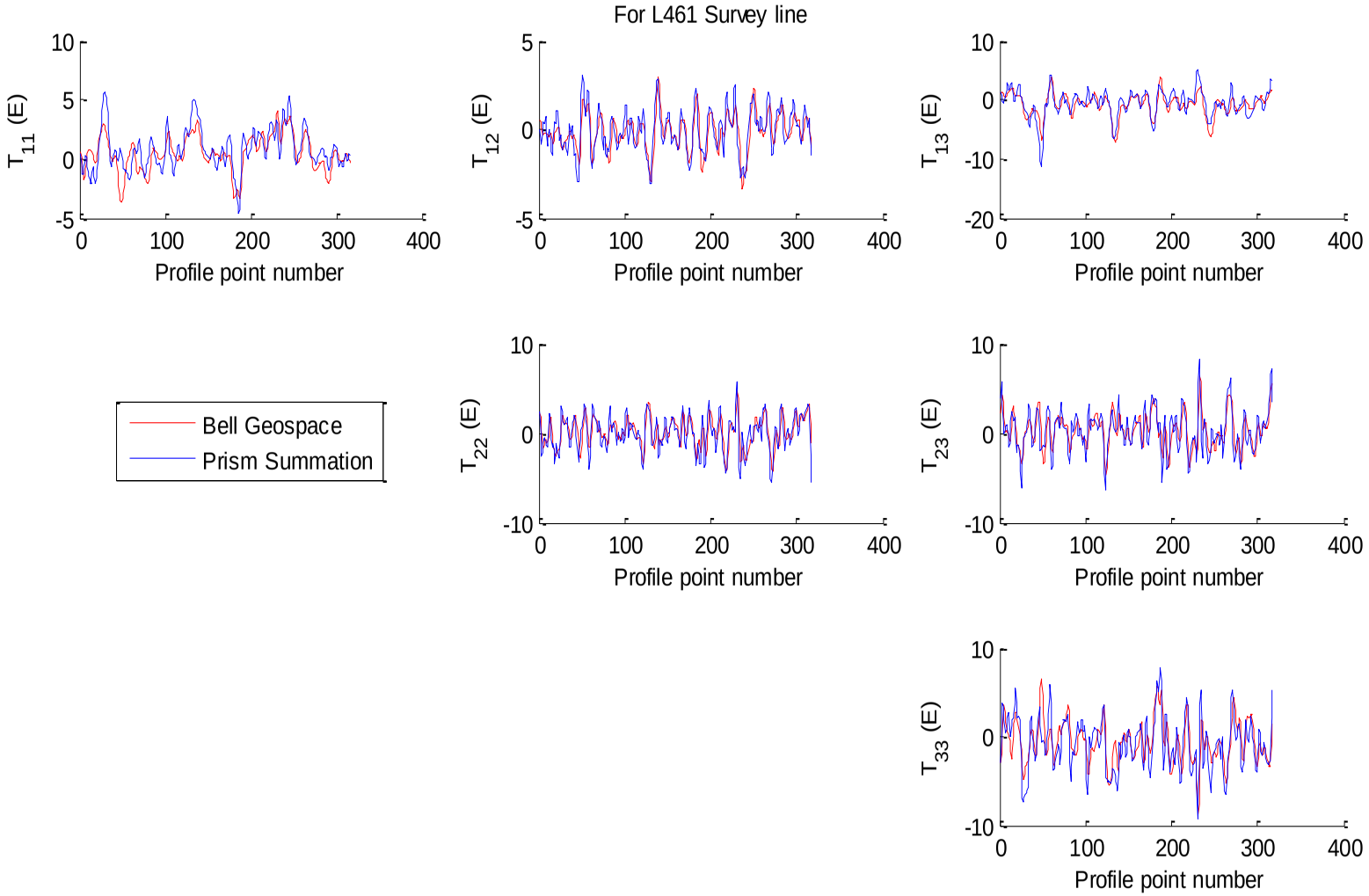

Figure 4.20 Terrain corrections of all gradients between two methods for L461 survey line

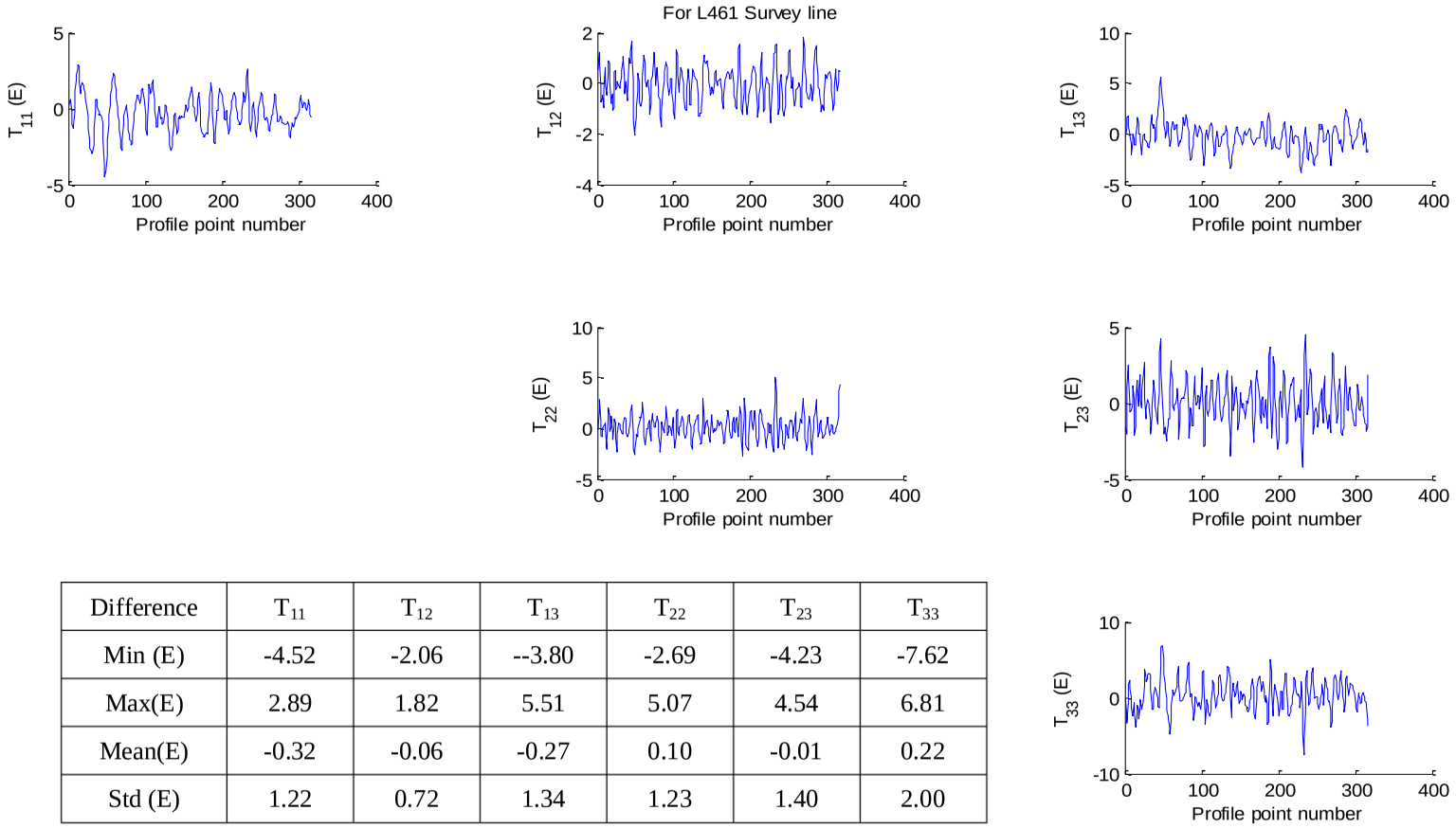

Difference	T_{11}	T_{12}	T_{13}	T_{22}	T_{23}	T_{33}
Min (E)	-4.52	-2.06	--3.80	-2.69	-4.23	-7.62
Max(E)	2.89	1.82	5.51	5.07	4.54	6.81
Mean(E)	-0.32	-0.06	-0.27	0.10	-0.01	0.22
Std (E)	1.22	0.72	1.34	1.23	1.40	2.00

Figure 4.21 Differences of terrain corrections of all gradients between two methods for L461 survey line

Next, we should determine the required extent of the terrain correction. Since we do not know the largest data area that will cause the variance of truncation error to converge for any particular extent, we select three DEMs concentric with the observation area, respectively $2^o \times 2^o$, $1^o \times 1^o$, and $0.5^o \times 0.5^o$. The SRTM 3″ DEM data for these three areas were downloaded from the website http://webmap.ornl.gov/wcsdown/wcsdown.jsp?dg_id=10008_2. Figure 4.15 outlines the three DEM areas with Vinton dome observation area: the outer area is $2^o \times 2^o$ with ranges in latitudes: 29.15°~31.15° and longitudes: -94.6°~-92.6°; the second is the $1^o \times 1^o$ area between latitudes: 29.65°~30.65° and longitudes: -94.1°~-93.1°; and the third is the $0.5^o \times 0.5^o$ area between latitudes: 29.9°~30.4° and longitudes: -93.85°~-93.35°. The innermost red area is the observation area bounded by latitudes: 30.07° ~ 30.23° and longitudes: -93.66° ~ -93.53°.

We use the geostatistical procedure described in chapter 2.2.2 to compute the variance of truncation error and variance of truncation error difference for three different sizes of DEMs by using equations (2.81) ~ (2.84). The observation height is set at h_p=80 m, which is about the average flight altitude. Next the extent of terrain correction was determined by letting the variance be smaller than the variance of typical instrument error, for example, high-accuracy airborne gradiometers with accuracy of 0.1 $E/\sqrt{Hz}$ (Jekeli, 2006); the results were shown in Figure 4.22, 4.23. Since the observation area is about 11.7 km x 16.7 km, so we set a pair of computation points separated with distance 20.7 km which is the longest distance within the observation area. It can be shown from the results in Figure 4.22 that the extent needed is about 35 km for $0.5^o \times 0.5^o$ area; 55 km for $1^o \times 1^o$ area, and 110 km for $2^o \times 2^o$ area based on the criterion of making the variance smaller than 10^{-2} E^2. For any pair of points separated by 20.7 km, it can be seen from Figure 4.23 that the extent needed from each point is about 25 km for $0.5^o \times 0.5^o$ area; 35km for $1^o \times 1^o$ area, 45 km for $2^o \times 2^o$ area based on the same criterion. Here the required extent differs for three different sizes of area and does not converge quickly even when the area size increases to $2^o \times 2^o$ because the topography in this area shows strong non-stationarity which is the assumption of our geostatistical analysis. On the other hand, if the topography is stationary, then these lines will converge quickly when the area size increasing (see Figure 4.8, Figure 4.32, 4.33 cases). Considering that the observation area is about 11.7 km x 16.7 km, and that Bell Geospace selected a DEM that extended 10 km along all directions of observation, their total extent of the DEM for the terrain correction is about 37 km, so their extent is enough to make sure the variance of truncation error for a single point is smaller than the criterion we set in terms of the variance of instrument error (i.e., 10^{-2} E^2).

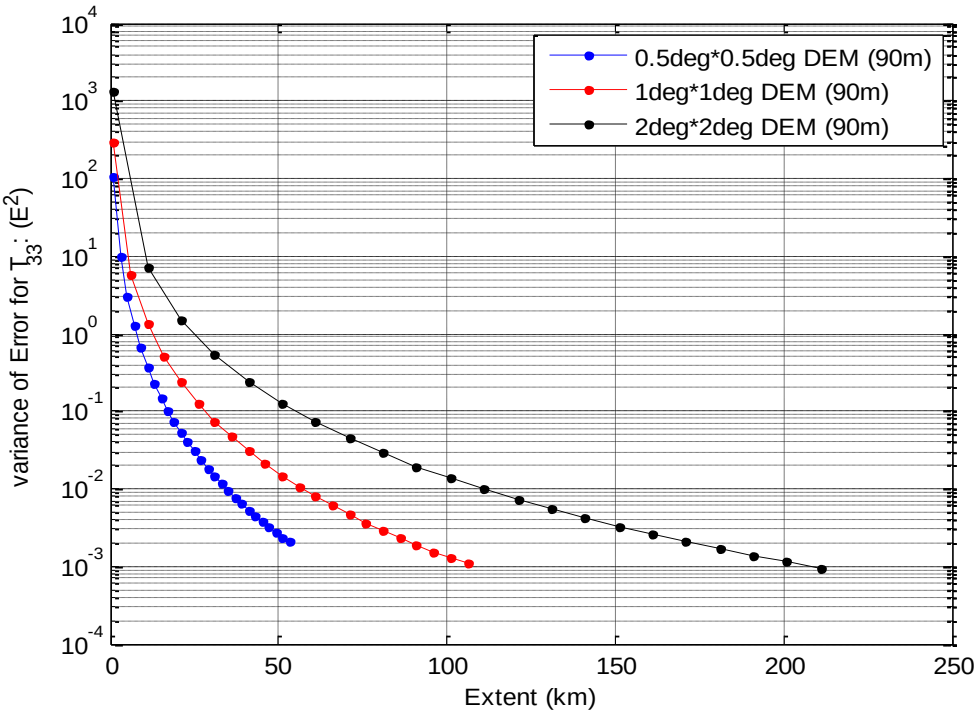

Figure 4.22 Variance of truncation error for three different sizes of DEM

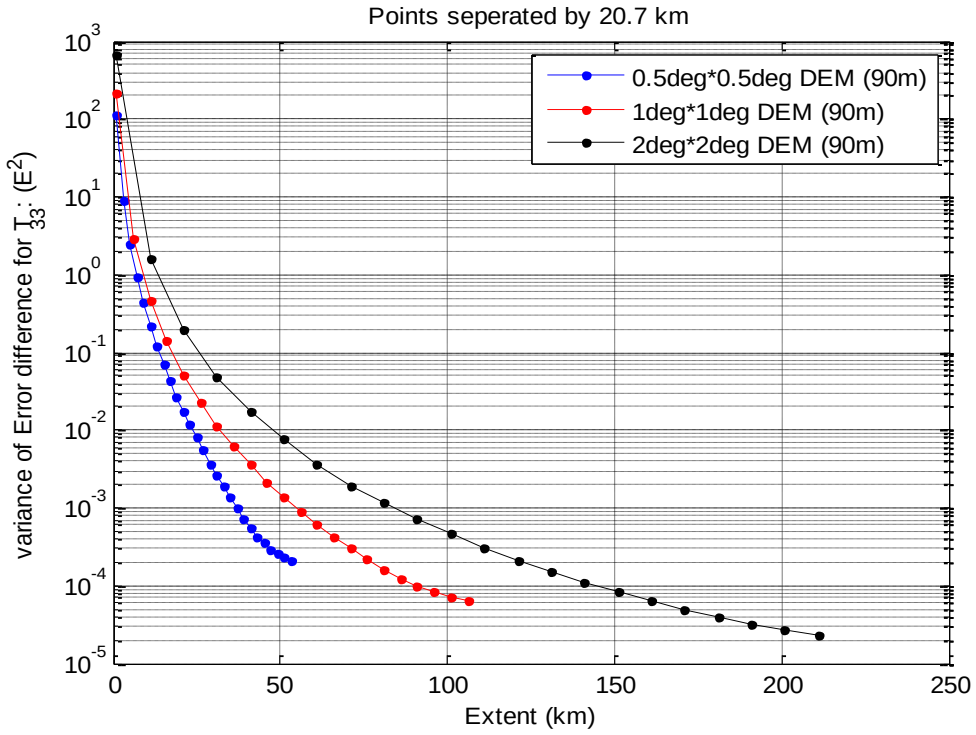

Figure 4.23 Variance of truncation error difference for three different sizes of DEM

4.3.2 Terrain correction of Air-FTG at Parkfield, CA

Bell Geospace also collected Air-FTG observations near Parkfield, California, from September 15, 2004 to September 17, 2004. Figure 4.24 shows the location of the survey area which covers about 100 km^2. Figure 4.25 shows the location of Air-FTG survey flight lines (Bell Geospace, 2004). The northwest-southeast flight lines are survey lines and the northeast-southwest flight lines are tie lines. There are 49 survey lines separated by 200 meters. Each survey line is about 11.2 km long. There are 10 tie lines separated by 1000 meters. Each tie line is about 10.3 km long. Table 4.5 shows the information of the terrain, altitude and clearance of the survey area. Bell Geospace uses the same procedure, method, and software package as that used for Vinton Dome area (Bell Geospace, 2008) to compute the terrain correction. The DEM data used for the terrain correction is the SRTM 1" dataset with about 30 m resolution.

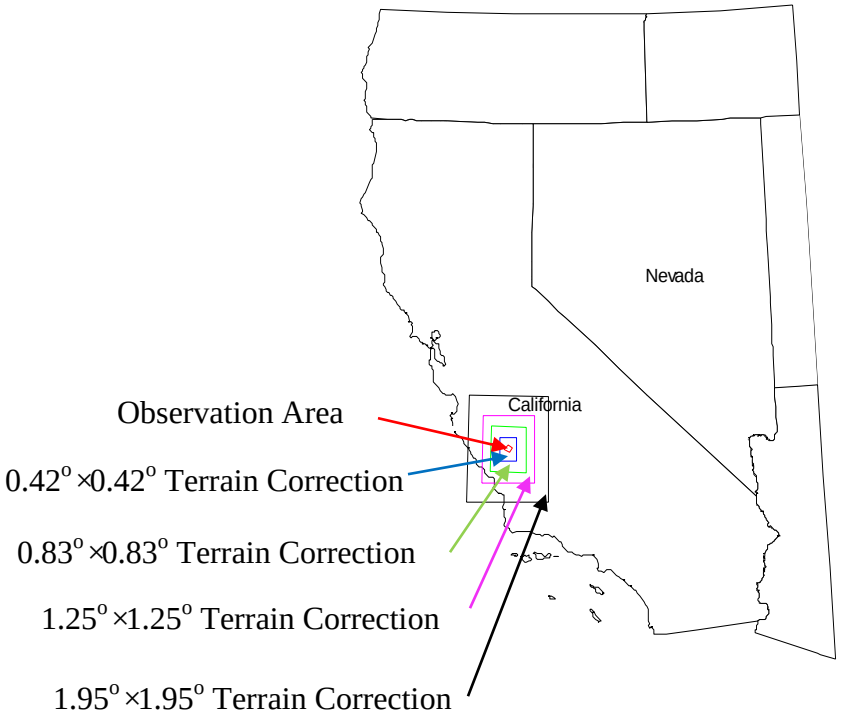

Figure 4.24 Location of survey area and terrain correction areas

Unit: m	Min	Max	Std. Dev.	Mean
Terrain	410	1064.3	108.0	705.7
GPS Altitude	839.4	1350.5	109.9	1096.4
Ground Clearance	183.4	674.5	93.5	390.7

Table 4.5 Flight altitude statistics

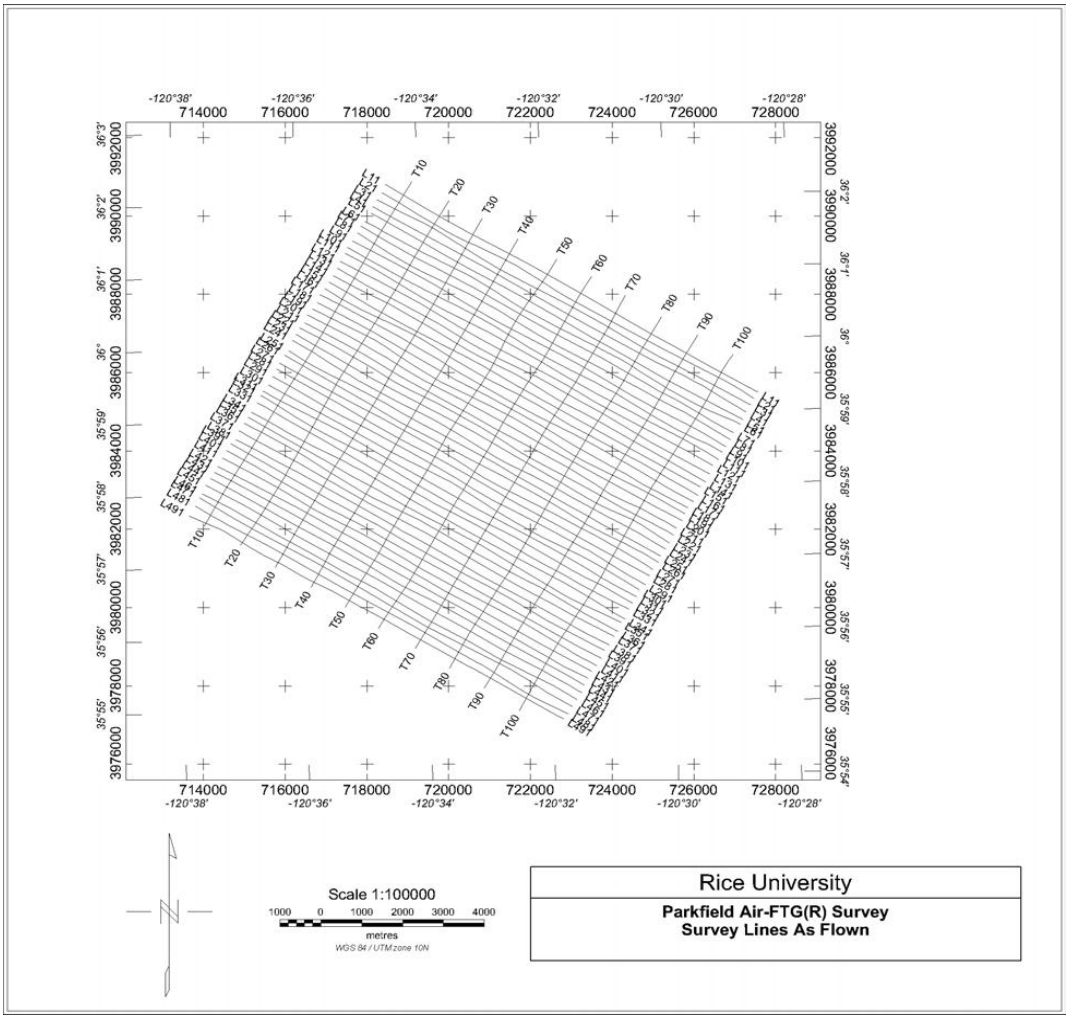

Figure 4.25 Air-FTG survey flight lines

Zhu (2007) also computed the terrain correction using the direct numerical integration methods. He used the USGS 1" DEM within the area defined by latitude: $35^{o}52^{'}28^{"} \sim 36^{o}04^{'}38^{"}$ and longitude: $-120^{o}41^{'}53^{"} \sim -120^{o}25^{'}30^{"}$; whereas, we used the

space prism summation method described in chapter 2.2.1. Two different sources of SRTM 1" DEM data were used for our computation, respectively; one dataset (named as DEM1) was downloaded from http://webmap.ornl.gov/wcsdown/wcsdown.jsp?dg_id=10008_2 and covers the same area as that of Zhu (2007), the other dataset (named as DEM2) is the dataset from the USGS website. The difference between the DEM1 and DEM2 datasets are shown in Figure 4.26, with their statistics listed in Table 4.6. The two DEMs have differences of about ±7 m, but the means of the terrain heights for two DEMs are almost same.

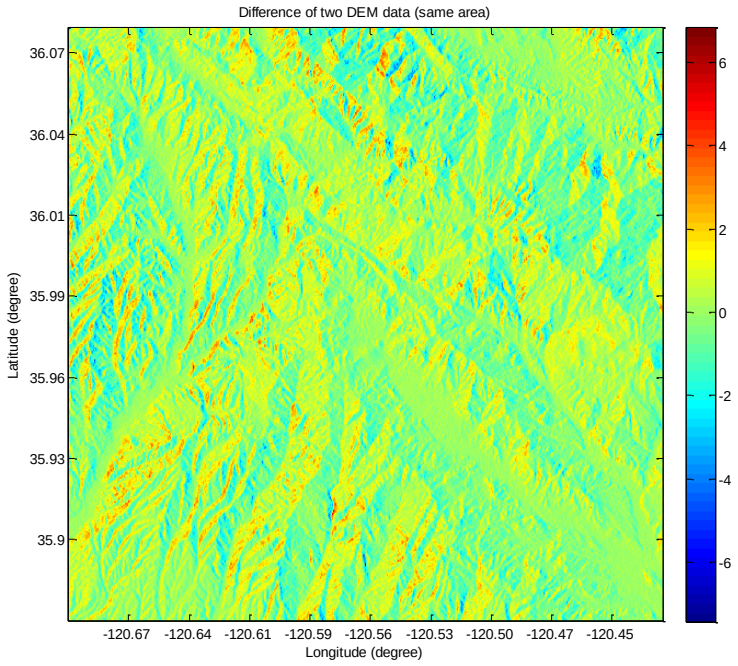

Figure 4.26 Height difference between DEM1 and DEM2 (unit: meter)

	Min	Max	Mean	Std.
Differences (m)	-7.42	6.85	0.01	1.0

Table 4.6 Statistics of difference between DEM1 and DEM2

Figure 4.27 shows our results using the DEM1 dataset compared with corresponding results from Jekeli and Zhu (2006) and Bell Geospace (2004) with respective differences shown in Figure 4.28. Figures 4.29, Figure 4.30 show results similar to Figure 4.27, and Figure 4.28, but for DEM2 dataset.

It can be seen from Figure 4.27, 4.29 that the three results are basically consistent with each other. Figures 4.28, 4.30 show that the differences with respect to Bell Geospace (2004) are between ±2 E using either the DEM1 dataset or the DEM2 dataset.

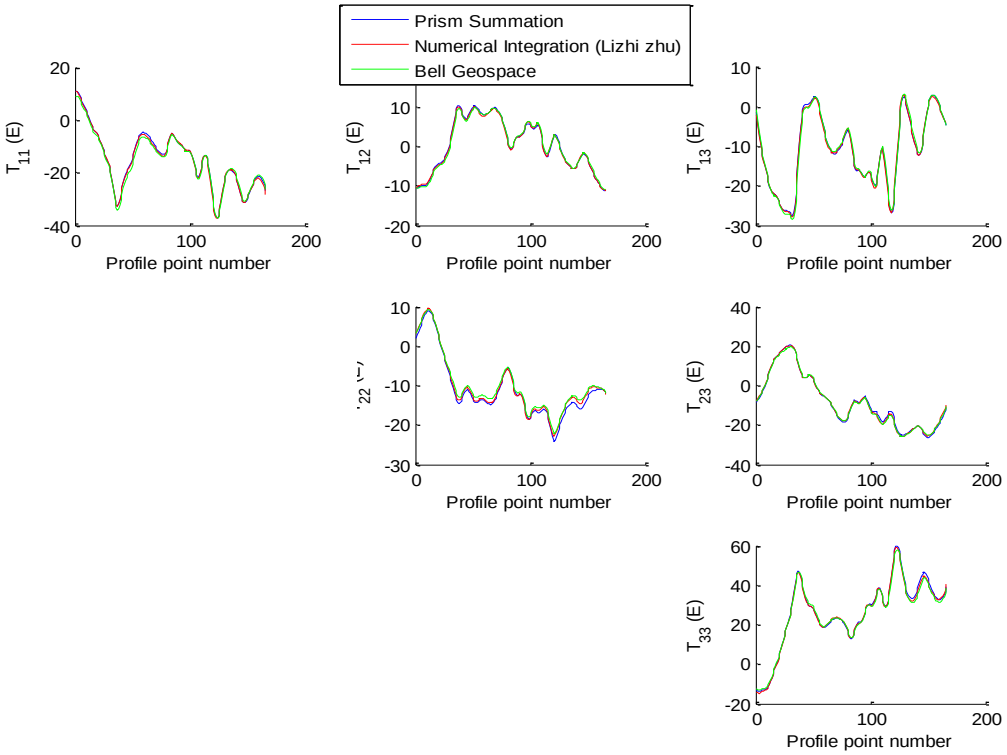

Figure 4.27 Terrain corrections of all gradients between three methods for Line 241

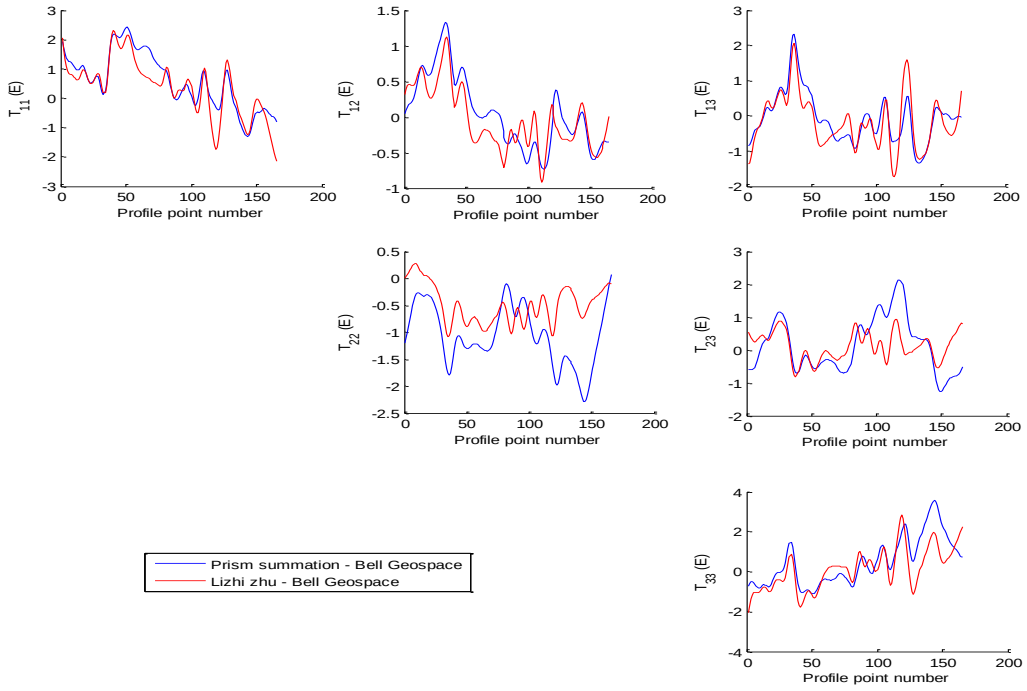

Figure 4.28 Differences of terrain corrections between three methods for Line 241

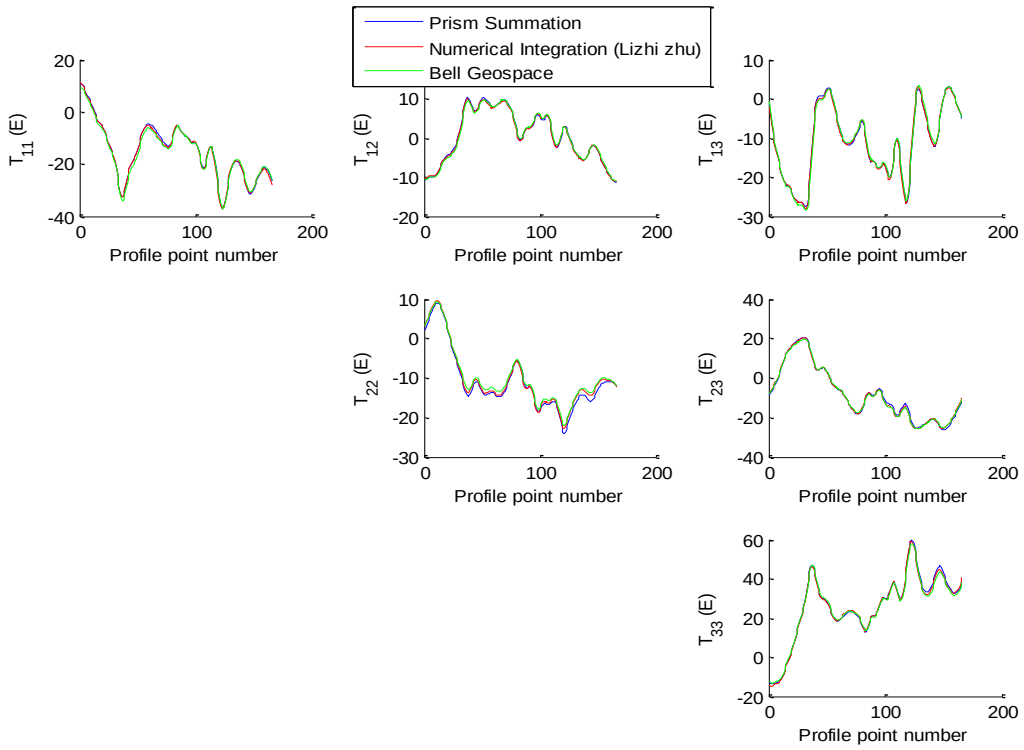

Figure 4.29 Terrain corrections of all gradients between three methods for Line 241

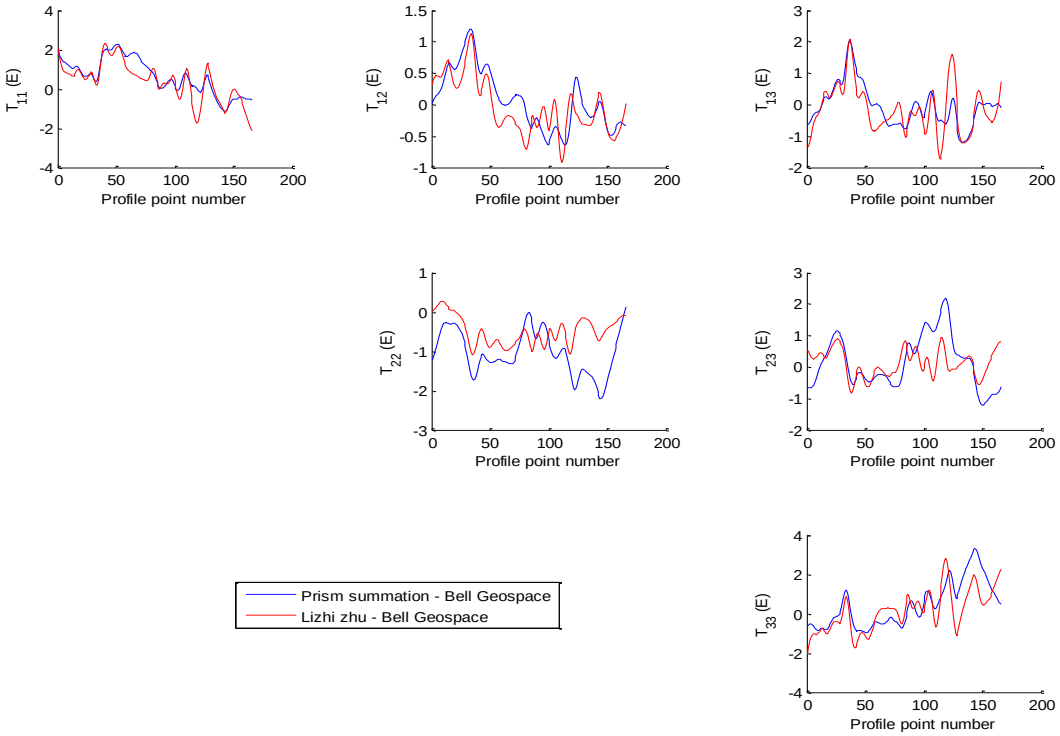

Figure 4.30 Differences of terrain corrections between three methods for Line 241

The differences of the terrain corrections for all gravity gradients between the DEM1 and DEM2 datasets are shown in Figure 4.31. Using the prism summation method these differences vary about ±0.4 E, which means the error of the DEM has little weight on the terrain corrections.

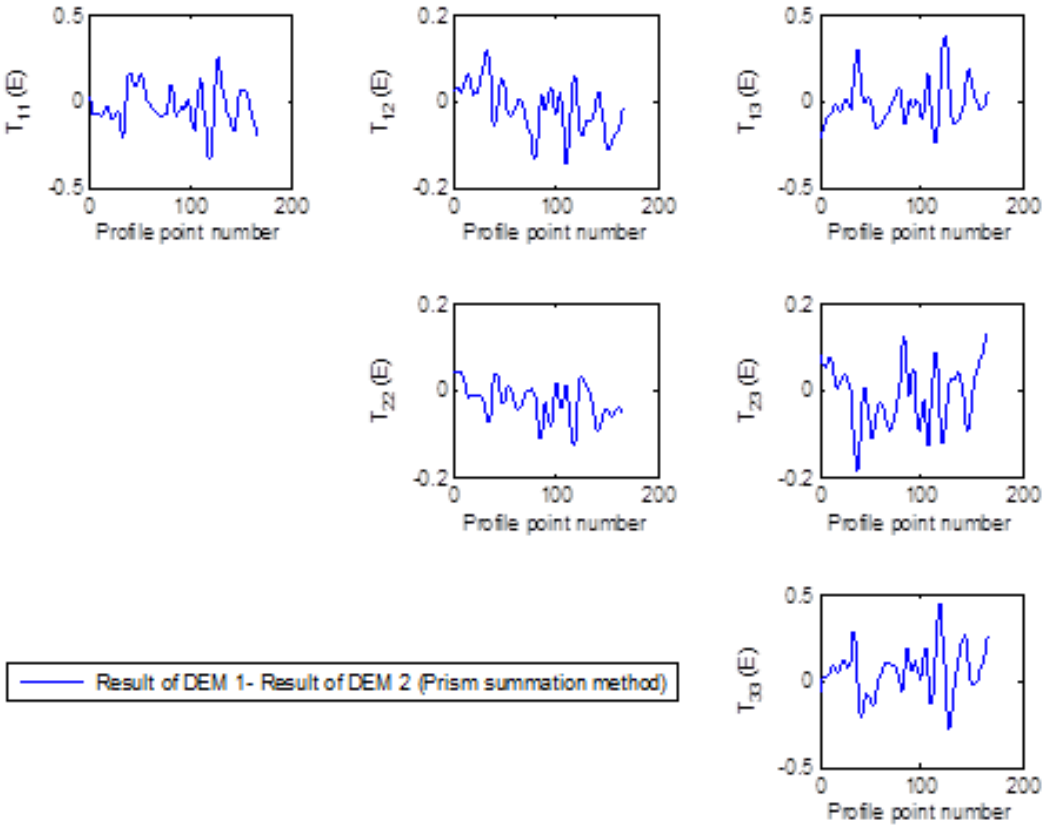

Figure 4.31 Differences of terrain corrections between DEM1 and DEM2 for Line 241

Next we select four DEM areas concentric with observation area, i.e., $1.95^o \times 1.95^o$, $1.25^o \times 1.25^o$, $0.83^o \times 0.83^o$ and $0.42^o \times 0.42^o$, respectively. The SRTM 3″ DEM data are downloaded from the website http://webmap.ornl.gov/wcsdown/wcsdown.jsp?dg_id=10008_2. Figure 4.24 shows the sketches of these DEM areas, where the innermost red area is observation area.

Following the same procedure as for the Vinton Dome area, we computed the variance of the truncation error and of the truncation error difference for four different sizes of DEMs. Then, the extent of the terrain correction was determined based on the variance. Since the observation area is about 10 km x 10 km, we considered a pair of computation points separated by 14 km, which is the longest distance within the observation area. The observation plane height is the average flight altitude of 1096.4 m. The results (for gradient T_{33}) are shown in Figures 4.32, and 4.33.

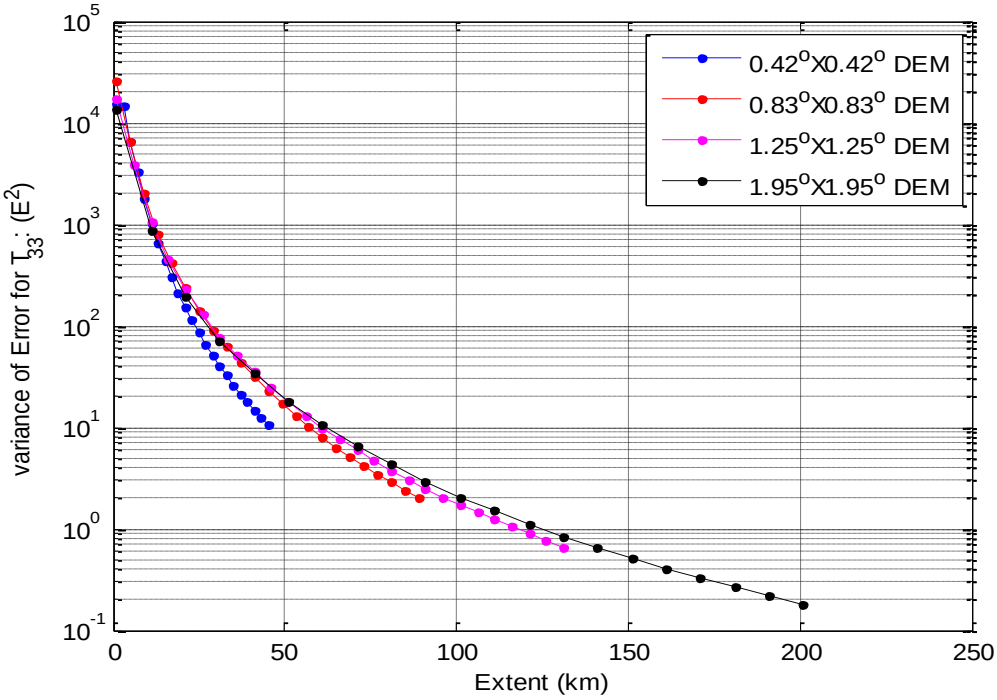

Figure 4.32 Variance of truncation error for four different sizes of DEM

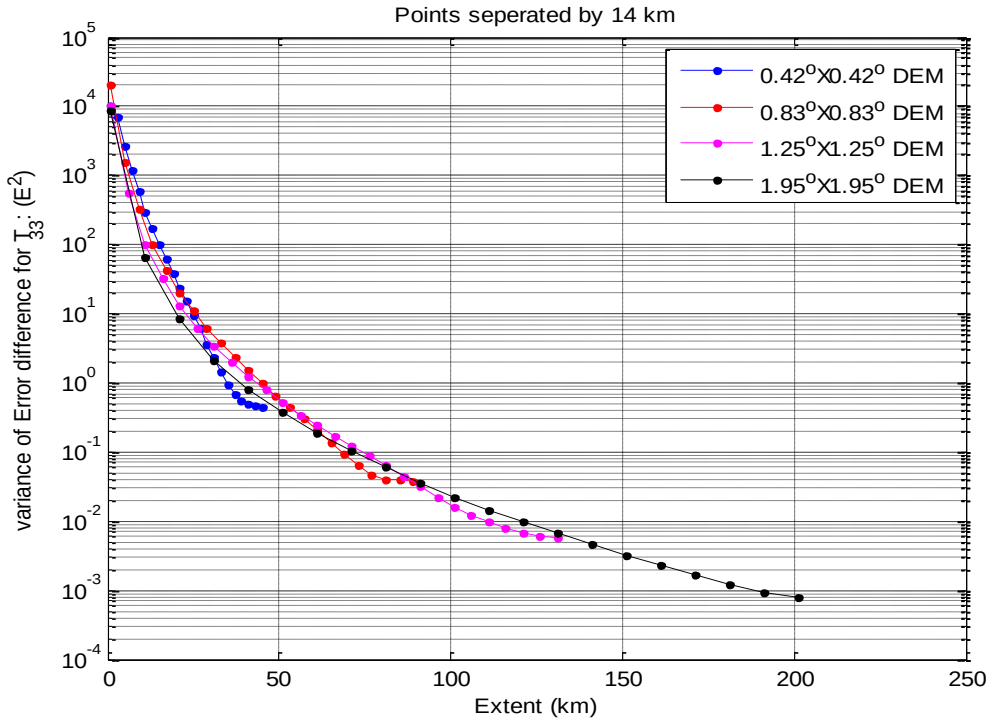

Figure 4.33 Variance of truncation error difference for four different sizes of DEM

It can be seen from Figure 4.32 that even if we corrected all the terrain within $1.95^o \times 1.95^o$, we still cannot reach the goal of making the variance smaller than 10^{-2} E^2. If we use the more realistic variance, such as 1 E^2, then the extent needed is 120 km for one single point and 40 km from each point for a pair of points within the $1.95^o \times 1.95^o$ DEM area in Parkerfield. It is because the area is rougher and the altitude of flight above the ground is much higher than for the Vinton Dome area. Likewise, for any pair of points separated by 14 km, the extent needed is about 120 km which is much larger than Bell Geospace's DEM correction area of about 16 km x 16 km.

4.3.3 Extent of terrain correction for different characters of topography

In the previous section, we determined the extent of terrain correction by computing the variance of truncation error through the geostatistical methods. The different types of topography can be quantified by geostatistics, so we can relate them directly to the corresponding required extent of terrain correction. For a specific observation area, we can just compute the geostatistics of the terrain around the observation area and find the required extent easily through a modeled relationship, thus avoiding extensive trial-and-error computations.

We selected three areas which contain distinctive characters (mostly flat, medium rough and mountainous) of topography and computed the covariance model of the terrain height, i.e., fitted an isotropic PSD to the empirical PSD of the height. The locations of three areas are shown in Figure 4.34.

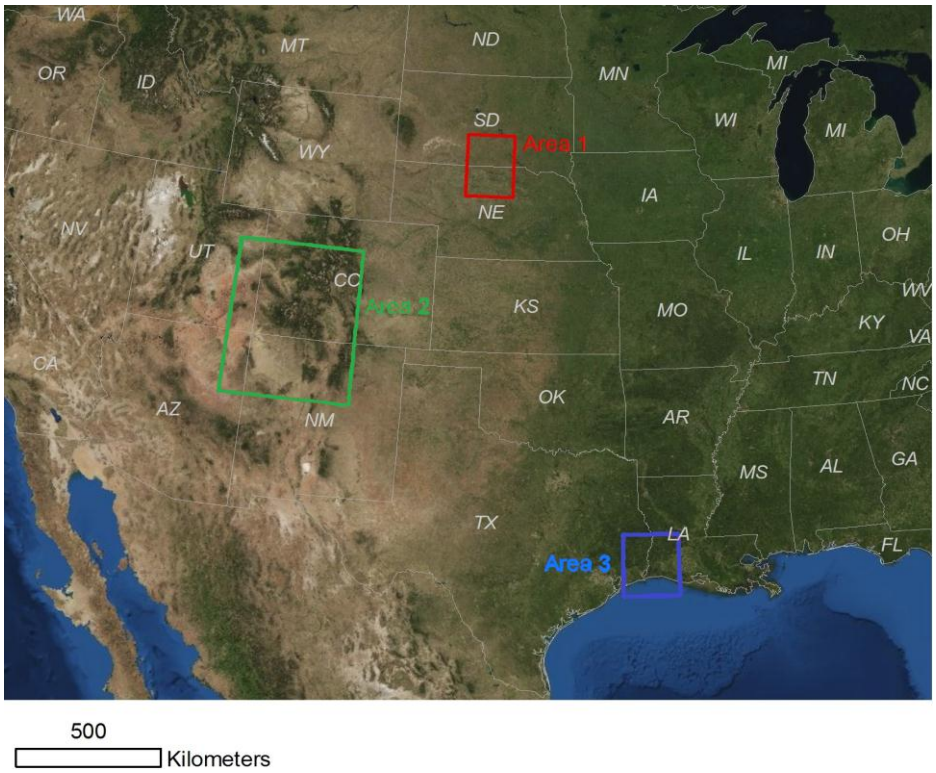

Figure 4.34 Three areas with distinctive characters of topography

Area 1 is $2^o \times 2^o$ with a range of latitudes: $42^o \sim 44^o$, and longitudes: $-101^o \sim -99^o$, and represents medium rough terrain. Area 2 is $5^o \times 5^o$ with a range of latitudes: $35^o \sim 40^o$, and longitudes: $-110^o \sim -105^o$, and represents mountainous terrain. Area 3 is $2^o \times 2^o$ with a range of latitudes: $29.15^o \sim 31.15^o$, and longitudes: $-94.6^o \sim -92.6^o$, and represents the mostly flat terrain. The reciprocal distance covariance model was fitted to the empirical PSDs of these three areas. We also determined the required extent of these three areas by using the geostatistical method. The results of these three covariance model and the corresponding variance of truncation error is given in Figure 4.35 for a single point, and in Figure 4.36 for a pair of points.

From the left plot of Figure 4.35 we can see that the PSD magnitude for the mountainous topography is 100 times that of the mostly flat topography comparing at medium wavelength; the corresponding extent determined for a certain variance magnitude of truncation error is about 4 times larger. For example, the required extent is 400 km for Area 2, while about 100 km for Area 3 provided the variance of truncation error is 10^{-2} E^2. For a pair of points separated by about 20 km, the required extent is 160 km for Area 2, while 40 km for Area 3 for the same truncation error variance. Alternatively, for a variance of 10^{-1} E^2, the required extent is 100 km for Area 2, and 25 km for Area 3. Thus, if we know the geostatistics of the terrain around our observation

area, we can easily know the required extent through the relationship. For other types of topography, the result can be obtained by interpolation.

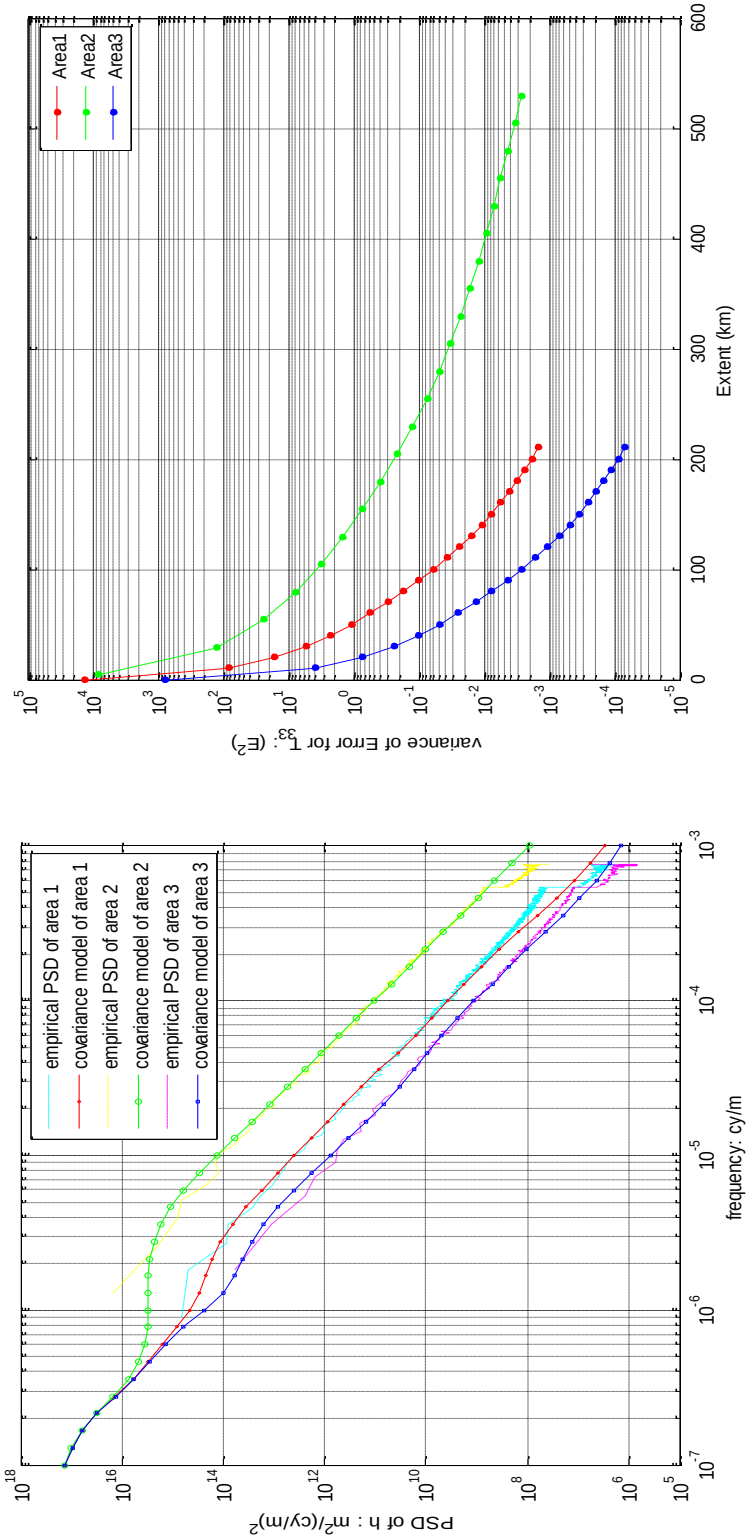

Figure 4.35 Covariance model and variance of truncation error of one point for three distinctive areas

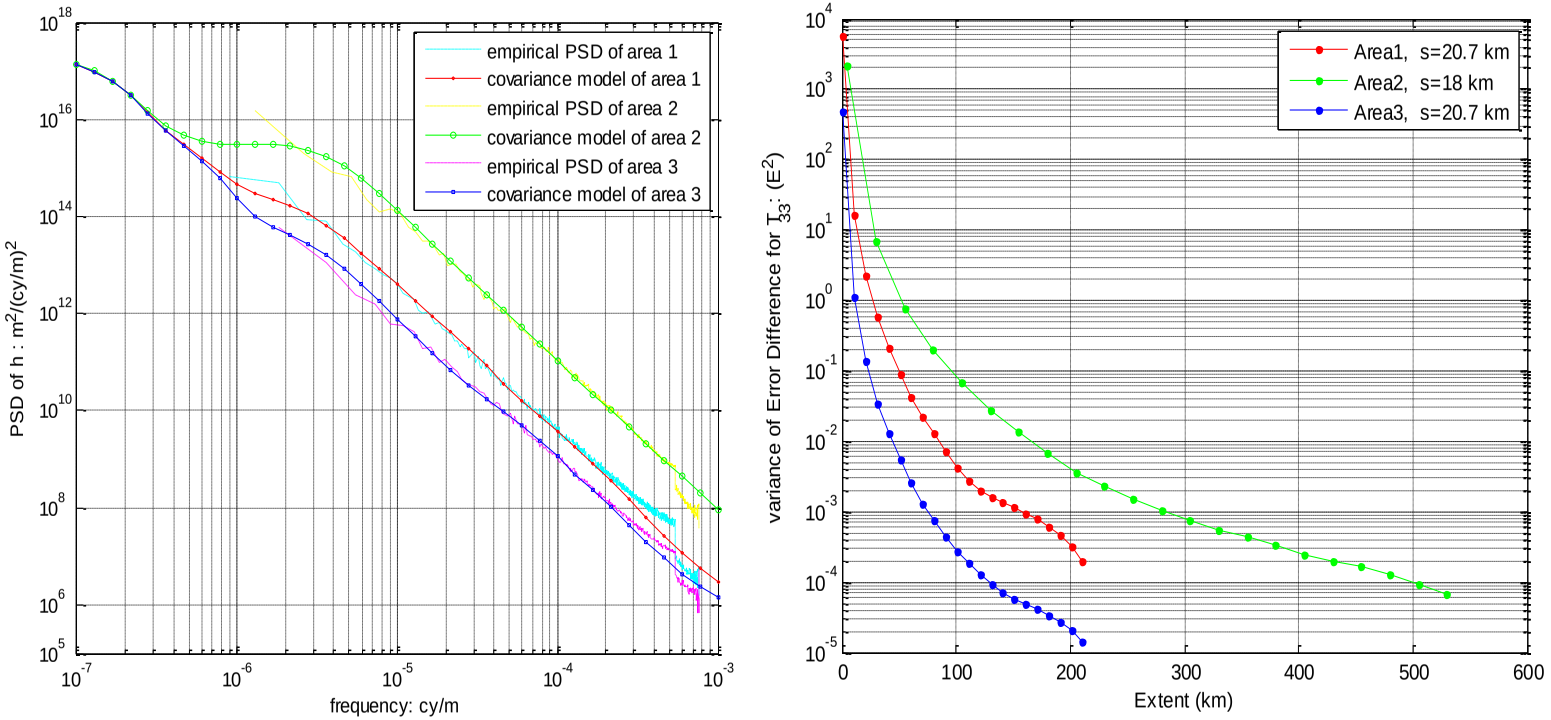

Figure 4.36 Covariance model and variance of truncation error difference of one pair of points for three distinctive areas

Chapter 5

Conclusion

In this study we developed a method to estimate the required extent of terrain correction of gravity gradients for geophysical studies based on a geostatistical method and truncation theory. The truncation theory was developed and applied to Forsberg's FFT method for the computation of the power spectral density and thus the covariance of the terrain. The truncation error represents the gravity gradient effect of neglecting the remote terrain beyond the specified area defined by truncation extent T. The variance of the error is based on the covariance analysis of the terrain in the neighborhood of the computation point. Therefore the necessary extent for the terrain correction of gravity gradients can be determined such that the truncation error variance is below a chosen value, e.g., the variance of the gradient measurement error. However, the effect of the remote zone will be nearly the same for two neighboring points of interest. The effect acts like a bias and like other biases is not of particular interest in a gravity gradient survey. For close points, the value of T will be smaller to obtain the same variance of error difference; for points further apart, the value of T will be larger. So if we consider the variance of the error difference for close points, then the needed extent of terrain correction should be decreased dramatically compared to the extent needed for single point.

The geostatistical analysis of the required extent can be done for different spectra of topography (smooth and rough). We confirmed the predicted truncation errors in each case by simulations using traditional terrain correction methods. We developed a method to simulate the different types of topography (smooth or rough with the desired resolution) based on the reciprocal distance covariance model. The low frequency part of topography can be obtained from known models, such as DTM2006, or from other available models, such as the SRTM DEM. Through the topography simulation, we can obtain different characters (smooth or rough), resolutions (even ultra-high resolutions) topography and also verified our procedure of geostatistical method for the determination of required extent of the terrain. We simulated 20 m resolution topographies based on DTM2006 5′ and SRTM 30″ data for two different types of area (smooth and rough), respectively.

We also validated our methods with the usual deterministic method by applying the analytical terrain correction formulas using the right rectangular prism to the simulated topography. The deterministic variances of the error or error difference are

computed from one thousand error samples in a Monte Carlo fashion by randomly selecting computation points within the same area used in the geostatistical method. These analyses show that two methods produce consistent results for our 3 km by 3 km high resolution (1 m) topography simulation. They differ only by 0.2 E^2 for a small truncation extent of 1 km; by 0.007 E^2 for a truncation extent of 2 km, and by 0.0009 E^2 for a truncation extent of 2.5 km. For a local gravity gradiometric survey (within 3 km by 3 km), the minimum extent we need to compute the terrain correction is 1.5 km in order that the variance of truncation error is smaller than 1 E^2. An extent of 2.5 km is needed in order to reduce the truncation error variance to 0.1 E^2.

Our previous result is based on an ultra-high resolution of topography for a very local survey. Considering the regional survey, the needed extent of terrain will also increase; at the same time, the curve line of the truncation error variance versus the extent should converge when we increase the outer boundary of the terrain. From our computation results, it shows that the curve line will converge quickly if the terrain is stationary; furthermore, the speed of convergence is slow if the terrain is not stationary. And based on the 3″ resolution DEM of such an area, it is concluded that the extent of terrain correction need to reach 400 km in order that the truncation error variance is smaller than 10^{-2} (E^2), or 230 km in order that the truncation error variance is smaller than 10^{-1} (E^2). It can be seen that the extent determined from the variance of truncation error difference for pairs of points is much less (especially for points separated by short distance) than that from the variance of truncation error for a single point. With the separated distance increasing, the required extent also increases. The simulation shows the required extent is 35 km for points separated by 0.9 km, 85 km for points separated by 4.5 km, 120 km for points separated by 9 km, 165 km for points separated by 18 km, 240 km for points separated by 45 km. And the above result is obtained from terrain correction of gravity gradient T_{33}. It is also concluded that the required extent for the terrain correction on gravity gradients T_{13}, T_{23} are much less than for other gravity gradient components.

We analyzed Bell Geospace's terrain correction computed for the Air-FTG observations at Vinton Dome, LA, and Parkfield, CA. Our computations of the terrain correction are consistent with Bell Geospace's result and that of Zhu (2007). The differences between these methods are about ±5 E for Vinton Dome area; ±2 E for Parkfield, CA area. Also by our geostatistical analysis, the extent needed is about 35 km for the terrain correction of gravity gradients in the Vinton Dome area, which agrees with Bell Geospace's assumed area, but it is about 120 km for the Parkfield area, which does not agree with Bell Geospace's use of only about 20 km. The reason why the latter needs much larger DEM extent is the much rougher terrain than in the vicinity of the Vinton Dome area. Also the flight clearance above the ground at Parkfield is much higher than

for Vinton Dome. Finally we determined the required extent for three different areas of typical topography, which are represented by mostly flat, medium rough and mountainous terrain. We also characterize these topographies using the reciprocal distance of covariance model, and we set up an empirical model between the required extent and the characteristic terrain. Thus the required extent for other characteristic terrain can be interpolated easily.

Further research still needs to be carried out to study the effect of different DEM resolution and of mass density variations on the determination of needed extent. Also our geostatistical method relies on some basic assumptions such as the stationarity, isotropy of the terrain, etc. However these assumptions may not be valid in some actual cases, thus the sensitivity of these assumptions should be tested and analyzed in future research. Also the future work should be done is to extend our theory to satellite altitude and solve the problem using the spherical approximation.

References

Asten, M.W., 2000. A technical review of the FALCON AIRBORNE gravity gradiometer: Technical Consultant's report, Section 6, Gravity Capital Limited, Melbourne.

Badekas J., 1967. The horizontal gradients of gravity in southwest ohio. Report of the department of geodetic science. Report NO.89.

Bell Geospace B, 2004. Final report of acquisition and processing onAir-FTG survey in Parkfield earthquake experiment area: technical report. Rice University, Houston

Bell Geospace B, 2008. Processing and Acquisition of Air-FTG DATA. Vionton Dome, Vinton, Louisiana. Houston, Texas. July, 2008.

Bod, L., Fischbach, E., Marx G. and NÁRAY-ZIEGLE, M., 1990. One hundred years of the Eotvos experiment. http://www.kfki.hu/eotvos/onehund.html.

Bullard, E.C., 1936. Gravity measurements in East Africa. Philosophical Transactions of the Royal Society, London 235,445-534.

Cassinis, G., Dore, P. and Ballarin, S., 1937. Fundamental tables for reducing gravity observed values. Tipografia Legatoria Mario Ponzio, 11-27.

Chapin, D.A., 1998b. Gravity measurements: Past, present, future. The Leading Edge,17,100-112.

Chen, J., and Macnae, J.C., 1997. Terrain corrections are critical for airborne gravity gradiometer data:Exploration Geophysics,28,21-25.

Chinnery, M.A., 1961. Terrain corrections for airborne gravity gradient measurements: Geophysics, 26, No. 4, P. 480-489.

Danes, Z.F., 1982. An analytic method for the determination of distant terrain corrections: Geophysics, 47, 1453-1455.

Dransfield, M. and Zeng, Y., 2009. Airborne gravity gradiometry: Terrain corrections and elevation error. Geophysics. Vol. 74, NO. 5, P. 137–142.

Difrancesco, D., 2007. Advances and Challenges in the Development and Deployment of Gravity Gradiometer Systems. EGM 2007 International Workshop. Innovation in EM, Grav and Mag Methods:a new Perspective for Exploration. Capri, Italy, April 15 – 18, 2007.

Farr, T. G., et al., 2007. The Shuttle Radar Topography Mission, Rev. Geophys., 45, RG2004, doi:10.1029/2005RG000183.

Freeden, W., Nashed, M.Z., Sonar, T., 2010. Handbook of geomathematics. Springer-Verlag Berlin Heidelberg.

Forsberg, R., 1984. A study of terrain reductions, density anomalies and geophysical inversion methods in gravity field modeling. Report no 355, Department of Geodetic Science and Survey, Ohio State University, Columbus, OH, 129pp.

Forsberg, R. 1985. Gravity field terrain effect computations by FFT. Bull.Geod. 59 (1985) pp. 342~360.

Grant, F.S. and Elsaharty A.F., 1962. Bouguer gravity corrections using a variable density:Geophysics,27,616-626.

Grant, F.S. and West, G.F., 1965. Interpretation Theory in Applied Geophysics, McGraw-Hill, New York (1965) pp.584.

Hammer, S., 1939. Terrain corrections for gravimeter stations. Geophysics 4, 184-194.

Hammer, S., 1976. Topographic corrections for gradients in airborne gravimetry: Geophysics 41,1346-1352.

Heiskanen, W.A. and Moritz, H., 1967, Physical Geodesy: W. H. Freeman and Co., SanFrancisco.

Hirt, C., Marti, U., Featherstone, W., 2010. Combining EGM2008 and SRTM/DTM2006.0 residual terrain model data to improve quasigeoid computations in mountainous areas devoid of gravity data. J Geod (2010) 84:557–567 DOI 10.1007/s00190-010-0395-1.

Hwang, C., Wang, C., Hsiao, Y., 2003. Terrain correction computation using Gaussian quadrature. Computers & Geosciences 29 (2003) 1259 – 1268.

Jekeli, C., 2003. Statistical Analysi of Moving-Base Gradiometry and Gravity Gradiometry. Report, NO.466. The Ohio State University.

Jekeli, C., 2006. Airborne Gradiometry Error Analysis. Surveys in Geophysics Volume 27, Number 2, 257-275, DOI: 10.1007/s10712-005-3826-4. Springer, 2006.

Jekeli, C., and Zhu, L., 2006. Comparison of methods to model the gravitational gradient from topographic data base: Geophysics Journal International, 166, 99–1014.

Journel, A.G., and Huijbregts, C. J., 1978. Mining Geostatitstics. Academic Press, San Diego, CA 92101. ISBN hardback: 0-12-391050-1.

Kass, M.A., and Li, Y., 2008. Practical aspects of terrain correction in airborne gravity gradiometry surveys: Exploration Geophysics, 39,198-203.

Ku, C.C., 1977. A direct computation of gravity and magnetic anomalies caused by 2- and 3-dimensional bodies of arbitrary shape and arbitrary magnetic polarization by equivalent-point method and a simplified cubic spline. Geophysics. Vol.42. NO.3 P. 610-622.

LaFehr, T.R., 1991b. An exact solution for the gravity curvature (Bullard B) correction. Geophysics 56, 1178–1184.

Li, Y.C., Sideris, M., 1994. Improved gravimetric terrain correction. Geophysical Journal International 119, 740-752.

Martinec, Z., Matyska, C., Grafarend E.W., and Vanicek, P., 1993. On Helmert's 2nd condensation method. Manusc. Geod.18: 417-421.

Martinec, Z., 1998. Boundary-Value Problems for Gravimetric Determination of a Precise *Geoid*. Heidelberg : Springer-Verlag. Lecture Notes in Earth Sciences. 223 p.

Moritz, H., 1980. Advanced Physical Geodesy. Abacus press, Tunbridge Wells, Kent.

Mueller, Ivan I., 1964. The horizontal gradients of gravity in geodesy. The Ohio State University, Department of geodetic science.

Nabighian, M.N., Ander, M.E., Grauch, V.J.S., Hansen, R.O., LaFehr, T.R., Li, Y., Pearson, W.C., Peirce, J.W., Phillips, J.D., Ruder, M.E., 2005. 75th Anniversary The

historical development of the gravity method in exploration. Geophysics. Vol.70.NO.6.

Nagy, D., 1966. The gravitational attraction of a right rectangular prism. Geophysics, 31 (1966), pp. 362–371.

Nahavandchi, H., and Sjöberg, L., 1998. Terrain correction to the power H^3 in gravimetric geoid determination. Journal of Geodesy 72, 124-135.

Nowell, D.A.G., 1999. Gravity terrain corrections - an overview. Journal of Applied Geophysics 42, 117-134.

Parker, R.L., 1972. The rapid calculation of potential anomalies: Geophysical Journal of the Royal Astronomical Society, 31,447-455.

Parker, R.L., 1995. Improved Fourier terrain correction, part one: Geophysics 60, 1007-1017.

Paul, M.K., 1974. The gravity effect of a homogeneous polyhedron for three-dimensional interpretation. Pure Appl Geophys 112:553 – 561.

Pavlis, N.K., Factor, J.K. and Holmes, S.A., 2007. Terrain-Related Gravimetric Quantities Computed for the Next EGM. Proceed of the 1st International Symposium of the International Gravity Field Service, Istanbul, Turkey, Harita Dergisi, Special Issue 18, pp 318-323.

Sideris, M.G., 1984. Computation of gravimetric terrain corrections using fast Fourier transform techniques, UCSE Rep, 20007, Dep. Of Surv. Eng., Univ. of Calgary, Calgary, Alberta.

Sideris, M. G., 1985. A fast Fourier transform method for computing terrain corrections. manuscripta geodaetica 10, 66–73.

Sjöberg, L.E., 2009. On the topographic bias in geoid determination by the external gravity field. J Geod 83:967-972.

Smith, W.H.F. and Sandwell, D.T., 1997. Global sea floor topography from satellite altimetry and ship depth soundings. Science, 277, pp. 1956-1962.

Sprenke, K.F., 1989. Efficient terrain corrections: a geostatistical analysis. Geophysics

54, 1622–1628.

Tsoulis, D.V., 1998. A combination method for computing terrain corrections. Phys. Chem. Earth, Vol.23, No.1 pp. 53-58.

Tsoulis, D.V., 2001. Terrain correction computations for a densely sampled DTM in the Bavarian Alps. J. Geod. 75, 291– 307.

Tziavos, I.N., Sideris, M.G., Forsberg, R. and Schwarz, K.P., 1988. The effect of the terrain on airborne gravity and gradiometry. Journal of Geophysical Research, Vol.93,NO.B8, P.9173-9186.

Tziavos, I.N., Sideris, M.G., and Sunkel, H., 1996. The effect of surface density variation on terrain modeling – A case study in Austria. Aristotle Univ. of Thessaloniki, Techniques for Local Geoid Determination p 99-110 (SEE N97-13487 01-46); FINLAND.

Vanicek, P., and Kleusberg, A., 1987. The Canadian geoid – Stokesian approach. Manusc. Geod., 12, 86-98.

Voigt, C., and Denker, H., 2006. A study of high frequency terrain effects in gravity field modelling. Proceedings of the 1st International Symposium of the International Gravity Field Service, “Gravity Field of the Earth”, Harita Dergisi, Special Issue 18, pp. 342–347, Ankara, Turkey.

Wang, YM. and Rapp, R. H., 1990. Terrain effects on geoid undulation computations. Manusc. geod., 15,23-29.

Zhu, L., 2007. Gradients Modeling with Gravity and DEM. Report No.483 Geodetic Science and Surveying, The Ohio State University, Columbus, OH, 43210.